

DEVELOPMENT  
OF  
A COMPUTER CONTROLLED  
SIX-PORT MICROWAVE MEASUREMENT SYSTEM

by

JAGDISH GIRIMAJI

A thesis  
presented to the University of Manitoba  
in partial fulfillment of the  
requirements for the degree of  
Master of Science  
in  
Electrical Engineering

Winnipeg, Manitoba, 1983

(c) JAGDISH GIRIMAJI, 1983

DEVELOPMENT  
OF  
A COMPUTER CONTROLLED  
SIX-PORT MICROWAVE MEASUREMENT SYSTEM

BY  
JAGDISH GIRIMAJI

A thesis submitted to the Faculty of Graduate Studies of  
the University of Manitoba in partial fulfillment of the requirements  
of the degree of

MASTER OF SCIENCE

© 1983

Permission has been granted to the LIBRARY OF THE UNIVER-  
SITY OF MANITOBA to lend or sell copies of this thesis, to  
the NATIONAL LIBRARY OF CANADA to microfilm this  
thesis and to lend or sell copies of the film, and UNIVERSITY  
MICROFILMS to publish an abstract of this thesis.

The author reserves other publication rights, and neither the  
thesis nor extensive extracts from it may be printed or other-  
wise reproduced without the author's written permission.



## ABSTRACT

This thesis presents a description and performance results of a computer controlled microwave six-port measurement system. In the six-port system concept a microwave circuit is synthesized in such a way that both the magnitude and phase of a load reflection coefficient is determined from four power readings generally derived from simple diode detection measurement circuitry. At present, complex reflection coefficient is measured by very time consuming slotted line techniques or by automatic network analysers (ANA) which are based on complex heterodyne detection methods. The appeal of the six-port system, therefore, lies in the simplicity of its amplitude detection system and its potential for use at millimeter wave frequencies where heterodyne detection is difficult.

The six-port system used in this research has been synthesized using a symmetric five-port junction and a directional coupler. The symmetric five-port junction has optimum properties for the accurate determination of complex load reflection coefficients and has been realized on stripline in the form of a ring type circuit with simple internal structure matching. All ports of the junction are well matched at the center frequency of 1 GHz and the junction has a useful bandwidth of at least 20%. A micro-computer, model HP-85, through an interface bus controls the experiment, acquires and processes data for the determination of the complex load reflection coefficient ( $\Gamma_L$ ). Using the six-port system  $\Gamma_L$  for various test loads has been determined over a 20% bandwidth and the results obtained have been compared with the computed values as well with readings obtained from the microwave network analyzer (MNA).

## ACKNOWLEDGEMENTS

The author wishes to express sincere appreciation to Professor E. Bridges, for his guidance, continuous interest, encouragement and patience through all phases of this work.

Special thanks are due to Mr. A. McKay of the Electronics shop and Mr. A. Symmons of the Machine shop. The cheerful cooperation provided by Mr. B. Tabachinick and Mr. D. Steinbach of the Antenna Laboratory is greatly appreciated.

## TABLE OF CONTENTS

	Page
ABSTRACT	i
ACKNOWLEDGEMENTS	ii
TABLE OF CONTENTS	iii
LIST OF FIGURES	vi
LIST OF TABLES	viii
CHAPTER I INTRODUCTION	1
1.1 Background	1
1.2 Review of Existing Six-port systems	2
CHAPTER II SIX-PORT THEORY	6
2.1 The Four Port Reflectometer	6
2.2 The Six-Port Network	9
2.3 Ideal q-Point Distribution	13
2.3 a The q-Point Distribution of a typical Six-Port	16
CHAPTER III THE SIX-PORT SYSTEM	19
3.1 Introduction	19
3.2 The Symmetric Five-Port Junction	19
3.3 Design of the Five-Port Junction	25
3.4 Experimental Performance of the Stripline Junction	31

		Page
CHAPTER	IV SIX-PORT IMPLEMENTATION	37
	4.1 The Six-Port Measurement System	37
	4.1 a System Operation	38
	4.2 Calibration of the Six-Port System	40
	4.3 An Expression for Determining Calibration Constants	43
	4.3 a A Closed Form Expression for the Constants $Z$ and $\phi_z$	45
	4.4 A Matrix Expression for $\Gamma_\ell$	50
	4.5 System Software	51
	4.5 a Calibration Program, REF - 6P	51
	4.5 b The Reflection Coefficient Measurement Program, REF - 6P	53
CHAPTER	V RESULTS AND DISCUSSIONS	54
	5.1 Introduction	54
	5.2 Six-Port Center Frequency Calibration	54
	5.3 Return Loss Calculation at 1 GHZ	55
	5.4 Measurement of $\Gamma_\ell$ at 1 GHZ	58
	5.5 Calibration of Six-Port System over a 220 MHZ Bandwidth	63
	5.6 Measurement of $\Gamma_\ell$ over the 220 MHZ Bandwidth	70

Page

CHAPTER VI	CONCLUSIONS	76
REFERENCES		79
APPENDIX A		81
APPENDIX B		84
APPENDIX C		88

## LIST OF FIGURES

Figure		Page
1.1	A six-port circuit as proposed by Engen.	2
1.2	Block diagram of dual six-port (Sperry Research Center).	4
1.3	Proposed MDL six-port configuration.	5
2.1	A directional coupler scheme employed to measure reflection coefficient.	7
2.2	Network analyzer set-up for the measurement of complex reflection coefficient.	8
2.3	Detector, source and load port arrangement.	9
2.4	Locus of $\Gamma_{\ell}$ when only two detector power measurements are used.	11
2.5	Loci of $\Gamma_{\ell}$ with three detector power measurements.	11
2.6	Loci of $\Gamma_{\ell}$ with four detector power measurements.	12
2.7	Six-port configuration.	16
2.8	Illustration of the q-point distribution for the circuit of figure 2.7.	17
3.1	Six-port configuration using a directional coupler and symmetric five-port junction.	20
3.2	A matched symmetric stripline five-port junction.	26
3.3	Circuit diagram of five-port junction.	27
3.4	Even-mode "half-circuit" of five-port junction.	28
3.5	Stripline symmetric five-port junction.	32
3.6	Insertion loss between ports 1-3, 1-4, 2-5, 2-4 and 3-5.	33

		Page
3.7	Insertion loss between ports 2-3, 4-3, 4-5, 1-5 and 1-2.	34
3.8	Results of return loss measurements at ports 1, 2, 3, 4 and 5 of the five-port junction.	35
4.1	Schematic representation of the six-port measurement system.	39
4.2	Phase distribution of reflection standards used.	42
4.3	Flow chart of software for setting system frequency.	42
5.1	Variable reflection standard.	58
5.2	Plot of reflection coefficient with varying stub length.	62
5.3	Variation of $Z/\rho_z$ with frequency (MHZ).	66
5.4	Variation of $X_1/\rho_{x1}$ with frequency (MHZ).	67
5.5	Variation of $X_2/\rho_{x2}$ with frequency	68
5.6	Variation of $X_3/\rho_{x2}$ with frequency (MHZ).	69
5.7	Plot of $\Gamma_\ell$ with frequency.	72
5.8	Plot of $\Gamma_\ell$ with change in frequency.	74

## LIST OF TABLES

5.1	Six-Port Calibration Constants at 1GHZ	55
5.2	Return Loss Measurement Results	57
5.3	Measurement of $\Gamma_{\ell}$ at 1GHZ	61
5.4	Calibration Constants over a 220 MHZ Bandwidth	65
5.5	Results of $\Gamma_{\ell}$ over (900-1100) MHZ	71
5.6	Results of $\Gamma_{\ell}$ over (900-1100) MHZ	75

## CHAPTER I

### INTRODUCTION

#### 1.1 Background

Almost twelve years ago, Hoer and Engen at the National Bureau of Standards (NBS) began to investigate the six-port junction as the heart of a simpler and less expensive network analyzer [1, 2]. Since then there has been considerable work in the analysis, design, and testing of six-port systems [3]. The application of automation to the field of microwave measurements is perhaps best illustrated by the automated network analyzer (ANA). The large reduction in measurement time and in operator effort which it provides are well known. Although techniques for measuring complex microwave impedance, scattering coefficients, etc., have been known since the inception of the art, until the advent of the ANA much of the subject of microwave measurements was focussed on the more easily determined scalar parameters such as power, attenuation and voltage standing wave ratio. In the absence of phase information, it was necessary to determine "worst case" limits for certain phase interactions which were labelled "mismatch errors." Prior to the introduction of the ANA, the key to improved measurement accuracy was often an improved hardware item, e.g., a directional coupler of higher directivity. Eventually it was recognized that the hardware would always be imperfect and the emphasis was shifted to methods for measuring these imperfections and correcting them [4]. In the existing ANA the phase information is obtained with a heterodyne detection system which requires multiple frequency conversions, local oscillators, phase detectors, etc. The need

for a costly and complex heterodyne system has been eliminated in the proposed six-port system where simple amplitude detectors are used for determining the complex reflection coefficient.

## 1.2 Review of Existing Six-Port Systems

Extensive work towards realizing a six-port system has been done in the U.S.A. at the National Bureau of Standards (NBS), the Sperry Research Center and Microwave Development Laboratory (MDL). In 1977 Glenn F. Engen working at NBS proposed one of the first six-port circuits [5]. The basic configuration of the six-port circuit is shown in figure 1.1.

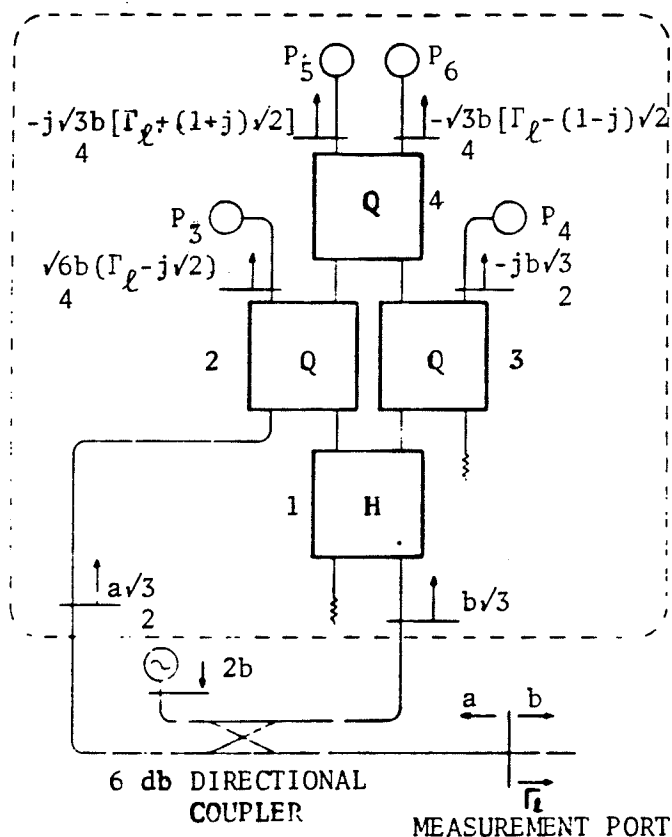


Figure 1.1 A six-port circuit as proposed by Engen [5]

It consists of three quadrature hybrids and one  $180^\circ$  hybrid plus a 6dB directional coupler. The emergent and incoming wave amplitudes at the measurement ports of this circuit are designated by 'b' and 'a', respectively. The wave amplitudes at other selected positions in the circuit are shown in figure 1.1.

The ideal performance of the six-port is dependent on a set of complex parameters called q-parameters. These q-parameters shall be discussed in depth and presented in Chapter II. At this stage it will suffice to know that for an ideal q-distribution the magnitudes of the q values should lie in the neighbourhood of 0.5 or 1.5 and their arguments should differ by about  $\pm 120^\circ$ . Although the NBS circuit fails to achieve the design objectives for the ideal q-point distribution it however is closer to the design goals than any other six-port devised until then. As compared with the  $\pm 120^\circ$  objective, the differences in the angles are  $135^\circ$ ,  $90^\circ$  and  $-135^\circ$ , respectively, with the magnitudes of the q's being 2, 2 and  $\sqrt{2}$  respectively.

Harry M. Cronson and Leon Susman [37], working at Sperry Research Center (SRC) extended the work done at NBS and developed a dual six-port system. The dual six-port is capable of measuring transmission coefficients in addition to reflection coefficients. The six-port junction used by Cronson and Susman is shown in figure 1.2 and consists of four quadrature hybrids and two power dividers. The SRC six-port is similar to the one used by Engen at NBS and the q-distribution is no closer to the design objective than that achieved by Engen at NBS.

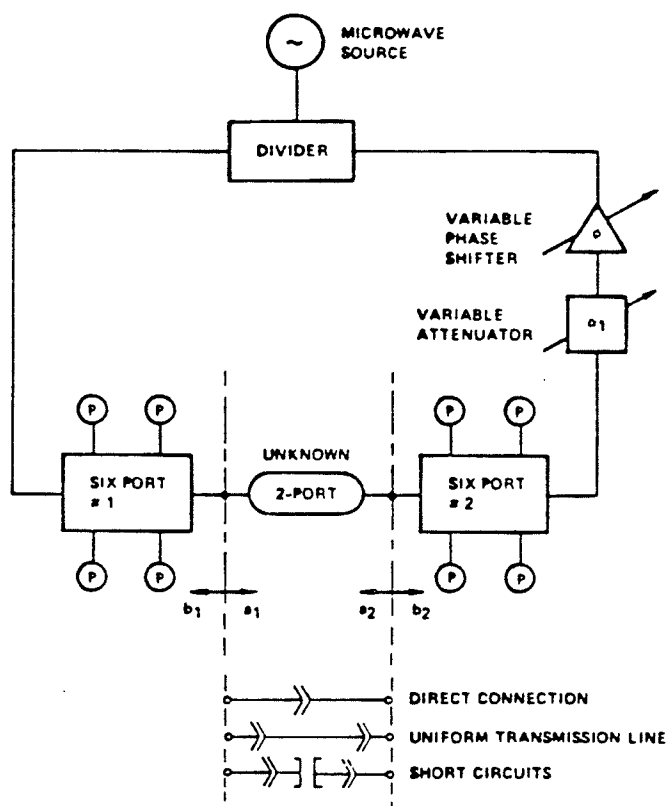


Figure 1.2 Block diagram of dual six-port (Sperry Research Center)

Till recent years the major thrust of published research has been towards developing the dual six-port system with the six-port itself consisting of quadrature hybrids and  $180^\circ$  hybrids. It was only in 1981 that Gordon P. Riblet and E.R. Bertil Hansson, working at the Microwave Development Laboratories (MDL), proposed a six-port circuit consisting of a symmetric five-port junction and a directional coupler [67]. With this circuit configuration they could achieve the ideal q-point distribution. The design details of their five-port junction has not been disclosed and their proposed six-port configuration is shown in figure 1.3.

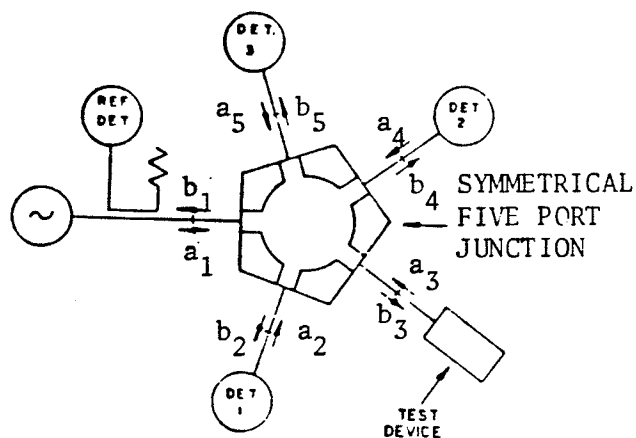


Figure 1.3 Proposed MDL six-port configuration.

This was the first six-port circuit of this kind to be realized without using hybrids. Based on the concept of the symmetric five-port junction developed at MDL our six-port also consists of a symmetric five-port junction, the design details of which are given in Chapter III.

The purpose of this thesis is to design, implement and test a single six-port system for the measurement of complex reflection coefficient. In Chapter II the six-port theory is presented defining the  $q$ -parameters and determining the ideal  $q$ -point distribution. In Chapter III the design of a six-port junction is covered and the performance results of the junction is presented. In Chapter IV the operation of the six-port measurement system is explained and the closed form expressions for the calibration constants determined. Finally, in Chapter V measurement results of return loss, complex reflection coefficient at 1GHZ and over a 200 MHZ band width are compared with theoretical results and also with values obtained from a commercial network analyzer instrument.

## CHAPTER II

### SIX-PORT THEORY

#### 2.1 The Four Port Reflectometer

The scattering parameters for a multiport network are defined as the ratio of the outgoing to the incoming wave variables. We have at the  $m$ 'th port the scattering coefficient  $S_{mn}$  which relates the outgoing wave  $b_m$  at the  $m$ 'th port to the power wave entering the  $n$ 'th port, expressed as

$$S_{mn} = \left. \frac{b_m}{a_n} \right| a_i = 0 \quad (i \neq n) \quad (2.1)$$

Thus, the evaluation of  $S_{mn}$  involves obtaining the ratio of two complex quantities,  $b_m$  and  $a_n$ . Network analyzers are designed so that they process signals which are proportional to  $b_m$  and  $a_n$ , in order to determine their complex ratio. Usually,  $a_m$ ,  $b_n$ , etc., cannot be measured right at their port locations, but are sampled with the help of a linear measurement network, e.g., a directional coupler circuit as shown in figure 2.1. Ports 1 and 2 in this circuit are the source and load ports, respectively, while ports 3 and 4 provide the measurement signals. The power waves emerging at ports 3 and 4 are given by [7, 8]

$$b_3 = Aa_2 + Bb_2 \quad (2.2)$$

$$b_4 = Ca_2 + Db_2 \quad (2.3)$$

where A, B, C, and D are the complex constants of the directional coupler circuit. The factors A and B give the fraction of the reflected and incident load port waves, respectively, coupled to port 3. Similarly C and

D give the fraction of the reflected and incident load port waves, respectively, coupled to port 4.

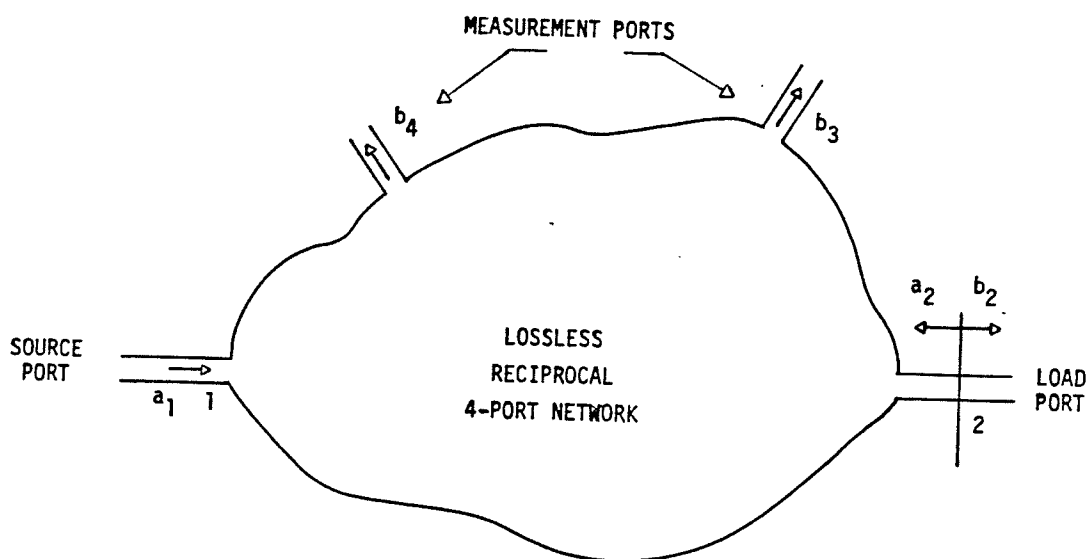


Fig. 2.1 A directional coupler scheme employed to measure reflection coefficient

In the practical four-port network analyzer A and D are made as close to zero as possible so that the measured waves  $b_3$  and  $b_4$  are essentially proportional to  $b_2$  and  $a_2$ , respectively. The basic set-up for such a microwave network analyzer utilizes a dual-directional coupler and is illustrated in figure 2.2. The constants B and C can be determined by applying standard loads to the load port. After having calibrated the system the ratio of  $a_2$  to  $b_2$  (reflection coefficient) for a given load can then be determined.

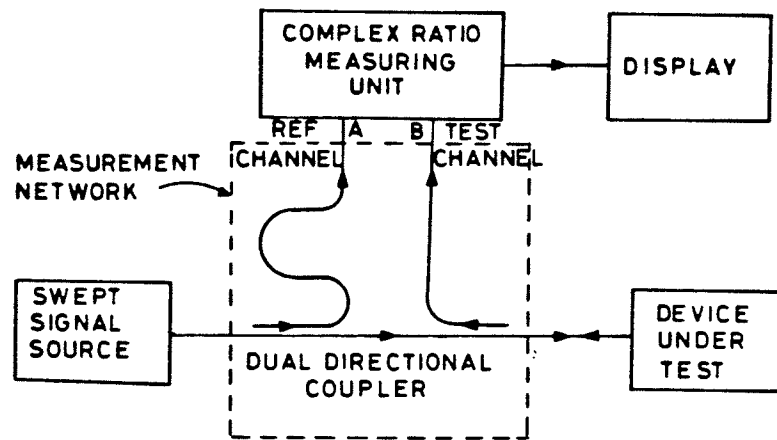


Fig. 2.2 Network analyser set-up for the measurement of complex reflection coefficient

If both the reflection coefficient magnitude and phase is required then frequency conversion is necessary in order to measure both the relative magnitude and the phase difference between  $b_3$  and  $b_4$ . If only the magnitude of the ratio of  $b_3$  to  $b_4$  is required only simple power detectors need be used. In present network analyzer systems the key signal operation is then the conversion of the test and reference signals to a lower frequency for the measurement of phase difference. This frequency conversion complicates the design of network analyzers and makes their cost high. It is possible, however, to eliminate the need for heterodyning by the addition of two more measurement ports, which makes the intervening four port network into a six-port.

## 2.2 The Six-Port Network

The configuration for the six-port circuit is shown in figure 2.3. The four measurement ports are terminated with power detectors. The power delivered to each of the detectors of the six-port is given by

$$P_3 = |Aa_2 + Bb_2|^2 \quad (2.4)$$

$$P_4 = |Ca_2 + Db_2|^2 \quad (2.5)$$

$$P_5 = |Ea_2 + Fb_2|^2 \quad (2.6)$$

$$P_6 = |Ga_2 + Hb_2|^2 \quad (2.7)$$

where A to H are complex constants determined by the properties of the six-port network.

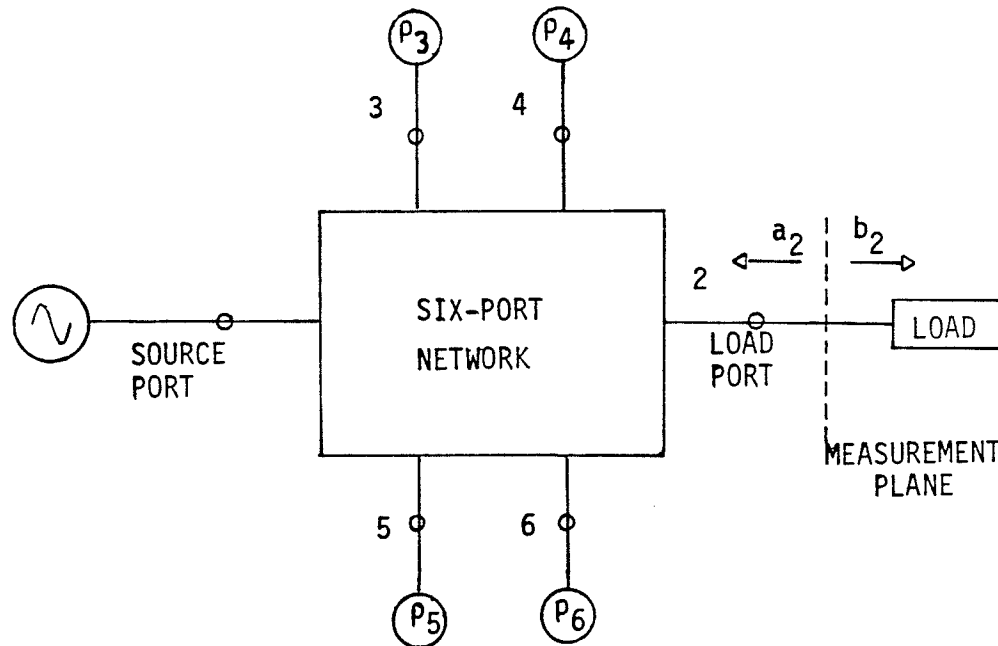


Fig. 2.3 Detector, source and load port arrangement of a six-port circuit.

In this six-port system one of the four measurement ports is essentially used only to monitor the input power. This has been selected to be port 4 and in practice, using nearly ideal components, it is possible to force the first term in equation (2.5) to zero. Thus we have  $C = 0$ , and (2.5) reduces to

$$P_4 = |D|^2 |b_2|^2 \quad (2.8)$$

Taking the ratios of several of the constants A to H we define a new set of parameters, called the q-parameters. These are,

$$q_3 = -B/A, \quad q_5 = -F/E, \quad q_6 = -H/G.$$

Appropriately substituting the above into (2.4), (2.6) and (2.7) and recognizing that  $\Gamma_\ell = a_2 / b_2$ , we obtain

$$P_3 = |A|^2 |b_2|^2 |\Gamma_\ell - q_3|^2 \quad (2.9)$$

$$P_5 = |E|^2 |b_2|^2 |\Gamma_\ell - q_5|^2 \quad (2.10)$$

$$P_6 = |G|^2 |b_2|^2 |\Gamma_\ell - q_6|^2. \quad (2.11)$$

Using (2.8) to eliminate  $|b_2|^2$  in these equations gives

$$|\Gamma_\ell - q_3|^2 = |D/A|^2 \times P_3/P_4 \quad (2.12)$$

$$|\Gamma_\ell - q_5|^2 = |D/E|^2 \times P_5/P_4 \quad (2.13)$$

$$|\Gamma_\ell - q_6|^2 = |D/G|^2 \times P_6/P_4 \quad (2.14)$$

In particular, let us examine (2.12). Given only two measurement results,  $P_3$  and  $P_4$ , and assuming  $q_3$  and  $|D/A|^2$  as known, the locus of possible values of  $\Gamma_\ell$  must lie on a circle with center at  $q_3$  and radius  $|\Gamma_\ell - q_3|$

as shown in figure 2.4. Similarly, assuming  $P_5$ ,  $q_5$  and  $|D/E|^2$  to be known, the locus of  $\Gamma_\ell$  in order to satisfy (2.13) is shown in figure 2.5.

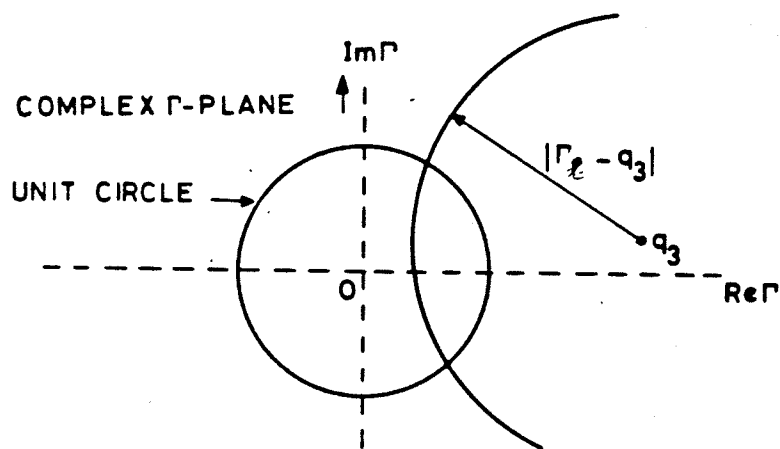


Fig. 2.4 Locus of  $\Gamma_\ell$  when only two detector power measurements are used

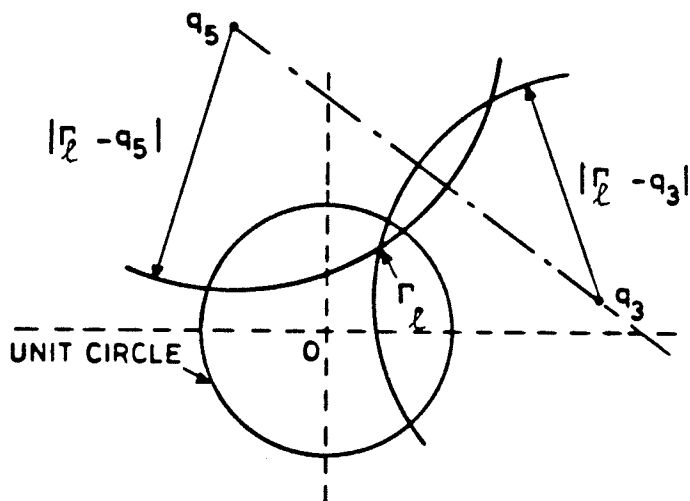


Fig. 2.5 Loci of  $\Gamma_\ell$  with three detector power measurements

Here, only two possible  $\Gamma_\ell$  values can satisfy both (2.12) and (2.13) and are given by the intersection points of the two circles. In figure 2.5 one of the intersection points falls outside the  $|\Gamma_\ell| = 1$  circle and we are able to choose between the two solutions on the basis that for passive networks  $|\Gamma_\ell| \leq 1$ . If both points of intersection happen to fall inside the  $|\Gamma_\ell| = 1$  circle, then it is clear that the reflection coefficient can not be determined unambiguously. However, the addition of a fourth power measurement results in an explicitly determined reflection coefficient. Assuming  $P_6$ ,  $q_6$  and  $|D/G|^2$  to be known a third circle can be drawn using (2.14) with center at  $q_6$  and radius  $|\Gamma_\ell - q_6|^2$  upon which  $\Gamma_\ell$  must lie. This situation is shown in figure 2.6.

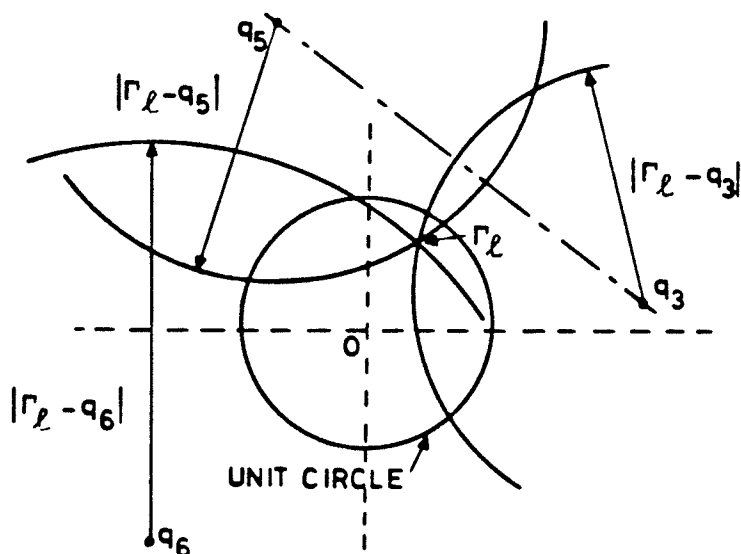


Fig. 2.6 Loci of  $\Gamma_\ell$  with four detector power measurements

For the typical q-point distribution used  $\Gamma_L$  is then determined unambiguously from the intersection of the three circles.

From inspection of (2.8) to (2.11) it is evident that  $|D|$ ,  $|A|$ ,  $|E|$  and  $|G|$  are scale factors, which for a given input signal level and depending upon the load at the output port determine the range of the power level at a measurement port. The dynamic range of the power measuring instrument determines the scale factors  $|A|$ ,  $|E|$ ,  $|G|$  and  $|D|$ . If, for instance bolometric-type power meters are assumed then the typical performance specifications might include an upper power limit of 10 mW. Hence, the values of  $|A|$ ,  $|E|$ ,  $|G|$  and  $|D|$  are chosen such that the 10 mW limit may not be exceeded for all possible values of  $\Gamma_L$  where  $|\Gamma_L| \leq 1$ .

It is in addition important to know what the optimum q-point distribution of the six-port circuit should be. A major design question centers around the choice of  $q_3$ ,  $q_5$ , and  $q_6$  and this shall be presented in the next section.

### 2.3 Ideal q-point distribution.

A rigorous mathematical proof for the ideal q-point distribution has not been undertaken and only a qualitative discussion followed closely along the lines provided by Engen [7] is presented. A typical q-point distribution is shown in figure 2.6. However, it is appropriate to question if a better choice would be to place one of the q's, say  $q_3$  at the centre of the unit circle? If this is done, one has a response ( $P_4$ ) which measures the incident wave ( $|b_2|$ ) while  $P_3$  now measures the reflected wave ( $|a_2|$ ). In this case the six-port incorporates the reflectometer.

There are several considerations, however, which argue against this choice for  $q_3$ . Assuming one could obtain the condition  $q_3 = 0$ , the prospect of achieving a direct measure of the reflection coefficient magnitude is indeed attractive. In actual fact, in the current state of the art, and even with this as a design goal, the expected deviations of  $q_3$  from zero are such as to largely negate the potential advantages. A more serious objection arises from dynamic range versus measurement precision considerations. This point is perhaps best illustrated by a specific example as given by Engen [7]:

In figure 2.6 let  $q_3$  be moved to the center of the diagram, let  $q_5=2$ , and  $q_6 = j2$ . Bolometric-type power meters will be assumed, for which typical performance specifications include upper power limit of 10mW and error 0.1 percent  $\pm 1 \mu\text{W}$ . Next, the values of  $|A|$ ,  $|E|$ ,  $|G|$  and  $|D|$  are so chosen that the 10-mW limit may be approached (but not exceeded) for all possible values of  $\Gamma_\ell$ , where  $|\Gamma_\ell| \leq 1$ . If one wishes to measure a termination for which  $|\Gamma_\ell| \approx 0.01$  (matched),  $P_3$  will be approximately  $1\mu\text{W}$ , thus the signal-to-noise ratio for this detector has dropped to unity. By contrast  $P_5$  and  $P_6$  will be operating at approximately 5mW, and the 0.1 percent will be the dominating error term. Since this applies to power, the error in  $|\Gamma_\ell - q_5|$  and  $|\Gamma_\ell - q_6|$  will be half of this. On the other hand, the nominal value of  $|\Gamma_\ell - q_5|$  or  $|\Gamma_\ell - q_6|$  in this example is 2, so that the uncertainty in the real and imaginary parts of a value of  $\Gamma_\ell$  in the neighborhood of the origin represents a 10% error. The interesting conclusion is that if one requires operation over the entire range of  $|\Gamma_\ell|$ , a point in the neighborhood of the origin should not be chosen. It is seen that the response of  $P_3$  contributes little or nothing to the determination of  $\Gamma_\ell$  when  $|\Gamma_\ell|$  is small, and it appears that a better

choice of  $q_3$  would be a value in the neighborhood of that shown in figure 2.6. Although the foregoing arguments do not necessarily hold for all choices of power meters, they do appear valid for the immediate candidates which include the bolometric and diode types.

Having disposed of the question of placing one of the  $q$ 's at the center of the unit circle, it now appears, from symmetry considerations, that  $q_3$ ,  $q_5$  and  $q_6$  should be located at the vertices of an equilateral triangle whose center is at the origin. This calls for  $|q_6| = |q_5| = |q_3|$ , while the arguments differ by  $\pm 120^\circ$ . Thus, the only remaining choice is the magnitude of  $|q_3|$ . It is unreasonable to choose a large value for  $|q_3|$ . In particular, since  $\Gamma_\ell$  is determined from its distances from  $q_3$ ,  $q_5$  and  $q_6$ , it is evident that an ill-conditioned situation will result if these distances become large in comparison with the distances between  $q_3$  and  $q_5$ ,  $q_3$  and  $q_6$ , or  $q_5$  and  $q_6$ . On the basis of these considerations, it appears that an optimum value for  $|q_3|$  might be expected to lie in the range 0.5-1.5. An experimental study with the aid of a computer done at NBS shows a decrease in the measurement accuracy when  $|\Gamma_\ell| \approx |q_3|$ . Since there is usually a substantial interest in values of  $\Gamma_\ell$  with a nominal magnitude of unity, there is a double reason for avoiding  $|q_3| \approx 1$ . Apart from values close to unity, the other region of primary interest is  $|\Gamma_\ell| < 0.3$ . In order to provide the largest possible bandwidth, a fairly loose tolerance on the performance of the individual components from which the six-port is constructed is desirable. This, now reduces the choice for  $|q_3|$  to values in the neighborhood of 0.5 or 1.5.

Now, having determined as to what the ideal  $q$ -point distribution should be it is of interest to find the  $q$  distribution of the six-port proposed by Engen, which has already been briefly touched upon in the



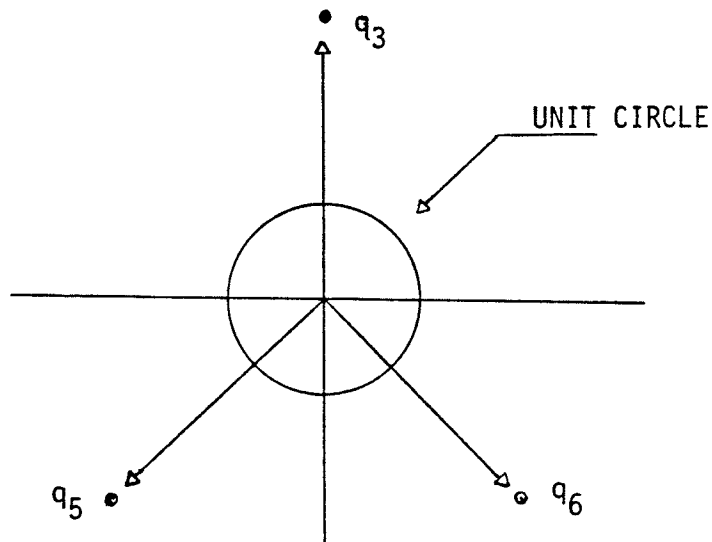


Fig. 2.8 Illustration of the q-point distribution for the circuit of Fig. 2.7

$b/\sqrt{3}$  as the incident power wave at the input to the hybrid 1. This hybrid, being an in-phase equal power divider, delivers  $\frac{b\sqrt{3}}{\sqrt{2}}$  to one of the inputs of quad 2. The other input to quad 2 being  $\frac{a\sqrt{3}}{2}$ . Thus the output of quad 2 is

$$\frac{j \frac{a\sqrt{3}}{2\sqrt{2}} - j \frac{b\sqrt{3}}{(\sqrt{2})(\sqrt{2})}} = \frac{\sqrt{6}}{4} (\Gamma_{\ell} - j\sqrt{2}) \quad (2.15)$$

where  $\Gamma_{\ell} = a_2 / b_2$

Hence  $P_3$  is given by

$$P_3 \propto \left(\frac{\sqrt{6}}{4}\right)^2 |b|^2 (\Gamma_{\ell} - j\sqrt{2})^2 \quad (2.16)$$

comparing (2.16) with (2.9) we have

$$q_3 = j\sqrt{2} \quad (2.17)$$

Thus,  $q_3$  has a magnitude of  $\sqrt{2}$  and the argument equals  $+90^\circ$ . In a similar manner we can determine  $q_5$  as  $\sqrt{2} \angle -135^\circ$  and  $q_6$  as  $2 \angle -45^\circ$  for this circuit with the distribution shown in figure 2.8. As a variant to the circuit configuration of figure 2.7, one may replace the 6dB directional coupler with a 3dB coupler. If this is done, the power level at the measurement port is doubled, but at the expense of the power levels at  $P_3 \dots P_6$ . In addition, the  $q$  magnitudes are multiplied by  $1/\sqrt{2}$ . Apart from a constant multiplier, the  $q$ -values are determined entirely by that portion of the circuit enclosed within the dotted lines in figure 2.7. Having determined the  $q$ -point distribution it is possible to obtain a visual display of the reflection coefficient on the oscilloscope [9]. For the circuit of figure 2.7 it has been shown that the powers  $P_3, P_4, P_5, P_6$  are proportional to  $|b(\Gamma_\ell - j\sqrt{2})|^2$ ,  $|b|^2$ ,  $|b(\Gamma_\ell + (1+j)\sqrt{2})|^2$  and  $|b(\Gamma_\ell - (1-j)\sqrt{2})|^2$ , respectively. In addition to obtaining an expression for  $\Gamma_\ell$  it is possible to get a real time display on the oscilloscope. The foregoing represents a straightforward and useful solution to the problem when measurement accuracy can be traded for computational simplicity. In order to make accurate measurements the  $q$ 's and the complex constants  $A, E, G$  and  $D$  have to be determined. An attempt to obtain  $A, E, G$  and  $D$  directly by using (2.8) - (2.11) results in numerical singularities [10]. However, using a calibration procedure which will be described in chapter four, the calibration constants are determined explicitly. Before proceeding to determine these constants, the design of the six-port systems which we have used is first presented, along with some performance results in the following chapter.

CHAPTER III  
THE SIX-PORT SYSTEM

### 3.1 Introduction

A six-port network using a symmetric five-port junction and a directional coupler has been designed to operate at a center frequency of 1 GHz. In section 3.2 the properties of the five-port junction is briefly studied and an expression for the complex reflection coefficient, assuming an ideal junction, is derived. In section 3.3 it is shown that the five-port junction is well matched at 1 GHz. Finally, in the concluding section the performance of the five-port obtained from measurements with a Hewlett-Packard model 8410S network analyzer system, is presented.

### 3.2 The Symmetric Five-Port Junction

The six-port configuration using a directional coupler and symmetric five-port junction is shown in figure 3.1. For a reciprocal junction, the junction scattering matrix  $[S]$  is symmetric so that  $S_{ij} = S_{ji}$ . Also, since the junction is completely matched we have  $S_{ii} = 0$  for  $i = 1 \dots 5$ . Employing these conditions, the scattering matrix for the five-port is written as

$$[S] = \begin{bmatrix} 0 & S_{12} & S_{13} & S_{14} & S_{15} \\ S_{12} & 0 & S_{23} & S_{24} & S_{25} \\ S_{13} & S_{23} & 0 & S_{34} & S_{35} \\ S_{14} & S_{24} & S_{34} & 0 & S_{45} \\ S_{15} & S_{25} & S_{35} & S_{45} & 0 \end{bmatrix} \quad (3.1)$$

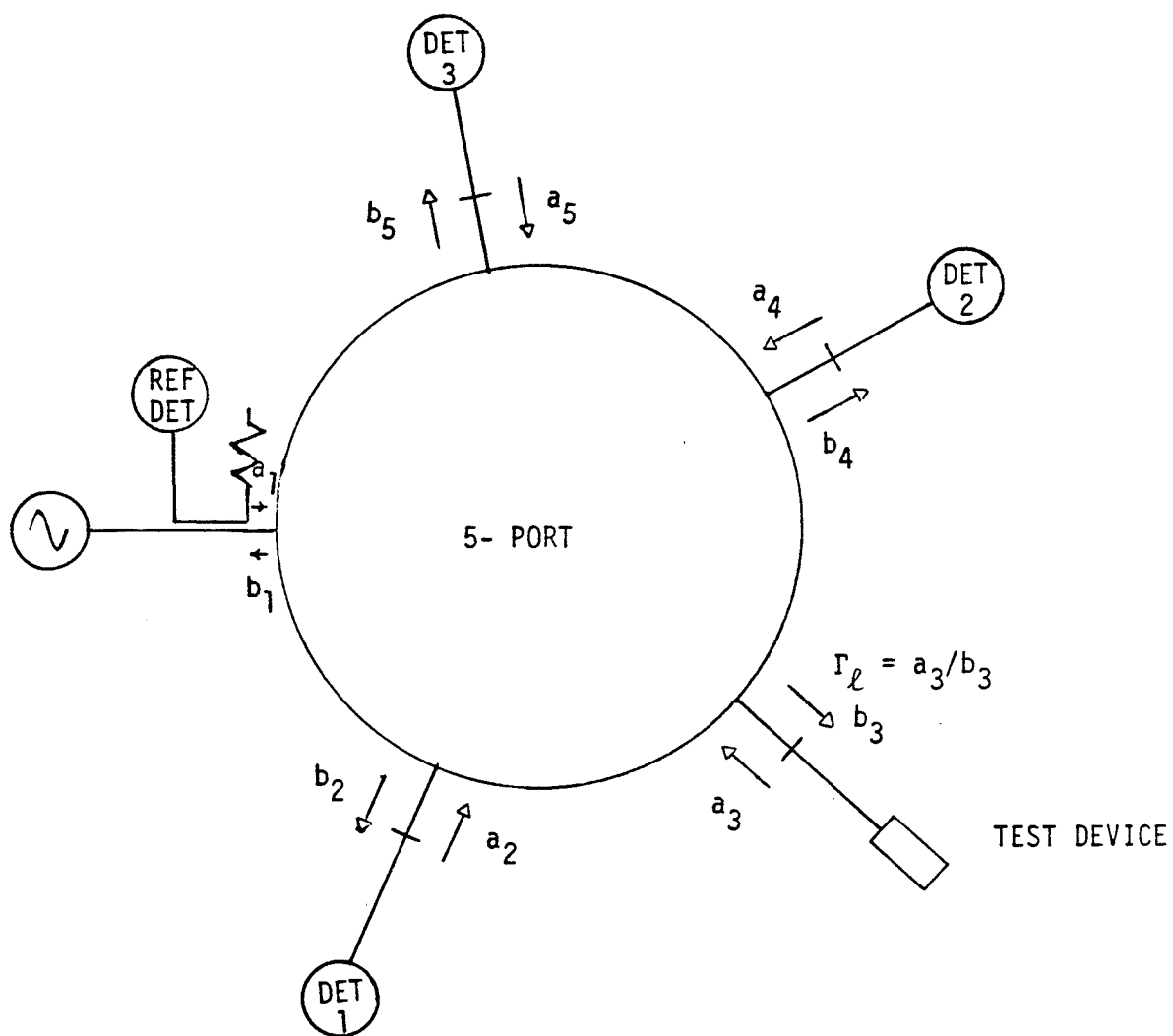


Fig. 3.1 Six-port configuration using a directional coupler and symmetric five-port junction.

Since the five-port junction is a lossless, reciprocal network the scattering matrix unitary property [1] must hold and

$$S^* S = 1.$$

From the junction symmetry the remaining scattering coefficients can only assume one of two possible values, thus

$$a = S_{12} = S_{23} = S_{34} = S_{45} = S_{15}$$

and

$$b = S_{13} = S_{25} = S_{35} = S_{24} = S_{14}$$

If the unitary condition is applied we get

$$\begin{bmatrix} 0 & a^* & b^* & b^* & a^* \\ a^* & 0 & a^* & b^* & b^* \\ b^* & a^* & 0 & a^* & b^* \\ b^* & b^* & a^* & 0 & a^* \\ a^* & b^* & b^* & a^* & 0 \end{bmatrix} \times \begin{bmatrix} 0 & a & b & b & a \\ a & 0 & a & b & b \\ b & a & 0 & a & b \\ b & b & a & 0 & a \\ a & b & b & a & 0 \end{bmatrix}$$

$$= \begin{bmatrix} 1 & 0 & 0 & 0 & 0 \\ 0 & 1 & 0 & 0 & 0 \\ 0 & 0 & 1 & 0 & 0 \\ 0 & 0 & 0 & 1 & 0 \\ 0 & 0 & 0 & 0 & 0 \end{bmatrix} \quad (3.2)$$

Equation (3.2) yields

$$2 | a |^2 + 2 | b |^2 = 1 \quad (3.3)$$

$$b^* a^* + a^* b + | b |^2 = 0 \quad (3.4)$$

$$b^* a + a^* b + | a |^2 = 0 \quad (3.5)$$

Subtracting (3.5) from (3.4) we get

$$| a | = | b | \quad (3.6)$$

Substitution of (3.6) into (3.3) shows that

$$\begin{aligned} | b |^2 = | a |^2 &= 1/4 \\ \text{or } | a | = | b | &= 1/2 \end{aligned} \quad (3.7)$$

If we select port reference planes so that

$$a = | a |$$

then (3.4) becomes

$$\begin{aligned} 1/2(b^* + b) + 1/4 &= 0 \\ \text{or } b^* + b &= -1/2 \end{aligned} \quad (3.8)$$

Let  $b = x + jy$ , then (3.8) becomes

$$\begin{aligned} x - jy + x + jy &= -1/2 \\ \text{or } x &= -1/4 \end{aligned}$$

Now, using the result and (3.7) we can write

$$\begin{aligned} | b |^2 &= 1/4 \\ x^2 + y^2 &= 1/4 \end{aligned}$$

$$y^2 = 1/4 - 1/16$$

$$y = \pm \frac{\sqrt{3}}{4} \quad (3.9)$$

Therefore

$$b = -1/4 \pm j \frac{\sqrt{3}}{4} = 1/4(-1 \pm j \sqrt{3}) = 1/2 \angle \pm 120^\circ \quad (3.10)$$

Having determined the S - parameters it can be readily seen that the incident power wave at each detector in the circuit of figure 3.1 can be evaluated. From the power readings for a matched load at the test port and assuming matched detectors, the q-point distribution can be obtained. Knowing the q-parameters it is possible to obtain an expression in terms of the detector power readings for the complex reflection coefficient for any test port load, suitable for visual display. The incoming and outgoing power waves at the various ports are labelled in figure 3.1 and are related to each other through the five-port junction scattering matrix. Assuming matched detectors we have

$$\begin{bmatrix} b_1 \\ b_2 \\ b_3 \\ b_4 \\ b_5 \end{bmatrix} = \begin{bmatrix} 0 & S_{12} & S_{13} & S_{13} & S_{13} \\ S_{12} & 0 & S_{12} & S_{13} & S_{13} \\ S_{13} & S_{12} & 0 & S_{12} & S_{13} \\ S_{13} & S_{13} & S_{12} & 0 & S_{12} \\ S_{12} & S_{13} & S_{13} & S_{12} & 0 \end{bmatrix} \begin{bmatrix} a_1 \\ 0 \\ a_3 \\ 0 \\ 0 \end{bmatrix} \quad (3.11)$$

From (3.11) we get

$$b_1 = S_{13} a_3 \quad (3.12)$$

$$b_2 = S_{12}a_1 + S_{12}a_3 \quad (3.13)$$

$$b_3 = S_{13}a_1 \quad (3.14)$$

$$b_4 = S_{13}a_1 + S_{12}a_3 \quad (3.15)$$

$$b_5 = S_{12}a_1 + S_{13}a_3 \quad (3.16)$$

The power delivered to each of the three detectors (refer to figure 3.1),  $P_1$ ,  $P_2$  and  $P_3$ , is proportional to  $|b_2|^2$ ,  $|b_4|^2$  and  $|b_5|^2$ , respectively.

Hence

$$\begin{aligned} P_1 \propto |b_2|^2 &= \left| S_{12}a_1 + \frac{S_{12}}{S_{13}} b_3 \right|^2 \\ &= |S_{12}|^2 |b_3|^2 \left| \Gamma_L - (-1/S_{13}) \right|^2 \end{aligned} \quad (3.17)$$

$$\begin{aligned} P_2 \propto |b_4|^2 &= |S_{12}a_3 + b_3|^2 \\ &= |S_{12}|^2 |b_3|^2 \left| \Gamma_L - (-1/S_{12}) \right|^2 \end{aligned} \quad (3.18)$$

$$\begin{aligned} P_3 \propto |b_5|^2 &= \left| S_{13}a_3 + \frac{S_{12}b_3}{S_{13}} \right|^2 \\ &= |S_{13}|^2 |b_3|^2 \left| \Gamma_L \frac{(-S_{12})}{(S_{13})^2} \right|^2 \end{aligned} \quad (3.19)$$

Comparing equations (3.17) - (3.19) with (2.9) - (2.11) shows that

$$q_1 = -1/S_{13}, \quad q_2 = -1/S_{12} \quad \text{and} \quad q_3 = -S_{12}/(S_{13})^2 \quad (3.20)$$

Since,  $|S_{12}| = |S_{13}| = 1/2$ , from (3.7) we get

$$|q_1| = |q_2| = |q_3| = 2 \quad (3.21)$$

We thus have  $|q's|$  in the neighborhood of 1.5 which as suggested by Engels [7] is an optimum value. Using (3.10) and (3.20) the arguments of the  $q's$  are

$$q_1 = q_2 - 2\pi/3 \quad (3.22)$$

$$q_3 = q_2 + 2\pi/3 \quad (3.23)$$

Substituting these  $q$  values in (3.17) - (3.19) we obtain the power readings  $P_1$ ,  $P_2$  and  $P_3$  as proportional to  $|S_{12}|^2 |b_3|^2 |\Gamma_\ell - q_1|^2$ ,  $|S_{12}|^2 |b_3|^2 |\Gamma_\ell - q_2|^2$  and  $|S_{13}|^2 |b_3|^2 |\Gamma_\ell - q_3|^2$ , respectively. The reference detector measures the input power  $P_R$  to the junction. Using (3.14) we may write

$$P_R = |a_1|^2 = \frac{|b_3|^2}{|S_{13}|^2} \quad (3.24)$$

From the four power readings  $\Gamma_\ell$  can be easily determined. It is vital to note at this point that the reflection coefficient so determined is only approximate since the properties of an ideal six-port have been assumed and this is difficult to realize in practice. Hence, the system needs to be calibrated in a more exacting manner and the resulting calibration coefficients can then be used to determine  $\Gamma_\ell$ . A procedure for a calibration process is given in the next chapter.

### 3.3 Design of the five-port junction

The five-port junction is shown in figure 3.2. It has been realized by using a ring type structure along with five radial short-circuited stubs. The stubs are spaced a quarter wave length apart and are an

eighth wavelength long and provide matching for the junction. The radial lines for the stubs have a characteristic impedance which is twice that of the transmission lines forming the ring structure. The five-port junction circuit diagram is given in figure 3.3. A brief analysis to obtain design equations for this junction follows:

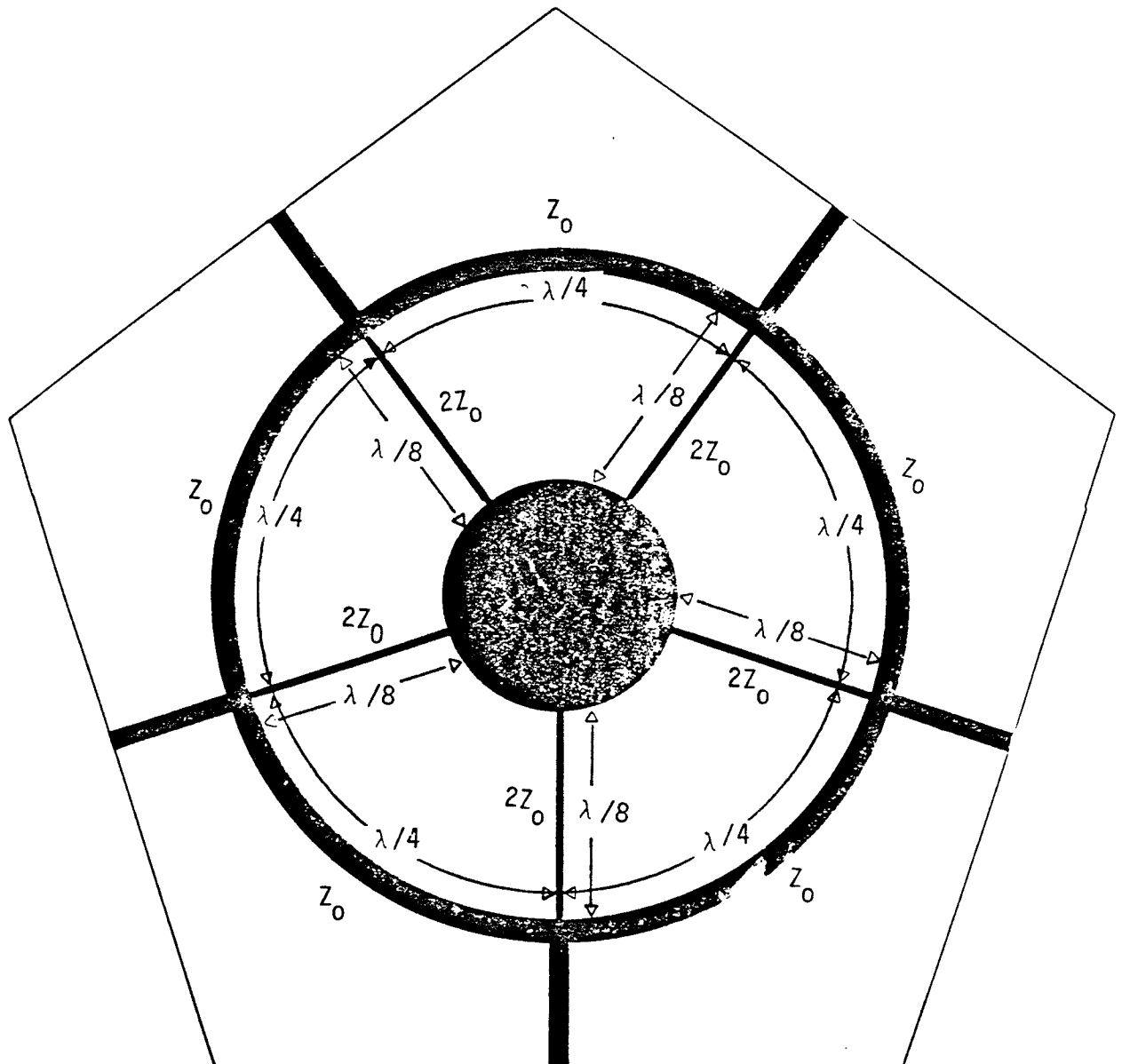


Figure 3.2 A matched symmetric stripline five-port junction

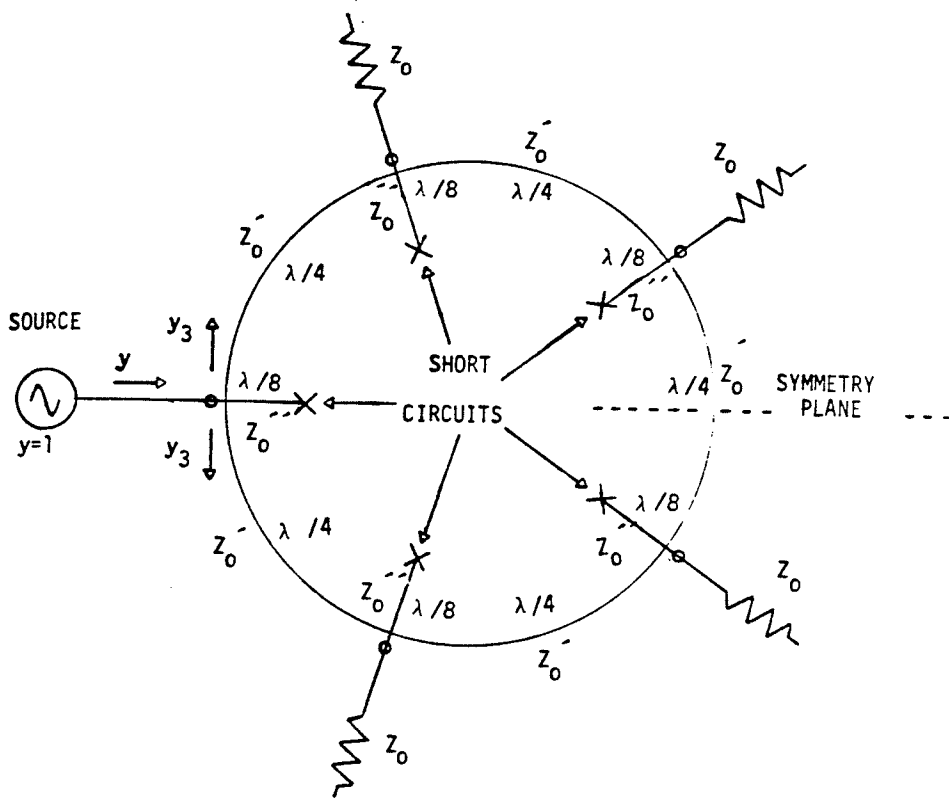


Fig. 3.3 Circuit diagram of five-port junction

In figure 3.3,  $Z_0$  is the characteristic impedance of the generator and load system while  $Z'_0$  and  $Z''_0$  are the characteristic impedances of the  $\lambda/4$  lines and  $\lambda/8$  stub lines, respectively. Application of a signal to port 1 of the junction is equivalent to an even-mode excitation of the network. The even mode "half-circuit" is shown in figure 3.4. The line admittances have been normalized with respect to  $Z_0$  and we have chosen  $Z''_0 = 2Z_0$ ; hence, the normalized line conductances are

$$g_0 = \frac{Z_0}{Z'_0}$$

$$g'_0 = \frac{Z_0}{Z''_0}$$

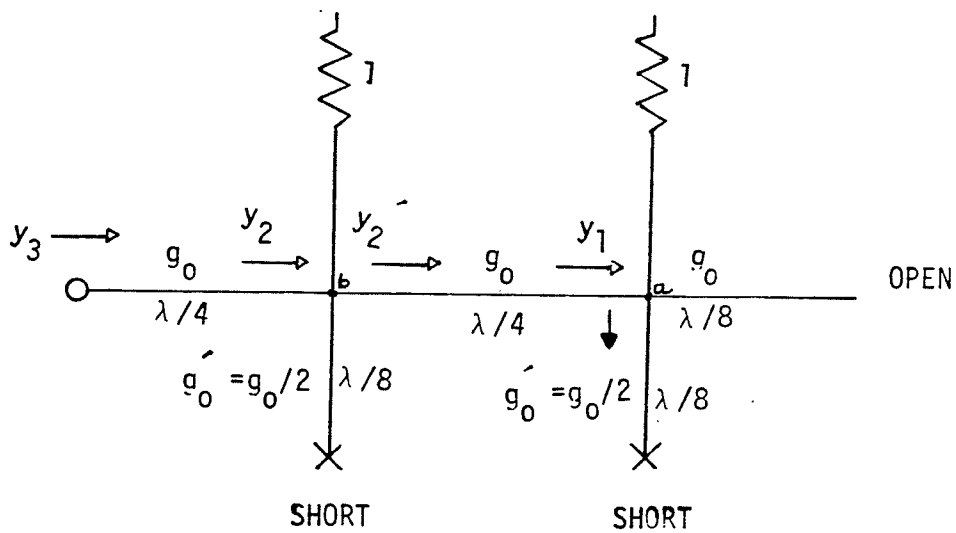


Fig. 3.4 Even-mode "half-circuit" of five-port junction.

The open-circuit terminated line is  $\lambda/8$  in length and has an input admittance  $+jg_0$ , while the  $\lambda/8$  long short-circuit terminated lines all have an input admittance  $-jg_0'$ . We are able to write the equivalent admittance  $y_1$ , at node - @ looking towards the open circuit, as

$$\begin{aligned} y_1 &= 1 + jg_0 - jg_0/2 \\ &= 1 + jg_0/2 \end{aligned} \quad (3.25)$$

The  $\lambda/4$  long line between node - @ and node - @ acts as an impedance transformer and at its input we have

$$Y_2' = g_0^2 / y_1$$

The admittance  $y_2$  at node - @ is

$$\begin{aligned}
 y_2 &= 1 - \frac{jg_0}{2} + \frac{g_0^2}{(1 + jg_0/2)} \\
 &= (1 + 5/4g_0^2) / (1 + jg_0/2)
 \end{aligned} \tag{3.26}$$

Finally, the input admittance  $y_3$  looking into the "half-circuit" is given by

$$\begin{aligned}
 y_3 &= g_0^2 / y_2 \\
 &= g_0^2 (1 + jg_0/2) / (1 + 5/4g_0^2)
 \end{aligned} \tag{3.27}$$

If  $y$  is the admittance of the match terminated five-port as seen from the source (refer to figure 3.3) we are able to write

$$y = 2y_3 - jg_0/2 \tag{3.28}$$

When (3.27) is substituted into (3.26) we obtain

$$\begin{aligned}
 y &= 2g_0^2 (1 + jg_0/2) / (1 + 5/4g_0^2) - jg_0/2 \\
 &= 2g_0^2 / (1 + 5/4g_0^2) + j \left( \frac{g_0^3 - g_0/2}{(1 + 5/4g_0^2)^2} \right)
 \end{aligned} \tag{3.29}$$

Now, in order for the imaginary part of (3.29) to be zero we require that

$$\begin{aligned}
 g_0^2 / (1 - 5/4g_0^2) &= 1/2 \\
 \text{or } g_0 &= 2 / \sqrt{3}
 \end{aligned} \tag{3.30}$$

When (3.30) is placed into (3.29) we find that the conductance part of  $y$  is of unit value. Thus, when (3.30) holds each port of the ideal five-

port circuit is perfectly matched at the design center frequency. From symmetry we see that equal powers are transmitted from port 1 towards port 2 and port 5. To establish that there is also an equal power split between ports 2 and 3 (or ports 4 and 5) we proceed in the following way. Assume a normalized voltage  $v_2$  at node -ⓑ of figure 3.4. A power  $v_2^2$  is then delivered to the unit load at this port. The admittance looking toward node -ⓐ and immediately to the right of node -ⓑ, is obtained by inspection to be

$$\begin{aligned} y_2' &= g_0^2 / (1 + jg_0/2) \\ &= g_0^2 (1 - jg_0/2) / (1 + g_0^2/4) \end{aligned} \quad (3.31)$$

The power delivered to node -ⓐ is given by  $v_2^2 \operatorname{Re} \{y_2'\}$  and clearly we require that  $\operatorname{Re} \{y_2'\}$  be of unit value in order for the power delivered to the unit load at node -ⓐ to be equal to the power delivered to the unit load at node -ⓑ. Hence

$$g_0^2 / (1 + g_0^2/4) = 1 \quad (3.32)$$

For  $g_0 = 2/\sqrt{3}$  this equality holds and the proposed five-port symmetric junction is matched at all ports and it acts as a four way power divider. Specifically, the values of  $Z_0'$  and  $Z_0''$ , when the source and load base characteristic impedance is 50 ohms, are

$$Z_0' = Z_0/g_0 = 43.3 \text{ ohms,}$$

$$Z_0'' = Z_0/g_0' = 86.6 \text{ ohms.}$$

Using these line impedance values a five-port stripline circuit has

been etched onto standard polyguide substrate. The strip widths for the various line impedances have been determined from the manufacturers graphical data (see Appendix A). Photographs of the fabricated strip-line five-port are shown in figure 3.5. Details of the performance of this junction is presented in the following section.

#### 3.4 Experimental Performance of the Strip-line Junction

Using a Hewlett-Packard model 8410S network analyzer, insertion loss and return loss measurements were made on the stripline junction. The results are presented in figures 3.6 to 3.8. The insertion loss between any two ports of the ideal junction is 6dB. From figure 3.6 it is seen that the measured insertion loss between the non-adjacent ports, e.g.,  $S_{13}$ ,  $S_{14}$  etc., all track very closely (within 0.5dB) together over the entire frequency range. At the center frequency of 1GHZ the insertion loss is about 6.5 dB. Below 1GHZ the loss is about 6.5 dB. Below 1GHZ the loss increases slowly to a value just over 7 dB, whereas, above 1GHZ it increases more rapidly to 10dB at 1200 MHz and then slowly to 12dB at 1.5GHZ. Over a 25% bandwidth, from 875 MHz to 1125 MHz the insertion loss remains within about 1dB of the ideal value of 6dB. Similarly from figure 3.7 it is seen that the measured insertion loss between adjacent ports, e.g.,  $S_{23}$ ,  $S_{43}$  etc., also all track closely (within 1 dB) together over the entire frequency range from 750 MHz to 1500 MHz. At the center frequency of 1GHZ the insertion loss is about 6.5 dB. Below 1GHZ the loss steadily increases to 8dB at 750 MHz, whereas above 1GHZ the loss remains constant at about 6.5dB till 1400 MHz before dropping down to a value of slightly under 5dB at

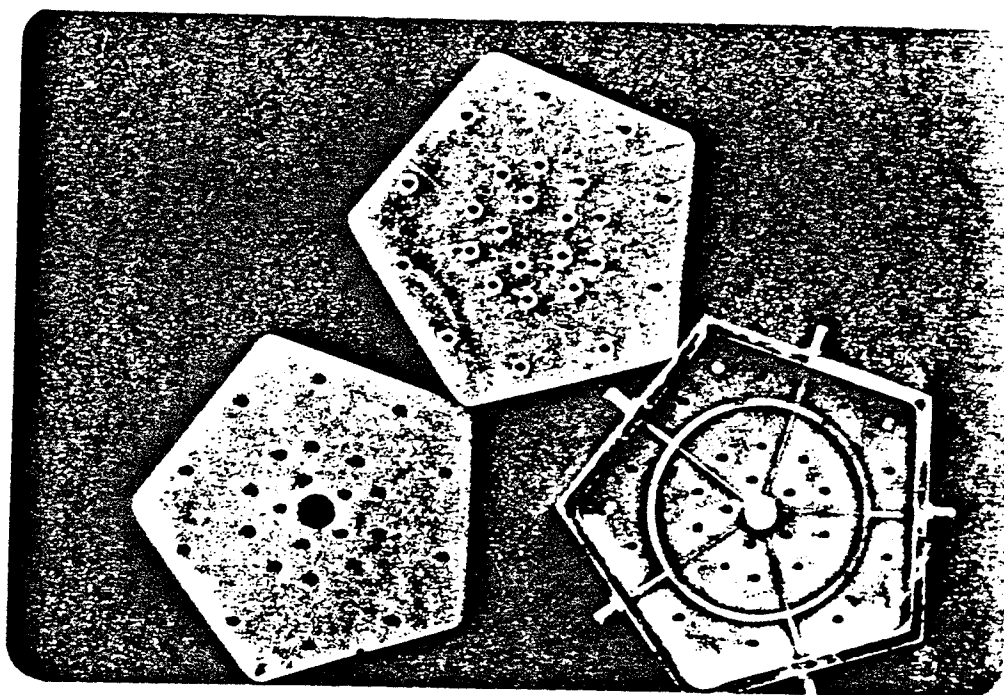
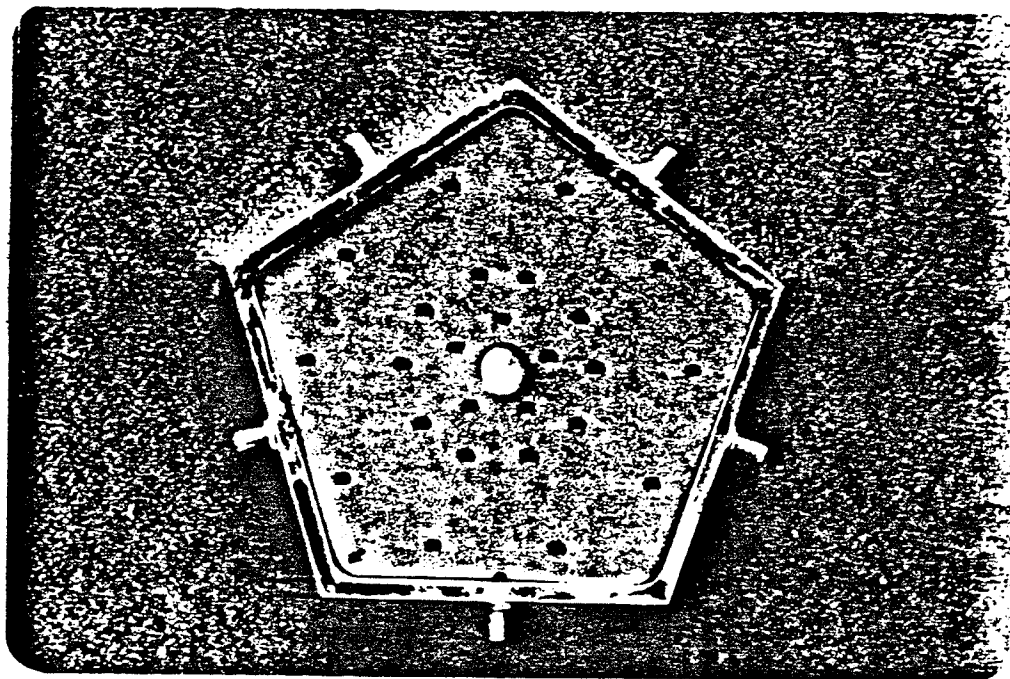


Fig. 3.5 Stripline symmetric five-port junction.

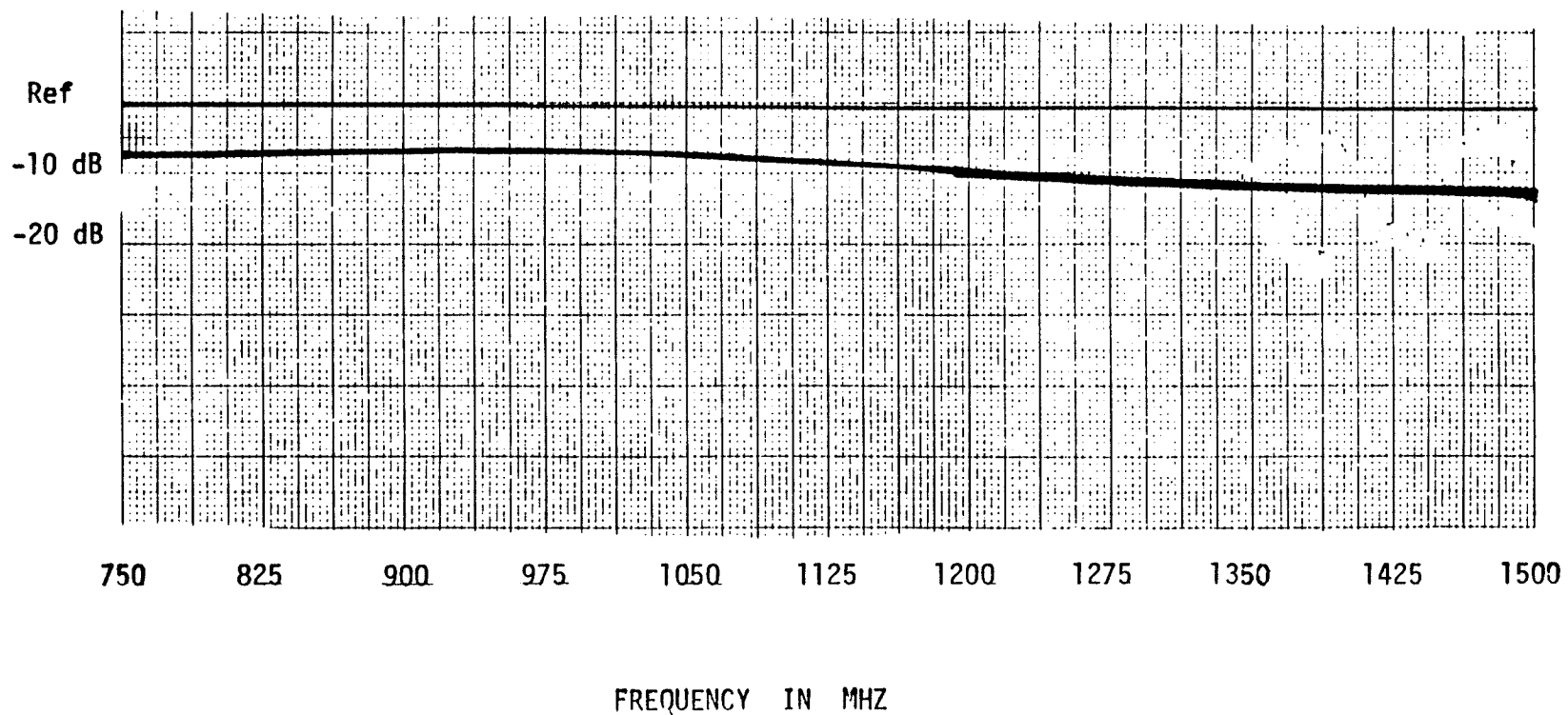


Fig. 3.6 Insertion loss between ports 1-3, 1-4, 2-5, 2-4, and 3-5.

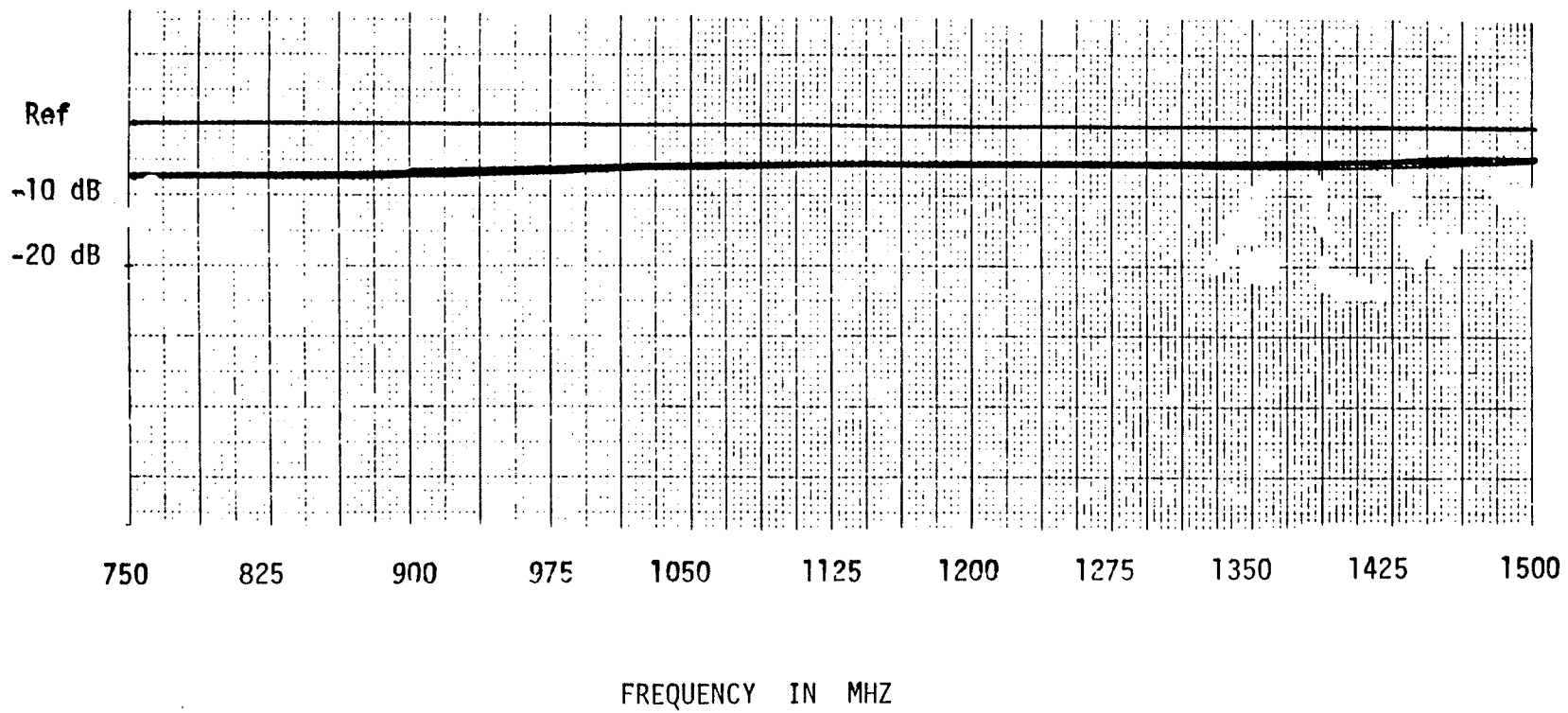


Fig. 3.7 Insertion loss between ports 2-3, 4-3, 4-5, 1-5, 1-2.

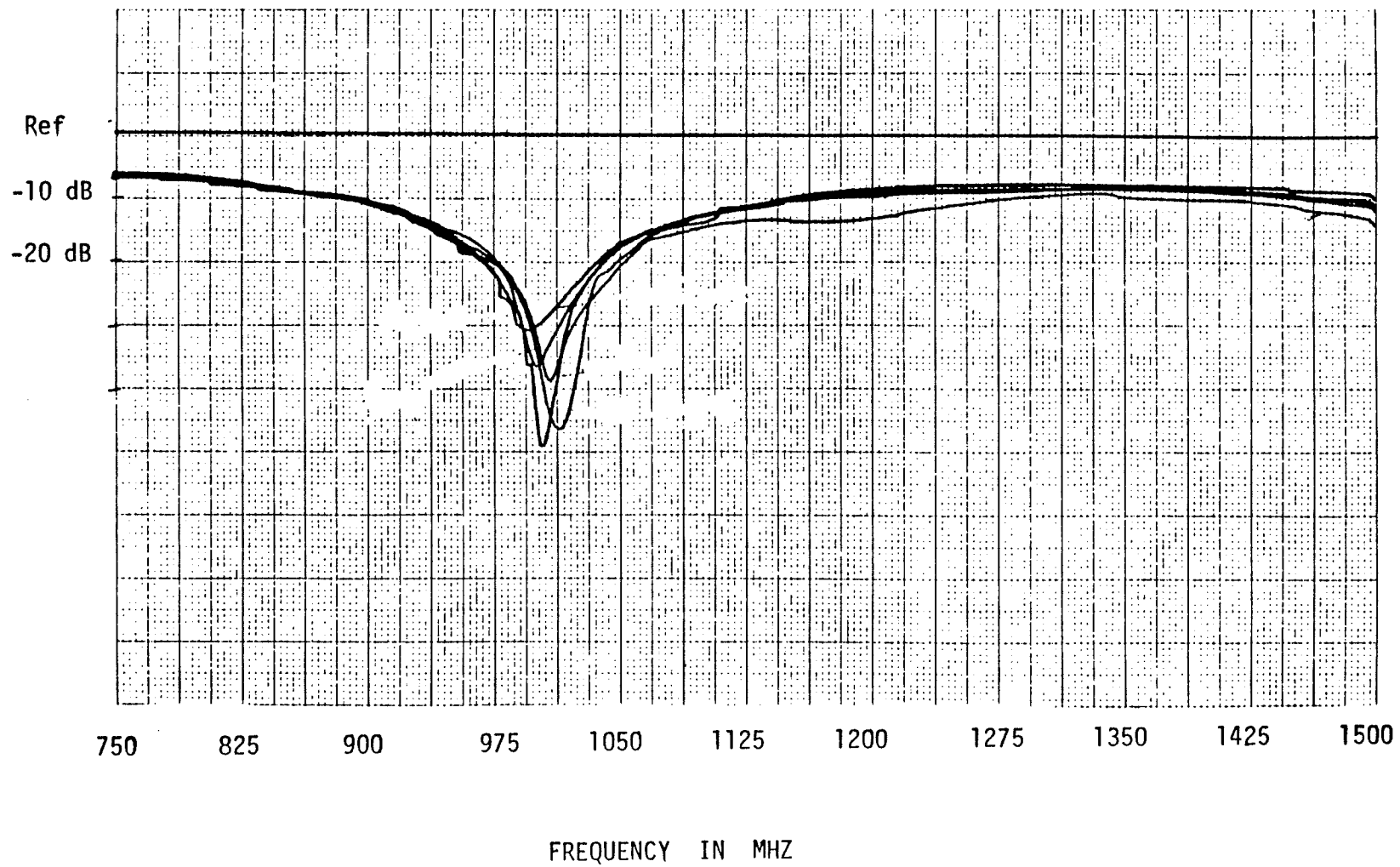


Fig. 3.8 Results of return loss measurements at ports 1,2,3,4 and 5 of the five-port junction.

1500 MHz. Over a 25% bandwidth from 875 MHz to 1125 MHz the insertion loss remains within about 1dB of the ideal value of 6dB. The results of the return loss measurements appear in figure 3.8. It is seen that for the frequency range 975-1050 MHz, each port of the five-port junction has a return loss of less than -20dB. Below 975 MHz the return loss rapidly increases to -10dB at a frequency of about 900 MHz and then slowly to a value of about -7dB at 750 MHz, similarly, above 1050 MHz the return loss increases to -10dB at 1150 MHz and stays around this value to 1500 MHz. Hence, if we consider a -10dB return loss as a sufficient port matching level a 25% bandwidth is readily obtainable with the junction power split remaining within 1dB of the ideal value of 6dB. Having designed, fabricated and tested a symmetric five-port stripline junction we are in a position to build a six-port measurement system based on this junction. The following chapter covers the development work for the six-port system.

## CHAPTER IV

### SIX-PORT IMPLEMENTATION

#### 4.1 The Six -Port Measurement System

The schematic representation of the six-port measurement system is shown in figure 4.1. In addition to the symmetric five-port and a directional coupler the six-port system consists of a power splitter, a set of four amplifiers connected to rf detectors, a source locking microwave counter, a sweep generator, a four channel A/D converter and a desk top computer. The counter, sweeper and A/D converter are controlled by the computer through the IEEE-488 interface bus (IB). The A/D converter, sweeper and counter are completely compatible with the IB, thus yielding complete system control to the computer through software. A Hewlett-Packard model 85A, desk top computer, functions as a system controller, data acquisition and computational device. It offers a fully integrated system including alphanumeric, editing, graphic and operator interaction capabilities. This fully integrated system is used to control the entire automated microwave measurement system using the BASIC software language. The Wiltron sweep generator, a model 610D mainframe and model 6247D multi-band rf plug-in, supplies the measurement system with a wide range of frequency coverage (10 MHz to 18GHz). The EIP model 371 source locking microwave counter is capable of automatically measuring any frequency within the range 20HZ to 18GHz. A bus controlled option of the counter enables the frequency output of the signal generator to be locked (using a feed back-loop process) at any desired frequency. The locking routine is capable with the aid of software to alter the sweep generator output

until the desired frequency is being generated. The advantage of the locking routine is that the generated frequency is of much higher accuracy than can be attained from the sweep generator itself. The HP model 59313A analog to digital converter digitizes the analog outputs from the four rf detectors and transmits signals via the IB to the computer for storage. A Hewlett-Packard model 11667A power splitter is used to divide the source signal between the counter and the six-port circuit. The detectors produce a dc output approximately proportional to the rf input power. The detector outputs are at a low level and in order to use the full range of the A/D converter ( $\pm 5$  volts) amplifiers are introduced between the detectors and the counter.

#### 4.1a System Operation

The six-port system shown in figure 4.1 operates as follows. Initially, the counter locks the sweeper at the first frequency called for by the computer. The A/D converter then takes signal samples from each of the four detectors and the digitized output is transmitted over the IB to the system controller where the data is stored for processing. It should be noted that the response characteristic of each of the four detectors has been characterized in the computer by a polynomial equation so that, from the voltage readings of the A/D converter, accurate power readings are obtained at the four measurement ports of the six-port circuit. Details of the detector calibration procedure and the characterizing

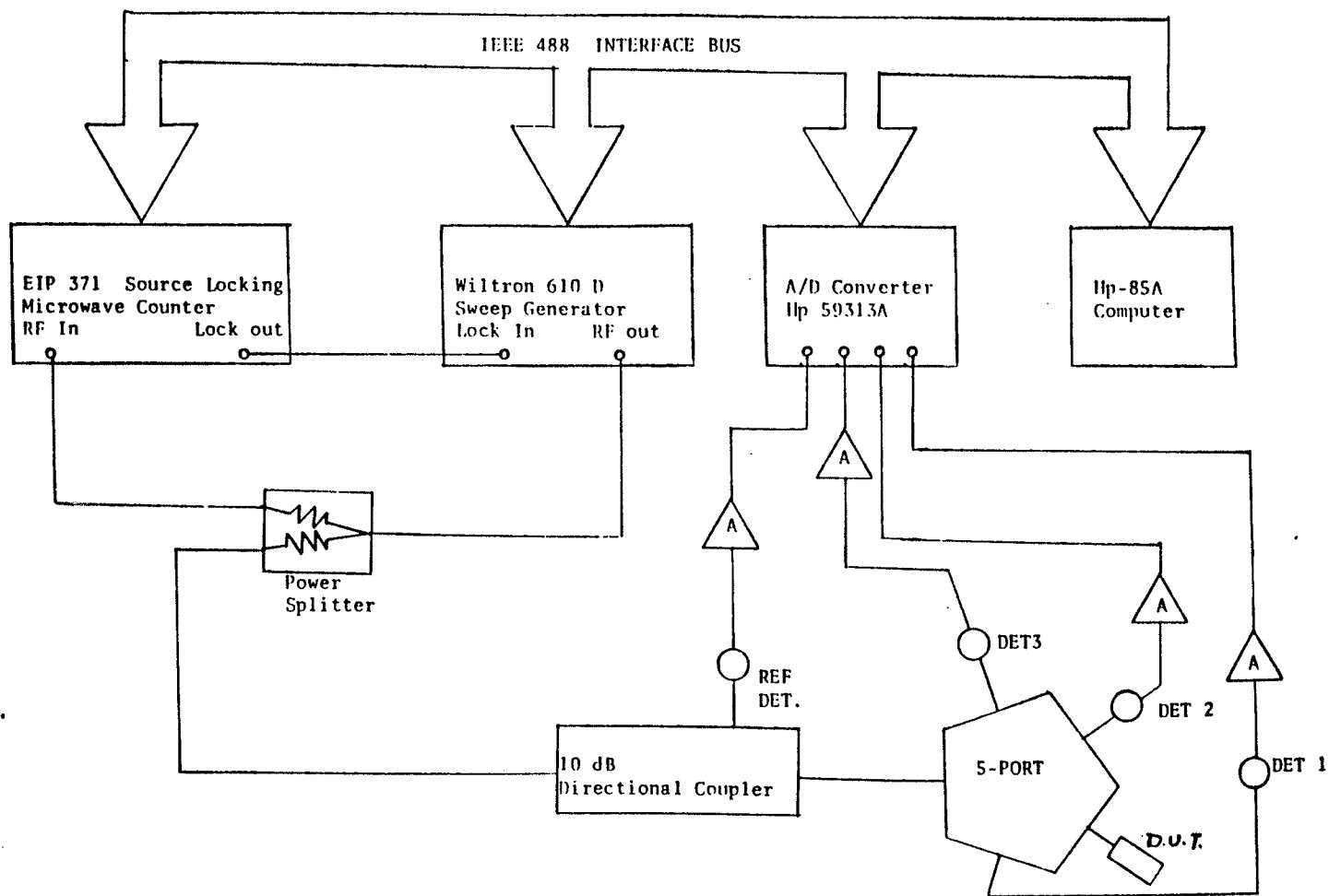


Fig. 4.1 Schematic representation of the six-port measurement system.

equations have been presented in Appendix B. The sweeper frequency is then incremented by the computer to the next frequency and the counter locks the sweeper and the process is repeated. After all the power readings have been collected the system controller processes the data to evaluate the complex reflection coefficient of the device under test (DUT) at each frequency. However, in order to determine these complex reflection coefficients the system needs to be calibrated. The process of calibration is necessary in order to determine all the complex constants in (4.19), (4.36) - (4.38) and (4.42).

#### 4.2 Calibration of the Six-Port System

From Chapter Two (equations (2.2) - (2.3)) the detector response at port 3 and reference port 4 are

$$b_3 = Aa_2 + Bb_2 \quad (4.1)$$

$$b_4 = Ca_2 + Db_2 \quad (4.2)$$

where A, B, C and D are complex constants. Dividing (4.1) by (4.2) and using

$$\Gamma_\ell = a_2 / b_2 \quad (4.3)$$

we get

$$\frac{b_3}{b_4} = \frac{B (A/B \Gamma_\ell + 1)}{C \Gamma_\ell + 1} \quad (4.4)$$

For convenience, the constants and  $\Gamma_\ell$  in (4.4) are redefined as

$$A/B = X e^{j\phi_x} \quad (4.5)$$

$$C = Z e^{j\phi_z} \quad (4.6)$$

$$\Gamma_\ell = |\Gamma_\ell| e^{j\phi_\ell} \quad (4.7)$$

where  $X$  and  $Z$  are real constants. In general the power emerging at a matched port is given by  $bb^*$ , so

$$\frac{P_3}{P_4} = \frac{b_3 b_3^*}{b_4 b_4^*} \quad (4.8)$$

Substituting (4.4) to (4.7) into (4.8) we have

$$\frac{P_3}{P_4} = B \left[ \frac{X e^{j\phi_x} |\Gamma_\ell| e^{j\phi_\ell} + 1}{Z e^{j\phi_z} |\Gamma_\ell| e^{j\phi_\ell} + 1} \right] X B^* \left[ \frac{X e^{-j\phi_x} |\Gamma_\ell| e^{-j\phi_\ell} + 1}{Z e^{-j\phi_z} |\Gamma_\ell| e^{-j\phi_\ell} + 1} \right] \quad (4.9)$$

$$= \frac{|B|^2 X^2 |\Gamma_\ell|^2 + 1 + 2 X |\Gamma_\ell| \cos(\phi_x + \phi_\ell)}{Z^2 |\Gamma_\ell|^2 + 1 + 2 Z |\Gamma_\ell| \cos(\phi_z + \phi_\ell)} \quad (4.10)$$

Generalizing (4.10) we can write [12]

$$\frac{P_i}{P_R} = |B_i|^2 \left[ \frac{X_i^2 |\Gamma_\ell|^2 + 1 + 2 X_i |\Gamma_\ell| \cos(\phi_{xi} + \phi_\ell)}{Z^2 |\Gamma_\ell|^2 + 1 + 2 Z |\Gamma_\ell| \cos(\phi_z + \phi_\ell)} \right] \quad (4.11)$$

where  $P_i$  ( $i = 1, 2, 3$ ) is the power emerging at each detector port of the five-port and  $P_R = P_4$  is the reference power delivered to the five-port junction. The purpose of the calibration procedure is to determine the constants  $|B_i|$ ,  $X_i$ ,  $\phi_{xi}$ , for  $i = 1, 2, 3$ , and  $Z$  and  $\phi_z$ . An examination of equation (4.11) reveals that a matched load ( $\Gamma_\ell = 0$ ) will suffice to determine  $|B_i|$ . The remaining constants are determined using the standard



loads. These standard loads, unfortunately, can not be of any arbitrary value. D. Woods [13] has shown that by choosing arbitrary values the calibration constants cannot be determined explicitly and numerical singularities are encountered. Renato G. Bosisio and Shire Li [10] have determined that the numerical singularities can however be avoided by carefully selecting four reflection standards ( $\Gamma_s$ ) such that  $|\Gamma_s| = 1$ .

We have chosen as reflection standards an open,  $\Gamma_s = 1$ , a short,  $\Gamma_s = -1$ , and two offset opens,  $\Gamma_s = j$  and  $\Gamma_s = -j$ . The phase distribution of the reflection standards used is shown in figure 4.2. Thus, to calibrate the six-port at each required frequency we need a matched load, a short, an open and two offset opens of  $\pm 90^\circ$  phase. There is no problem at low microwave frequencies in using the same matched load, open and short standards for the different required frequencies, however, the length

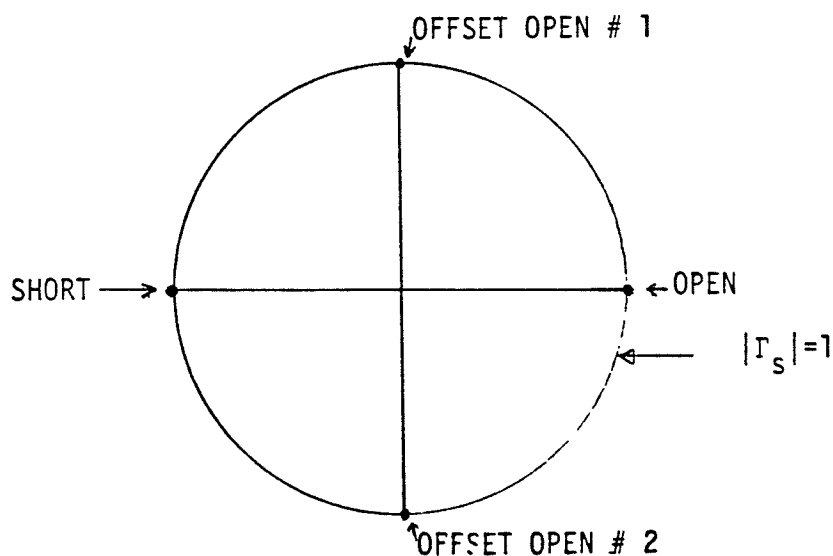


Fig. 4.2 Phase distribution of reflection standards used

of the offset load standards has to be changed for each calibration frequency. Hence a method of fairly accurately obtaining these offset standards is required.

A load with a unit reflection coefficient modulus and of varying phase is generated by terminating a length of transmission line with a sliding short. A network analyzer was used to set the phase of the reflection coefficient of this circuit.

### 4.3 An Expression for determining Calibration Constants

As mentioned earlier the constants  $|B_i|$  are determined by connecting a matched load to the test port. When a matched load  $\Gamma_\ell = 0$  is used, from (4.11), we get

$$|B_i|^2 = P_i/P_R \quad (4.12)$$

To determine the remaining calibration constants four loads of unit reflection coefficient magnitude, but separated in phase by  $90^\circ$  are used. Assuming that  $Z$  and  $\theta_z$  are known (a procedure is given in section 4.3a for separately determining these constants) we define a normalized power ratio  $(P_i/P_R)'$  such that

$$\left[ \frac{P_i}{P_R} \right]' = \left[ \frac{P_i}{P_R} \right] / |B_i|^2 \left[ 1 + 2Z |\Gamma_\ell| \cos(\theta_z + \theta_\ell) + Z^2 |\Gamma_\ell|^2 \right] \quad (4.13)$$

Substituting (4.13) in (4.11) we have

$$\left[ \frac{P_j}{P_R} \right]' = 1 + 2x_i |\Gamma_\ell| \cos(\theta_{xi} + \theta_\ell) + x_i^2 |\Gamma_\ell|^2 \quad (4.14)$$

Using an open standard at the test port plane of reference we get

$$\left[ \frac{P_i}{P_R} \right]_1 = 1 + 2X_i \cos \theta_{xi} + x_i^2 \quad (4.15)$$

Next, we obtain for a short standard

$$\left[ \frac{P_i}{P_R} \right]_2 = 1 - 2X_i \cos \theta_{xi} + x_i^2 \quad (4.16)$$

For an offset open standard of  $90^\circ$  electrical length we get

$$\left[ \frac{P_i}{P_R} \right]_3 = 1 - 2X_i \sin \theta_{xi} + x_i^2 \quad (4.17)$$

and finally for the offset open standard of  $270^\circ$  electrical length,

$$\left[ \frac{P_i}{P_R} \right]_4 = 1 + 2X_i \sin \theta_{xi} + x_i^2 \quad (4.18)$$

Re-arranging (4.15) to (4.18) in matrix form results in

$$\begin{bmatrix} x_i \cos \theta_{xi} \\ x_i \sin \theta_{xi} \end{bmatrix} = 1/4 \begin{bmatrix} 1 & -1 & 0 & 0 \\ 0 & 0 & -1 & 1 \end{bmatrix} \begin{bmatrix} (P_i/P_R)_1 \\ (P_i/P_R)_2 \\ (P_i/P_R)_3 \\ (P_i/P_R)_4 \end{bmatrix} \quad (4.19)$$

Hence, knowing  $\frac{P_i}{P_R}_K$ ,  $K = 1, 2, 3, 4$ , we can determine  $X_i \cos \theta_{xi}$

and  $X_i \sin \theta_{xi}$ .

### 4.3a A Closed Form Expression for the Constants $Z$ and $\theta_z$ [14]

Let  $R_0(i)$ ,  $R_1(i)$ ,  $R_2(i)$ ,  $R_3(i)$ ,  $i=1, 2, 3$ , be the measured normalized powers at the three detector ports for four unit magnitude offset load standards with phase angles  $\theta_0$ ,  $\theta_1$ ,  $\theta_2$  and  $\theta_3$ , respectively. Writing

$$R_K(i) = \left[ \frac{P_i}{P_R} \right] / |B_i|^2 ; K = 0, 1, 2, 3 \quad (4.20)$$

and substituting (4.20) into (4.11) we have the following:

$$\begin{aligned} R_0(i) (1 + z^2) + R_0(i) \cos \theta_0 2z \cos \theta_z - R_0(i) \sin \theta_0 2z \sin \theta_z \\ = 1 + x_i^2 + \cos \theta_0 2x_i \cos \theta_{xi} - \sin \theta_0 2x_i \sin \theta_{xi} \end{aligned} \quad (4.21)$$

$$\begin{aligned} R_1(i) (1 + z^2) + R_1(i) \cos \theta_1 2z \cos \theta_z - R_1(i) \sin \theta_1 2z \sin \theta_z \\ = 1 + x_i^2 + \cos \theta_1 2x_i \cos \theta_{xi} - \sin \theta_1 2x_i \sin \theta_{xi} \end{aligned} \quad (4.22)$$

$$\begin{aligned} R_2(i) (1 + z^2) + R_2(i) \cos \theta_2 2z \cos \theta_z - R_2(i) \sin \theta_2 2z \sin \theta_z \\ = 1 + x_i^2 + \cos \theta_2 2x_i \cos \theta_{xi} - \sin \theta_2 2x_i \sin \theta_{xi} \end{aligned} \quad (4.23)$$

$$\begin{aligned} R_3(i) (1 + z^2) + R_3(i) \cos \theta_3 2z \cos \theta_z - R_3(i) \sin \theta_3 2z \sin \theta_z \\ = 1 + x_i^2 + \cos \theta_3 2x_i \cos \theta_{xi} - \sin \theta_3 2x_i \sin \theta_{xi} \end{aligned} \quad (4.24)$$

Writing (4.22) to (4.24) in matrix form we get

$$\begin{bmatrix} R_1(i) & R_1(i) \cos \theta_1 & -R_1(i) \sin \theta_1 \\ R_2(i) & R_2(i) \cos \theta_2 & -R_2(i) \sin \theta_2 \\ R_3(i) & R_3(i) \cos \theta_3 & -R_3(i) \sin \theta_3 \end{bmatrix} \begin{bmatrix} 1 + z^2 \\ 2z \cos \theta_z \\ 2z \sin \theta_z \end{bmatrix}$$

$$= \begin{bmatrix} 1 & \cos \theta_1 & -\sin \theta_1 \\ 1 & \cos \theta_2 & -\sin \theta_2 \\ 1 & \cos \theta_3 & -\sin \theta_3 \end{bmatrix} \begin{bmatrix} 1 + x_i^2 \\ 2x_i \cos \theta_{xi} \\ 2x_i \sin \theta_{xi} \end{bmatrix} \quad (4.25)$$

This yields

$$\begin{bmatrix} 1 + x_i^2 \\ 2x_i \cos \theta_{xi} \\ 2x_i \sin \theta_{xi} \end{bmatrix} = \left[ \sin(\theta_1 - \theta_2) + \sin(\theta_2 - \theta_3) + \sin(\theta_3 - \theta_1) \right]^{-1} \times$$

$$\begin{bmatrix} \sin(\theta_2 - \theta_3) & \sin(\theta_3 - \theta_1) & \sin(\theta_1 - \theta_2) \\ \sin \theta_3 - \sin \theta_2 & \sin \theta_1 - \sin \theta_3 & \sin \theta_2 - \sin \theta_1 \\ \cos \theta_3 - \cos \theta_2 & \cos \theta_1 - \cos \theta_3 & \cos \theta_2 - \cos \theta_1 \end{bmatrix} \times$$

$$\begin{bmatrix} R_1(i) & R_1(i) \cos \theta_1 & -R_1(i) \sin \theta_1 \\ R_2(i) & R_2(i) \cos \theta_2 & -R_2(i) \sin \theta_2 \\ R_3(i) & R_3(i) \cos \theta_3 & -R_3(i) \sin \theta_3 \end{bmatrix} \begin{bmatrix} 1 + z^2 \\ 2z \cos \theta_z \\ 2z \sin \theta_z \end{bmatrix} \quad (4.26)$$

From (4.26) we get expressions for  $1 + x_i^2$ ,  $2x_i \cos \theta_{xi}$  and  $2x_i \sin \theta_{xi}$ .

There are as follows:

$$1 + x_i^2 = \left[ \sin(\theta_1 - \theta_2) + \sin(\theta_2 - \theta_3) + \sin(\theta_3 - \theta_1) \right]^{-1} \times$$

$$\left[ (1 + z^2) \left[ \sin(\theta_2 - \theta_3) R_1(i) + \sin(\theta_3 - \theta_1) R_2(i) + \right. \right.$$

$$\left. \sin(\theta_1 - \theta_2) R_3(i) \right] + (2z \cos \theta_z) \left[ \sin(\theta_2 - \theta_3) R_1(i) \cos \theta_1 + \right.$$

$$\left. \sin(\theta_3 - \theta_1) R_2(i) \cos \theta_2 + \sin(\theta_1 - \theta_2) R_3(i) \cos \theta_3 \right] -$$

$$(2z \sin \theta_z) \left[ \sin(\theta_2 - \theta_3) R_1(i) \sin \theta_1 + \sin(\theta_3 - \theta_1) \right.$$

$$\left. R_2(i) \sin \theta_2 + \sin(\theta_1 - \theta_2) R_3(i) \sin \theta_3 \right] \quad (4.27)$$

$$\begin{aligned}
2x_i \cos \theta_{xi} = & \left[ \sin (\theta_1 - \theta_2) + \sin (\theta_2 - \theta_3) + \sin (\theta_3 - \theta_1) \right]^{-1} \times \\
& \left[ (1 + z^2) \left[ (\sin \theta_3 - \sin \theta_2) R_1(i) + (\sin \theta_1 - \sin \theta_3) R_2(i) + \right. \right. \\
& \left. \left. (\sin \theta_2 - \sin \theta_1) R_3(i) \right] + (2z \cos \theta_z) \left[ (\sin \theta_3 - \sin \theta_2) \right. \right. \\
& \left. \left. R_1(i) \cos \theta_1 + (\sin \theta_1 - \sin \theta_3) R_2(i) \cos \theta_2 + \right. \right. \\
& \left. \left. (\sin \theta_2 - \sin \theta_1) R_3(i) \cos \theta_3 \right] - (2z \sin \theta_z) \times \right. \\
& \left. \left[ (\sin \theta_3 - \sin \theta_2) R_1(i) \sin \theta_1 + (\sin \theta_1 - \sin \theta_3) \right. \right. \\
& \left. \left. R_2(i) \sin \theta_2 + (\sin \theta_2 - \sin \theta_1) R_3(i) \sin \theta_3 \right] \right] \quad (4.28)
\end{aligned}$$

$$\begin{aligned}
2x_i \sin \theta_{xi} = & \left[ \sin (\theta_1 - \theta_2) + \sin (\theta_2 - \theta_3) + \sin (\theta_3 - \theta_1) \right]^{-1} \times \\
& \left[ (1 + z^2) \left[ (\cos \theta_3 - \cos \theta_2) R_1(i) + (\cos \theta_1 - \cos \theta_3) R_2(i) \right. \right. \\
& \left. \left. + (\cos \theta_2 - \cos \theta_1) R_3(i) \right] + (2z \cos \theta_z) \left[ (\cos \theta_3 - \right. \right. \\
& \left. \left. \cos \theta_2) R_1(i) \cos \theta_1 + (\cos \theta_1 - \cos \theta_3) R_2(i) \cos \theta_2 \right. \right. \\
& \left. \left. + (\cos \theta_2 - \cos \theta_1) R_3(i) \cos \theta_3 \right] - (2z \sin \theta_z) \right. \\
& \left. \left[ (\cos \theta_3 - \cos \theta_2) R_1(i) \sin \theta_1 + (\cos \theta_1 - \cos \theta_3) \right. \right. \\
& \left. \left. R_2(i) \sin \theta_2 + (\cos \theta_2 - \cos \theta_1) R_3(i) \sin \theta_3 \right] \right] \quad (4.29)
\end{aligned}$$

Returning to (4.21) we see that by selecting  $\theta_0 = 0^\circ$  (open standard used as reference) (4.21) reduces to

$$R_0(i) (1 + z^2) + R_0(i) 2z \cos \theta_z = 1 + x_i^2 + 2 x_i \cos \theta_{xi} \quad (4.30)$$

Substituting (4.27) and (4.28) into (4.30) and re-arranging terms gives

$$\begin{aligned}
(1 + z^2) \left[ (R_0(i) \left[ \sin (\theta_2 - \theta_3) + \sin (\theta_3 - \theta_1) + \sin (\theta_1 - \theta_2) \right] + R_1(i) \left[ \sin \theta_2 - \right. \right. \right. \\
\left. \left. \sin \theta_3 - \sin (\theta_2 - \theta_3) \right] + R_2(i) \left[ \sin \theta_3 - \sin \theta_1 - \sin (\theta_3 - \theta_1) \right] + \right.
\end{aligned}$$

$$\begin{aligned}
& R_3(i) \left[ \sin \theta_1 - \sin \theta_2 - \sin (\theta_1 - \theta_2) \right] + (2z \cos \theta_2) \left[ R_0(i) \left[ \sin (\theta_2 - \theta_3) + \right. \right. \\
& \left. \left. \sin (\theta_3 - \theta_1) + \sin (\theta_1 - \theta_2) \right] + R_1(i) \cos \theta_1 \left[ \sin \theta_2 - \sin \theta_3 - \right. \right. \\
& \left. \left. \sin (\theta_2 - \theta_3) \right] + R_2(i) \cos \theta_2 \left[ \sin \theta_3 - \sin \theta_1 - \sin (\theta_3 - \theta_1) \right] + \right. \\
& \left. R_3(i) \cos \theta_3 \left[ \sin \theta_1 - \sin \theta_2 - \sin (\theta_1 - \theta_2) \right] \right] - (2z \sin \theta_2) \\
& \left[ R_1(i) \sin \theta_1 \left[ \sin \theta_2 - \sin \theta_3 - \sin (\theta_2 - \theta_3) \right] + R_2(i) \sin \theta_2 \left[ \sin \theta_3 - \right. \right. \\
& \left. \left. \sin \theta_1 - \sin (\theta_3 - \theta_1) \right] + R_3(i) \sin \theta_3 \left[ \sin \theta_1 - \sin \theta_2 - \sin (\theta_1 - \theta_2) \right] \right] = 0
\end{aligned} \tag{4.31}$$

$$\begin{bmatrix} R_1(i) - R_0(i) & R_2(i) - R_0(i) & R_3(i) - R_0(i) \\ R_1(i) \cos \theta_1 - R_0(i) & R_2(i) \cos \theta_2 - R_0(i) & R_3(i) \cos \theta_3 - R_0(i) \\ -R_1(i) \sin \theta_1 & -R_2(i) \sin \theta_2 & -R_3(i) \sin \theta_3 \end{bmatrix} \times$$

$$\begin{bmatrix} \sin \theta_2 - \sin \theta_3 - \sin (\theta_2 - \theta_3) \\ \sin \theta_3 - \sin \theta_1 - \sin (\theta_3 - \theta_1) \\ \sin \theta_1 - \sin \theta_2 - \sin (\theta_1 - \theta_2) \end{bmatrix} \times \begin{bmatrix} 1 + z^2 \\ 2z \cos \theta_2 \\ 2z \sin \theta_2 \end{bmatrix} = 0 \tag{4.32}$$

If we make the following definition

$$\begin{bmatrix} R_1(i) - R_0(i) & R_2(i) - R_0(i) & R_3(i) - R_0(i) \\ R_1(i) \cos \theta_1 - R_0(i) & R_2(i) \cos \theta_2 - R_0(i) & R_3(i) \cos \theta_3 - R_0(i) \\ -R_1(i) \sin \theta_1 & -R_2(i) \sin \theta_2 & -R_3(i) \sin \theta_3 \end{bmatrix} \times$$

$$\begin{bmatrix} \sin \theta_2 - \sin \theta_3 - \sin (\theta_2 - \theta_3) \\ \sin \theta_3 - \sin \theta_1 - \sin (\theta_3 - \theta_1) \\ \sin \theta_1 - \sin \theta_2 - \sin (\theta_1 - \theta_2) \end{bmatrix} = \begin{bmatrix} A_{i1} \\ A_{i2} \\ A_{i3} \end{bmatrix}$$

$$i = 1, 2, 3$$

then from (4.32) we obtain

$$A_{11} (1 + z^2) + A_{12} (2z \cos \theta_z) + A_{13} (2z \sin \theta_z) = 0 \quad (4.33)$$

$$A_{21} (1 + z^2) + A_{22} (2z \cos \theta_z) + A_{23} (2z \sin \theta_z) = 0 \quad (4.34)$$

$$A_{31} (1 + z^2) + A_{32} (2z \cos \theta_z) + A_{33} (2z \sin \theta_z) = 0 \quad (4.35)$$

From (4.33) - (4.35) we get three expressions for  $\theta_z$

$$\theta_z = \tan^{-1} \left[ \frac{A_{21} A_{12} - A_{11} A_{22}}{A_{11} A_{23} - A_{21} A_{13}} \right] \quad (4.36)$$

$$\theta_z = \tan^{-1} \left[ \frac{-A_{22} A_{31} + A_{32} A_{21}}{-A_{33} A_{21} + A_{23} A_{31}} \right] \quad (4.37)$$

$$\theta_z = \tan^{-1} \left[ \frac{A_{31} A_{12} + A_{32} A_{11}}{A_{33} A_{11} - A_{31} A_{13}} \right] \quad (4.38)$$

Having determined the value of  $\theta_z$  from any of the three expressions given above, it is then substituted in (4.33) to give

$$A_{11} (1 + z^2) + A_{12} (2z \cos \theta_z) + A_{13} (2z \sin \theta_z) = 0 \quad (4.39)$$

Dividing (4.39) by  $2z$  and re-arranging, results in

$$\left[ \frac{1+z^2}{2z} \right] = - \left[ \frac{A_{12} \cos \theta_z + A_{13} \sin \theta_z}{A_{11}} \right] \quad (4.40)$$

Let

$$x = - \frac{(A_{12} \cos \theta_z + A_{13} \sin \theta_z)}{A_{11}} \quad (4.41)$$

Equation (4.40) reduces to  $z^2 - 2xz + 1 = 0$ , which has the solution

$$z = x \pm \sqrt{x^2 - 1} \quad (4.42)$$

For  $z$  to be real we need  $x$  greater than unity. As  $z$  is the coupling coefficient (see (4.6)) we therefore have  $z \leq 1$  ( for passive devices ) and must choose the - ve sign in (4.42). Having determined  $z$  and  $\theta_z$  the remaining constants, using (4.19), can now be evaluated.

Knowing all the calibration constants it is quite simple and straight forward using (4.11) to determine from the six-port power readings the complex reflection coefficient of the DUT.

#### 4.4 A Matrix Expression for $\Gamma_\ell$

Re-arranging and writing (4.11) in matrix form we have

$$\begin{bmatrix} S_{11} & S_{12} & S_{13} \\ S_{21} & S_{22} & S_{23} \\ S_{31} & S_{32} & S_{33} \end{bmatrix} \begin{bmatrix} |\Gamma_\ell|^2 \\ 2|\Gamma_\ell| \cos \theta_\ell \\ 2|\Gamma_\ell| \sin \theta_\ell \end{bmatrix} = \begin{bmatrix} 1 - P_1 / (P_R \times B_1) \\ 1 - P_2 / (P_R \times B_2) \\ 1 - P_3 / (P_R \times B_3) \end{bmatrix} \quad (4.43)$$

where,

$$S_{11} = [P_1 / (P_R \times B_1)] z^2 - x_1^2 ; S_{21} = [P_2 / (P_R \times B_2)] z^2 - x_2^2 ; S_{31} = [P_3 / (P_R \times B_3)] z^2 - x_3^2$$

$$S_{12} = [P_1 / (P_R \times B_1)] z \cos \theta_z - x_1 \cos \theta_{x1} ; S_{22} = [P_2 / (P_R \times B_2)] z \cos \theta_z - x_2 \cos \theta_{x2}$$

$$S_{32} = [P_3 / (P_R \times B_3)] z \cos \theta_z - x_3 \cos \theta_{x3} ; S_{13} = x_1 \sin \theta_{x1} - z [P_1 / (P_R \times B_1)] \sin \theta_z$$

$$S_{23} = x_2 \sin \theta_{x2} - z [P_2 / (P_R \times B_2)] \sin \theta_z ; S_{33} = x_3 \sin \theta_{x3} - z [P_3 / (P_R \times B_3)] \sin \theta_z.$$

From (4.43) the values of  $\Gamma_\ell$  and  $\theta_\ell$  can easily be determined.

## 4.5 System Software

The computer software which has been developed allows automated operation of the six-port measurement system. The six-port has been calibrated for use in the frequency range 890-1110 MHz. The calibration constants have been determined at eleven frequency points at 20 MHz intervals. These constants are determined using the program 6PCAL which is described in the next section.

### 4.5a Calibration Program, 6PCAL

The program 6PCAL determines the calibration constants at all the required frequencies between 890 to 1110 MHz and a program listing is given in Appendix C. First, the user is prompted to input the desired frequency range and the required frequency increments at which the system has to be calibrated. The counter locks the sweeper at each desired frequency as follows. A sweeper output within 10MHz of the required frequency allows the counter locking procedure to be initiated. If the sweeper output is not within 10MHz of the desired frequency, then the sweep frequency is raised/lowered until the frequency output of the sweeper is within the locking range of the counter. A flow chart for this procedure is shown in figure 4.3. After having locked the sweeper the user is prompted to connect a matched load ( $50 \Omega$ ) and then the A/D converter, starting from channel 1 through channel 4, samples the analog inputs and transmits the digital data to the system controller over the IB. The Hp-85 computer stores these readings. The process is repeated for the remaining four loads namely, a short, an open and two offset opens ( $\pm 90^\circ$ ). After having done this the calibration constants are calculated

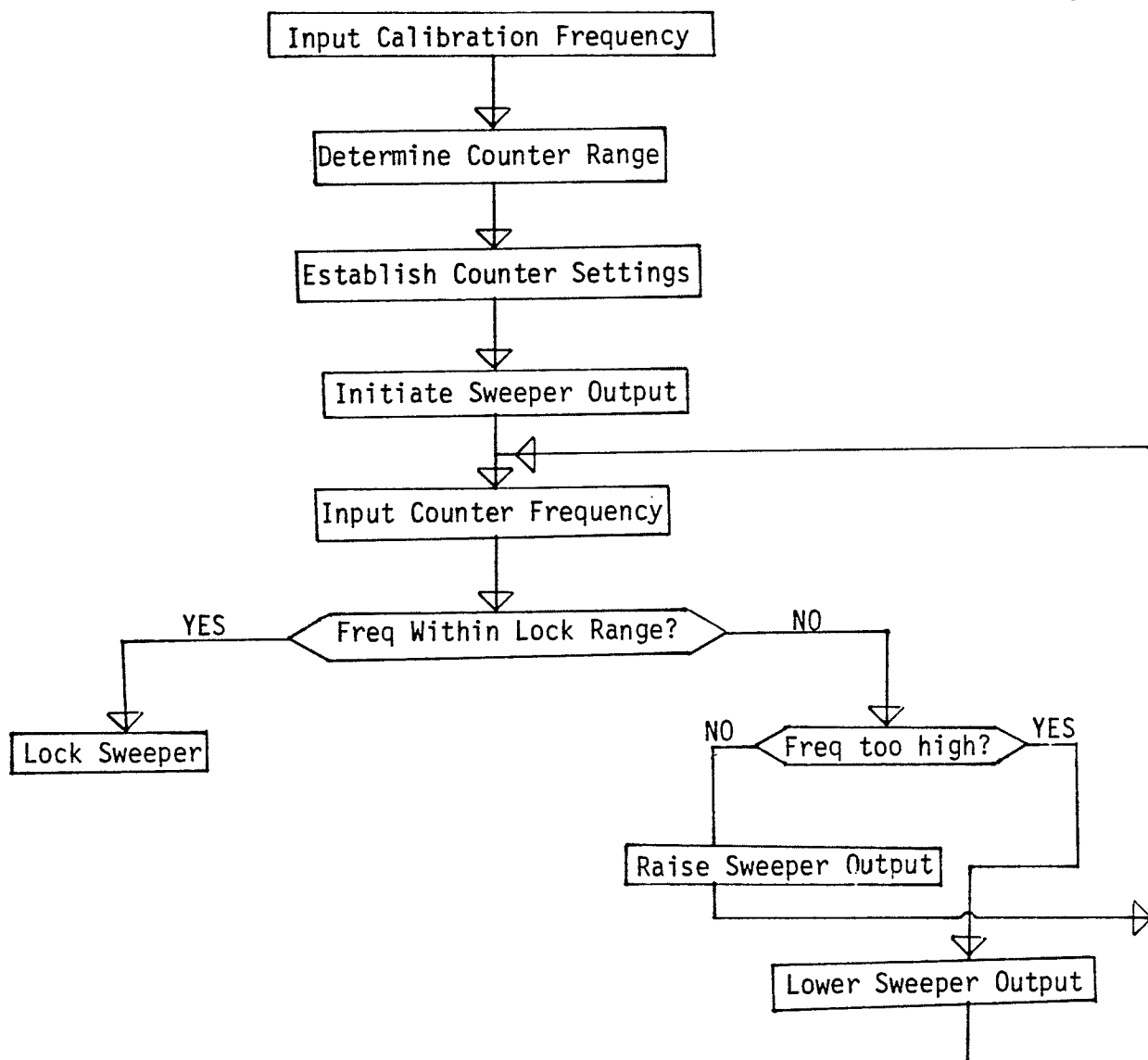


Fig. 4.3 Flowchart of software for setting system frequency.

using the equations determined in the previous sections. Next, the frequency is incremented and the process is repeated. This is repeated till the calibration constants at all frequencies have been determined explicitly.

#### 4.5b The Reflection Coefficient Measurement Program, REF-6P

The reflection coefficient for a DUT is determined using the program REF-6P, which is now briefly explained. A listing of the program is given in Appendix C. The programs REF-6P and 6PCAL are written as two separate programs because of the operator skill required to perform the calibrations and also because recalibration is not required each time the system is used. As in the calibration program the user is first prompted to input the desired frequency range and the required frequency increments. The counter locks the sweeper at each desired frequency and the A/D converter samples the signal with the DUT connected. These readings, along with the appropriate set of calibration constants and the system of equations derived in the previous sections, are used to determine the magnitude and phase of the reflection coefficient at each required frequency. It shall be shown in the following chapter that the calibration constants vary slowly with frequency and for the purposes of this thesis it has been assumed to be constant over a 20MHZ frequency interval. Hence, the system has been calibrated at 20MHZ frequency intervals.

## Chapter V

### Results and Discussion

#### 5.1 Introduction

Employing the six-port system described in the previous chapters measurements on various test loads have been performed at the center frequency of 1 GHz and over a bandwidth of frequencies. In section 5.2 the calibration constants determined at 1 GHz are presented. Using these constants return loss measurements made at the center frequency have been reported in section 5.3. A variable reflection coefficient load standard has been used to test the six-port system at 1 GHz and the results obtained have been compared with those obtained with a MNA and also with computed values and have been recorded in section 5.4. Next, to test the six-port system over the 900-1100 MHz bandwidth, calibration constants have been determined at 20 MHz frequency intervals and are tabulated in section 5.5. Finally, in section 5.6 the load reflection coefficient has been measured over the 900-1100 MHz bandwidth, using the calibration constants determined in the previous section. The results obtained using the six port system have been compared with those obtained with a MNA and also with the computed values.

#### 5.2 Six-Port Center Frequency Calibration

To establish some confidence in the accuracy of the six-port system return loss measurements were initially made on a short-circuit terminated attenuator (HP-model 8494H) set at various attenuation levels and at the center frequency of 1 GHz. In order to perform these measurements the system had to be calibrated at the center frequency. As described in

Chapter IV the load standards used for this calibration are a matched load, an open, a short, and two offset opens of  $\pm 90^\circ$  phase. The  $\pm 90^\circ$  offset open load standards have been obtained by properly adjusting the length of a short-circuit terminated line using the HP microwave network analyzer. The six-port calibration constants so determined are listed in table 5.1.

$z \angle \phi_z$	0.051	$\angle 266.7^\circ$
$x_1 \angle \phi_{x1}$	0.410	$\angle 69.7^\circ$
$x_2 \angle \phi_{x2}$	0.520	$\angle 197.7^\circ$
$x_3 \angle \phi_{x3}$	0.482	$\angle -58.6^\circ$
$ B_1 $	0.273	
$ B_2 $	0.232	
$ B_3 $	0.251	

Table 5.1: Six-Port Calibration Constants at 1GHZ

These calibration constants were used in the return loss measurements and as well in further measurements in order to evaluate the performance of the six-port system. These measurements are described and presented in the following two sections.

### 5.3 Return Loss Calculation at 1GHZ

A HP model 8494H attenuator terminated with a short circuit was connected to the load port of the six-port and its input reflection co-

efficient measured. The return loss (RL) was calculated from the measured coefficient using the relationship.

$$RL = 20 \log (1/|\Gamma_{\ell}|)$$

and the result then compared with the expected value based on the attenuator setting, i.e.,  $RL = 2A$  where  $A$  is the attenuation value. The HP model 8494H attenuator allowed the attenuation to be varied in 1-dB steps. The load reflection coefficient for each 1 dB step of the attenuation was measured using both the six-port system and the HP microwave network analyzer. The measurement results obtained from the network analyzer and the six-port system are tabulated in Table 5.2. From table 5.2 it is seen that the RL as measured using the MNA and six-port track closely and there is less than 5% difference between the two sets of readings for all values of attenuator settings up to 9dB. Beyond this value the difference increases to about 10% at 11dB. It is also seen that both sets of measured RL values compare well with the theoretical values for the attenuator settings up to 8dB. Beyond 8dB the readings do not agree closely. We should note that for an 8dB attenuator setting  $|\Gamma_{\ell}|$  is 0.158. It is hence concluded that the six-port provides fairly accurate readings of reflection coefficient for  $|\Gamma_{\ell}|=0.2$ . It is useful to mention that  $|\Gamma_{\ell}| = 0.2$  corresponds to a return loss of 14dB (a reflected power of 4%) which for many practical purposes can be considered to be a sufficiently well matched load. Hence, it will suffice if the six-port can accurately measure  $|\Gamma_{\ell}| \geq 0.2$ ; which it does. For  $|\Gamma_{\ell}| < 0.2$ , the accuracy obtained using the six-port system is poor as one would generally expect.

Attenuation Setting (dB) $\pm$ attenuation accuracy (dB)	Reflection Coefficient ( $\Gamma_{\ell}$ )		Return Loss (dB)		
	MNA	Six-Port	MNA	Six-Port	Attenuator System
1 $\pm$ 0.3	0.75 $\angle -8^{\circ}$	0.740 $\angle -8.32^{\circ}$	2.50	2.60	1.4 to 2.6
2 $\pm$ 0.3	0.61 $\angle -11^{\circ}$	0.615 $\angle -11.59^{\circ}$	4.30	4.22	3.4 to 4.6
3 $\pm$ 0.4	0.50 $\angle -17^{\circ}$	0.497 $\angle -16.60^{\circ}$	6.00	6.07	5.2 to 6.8
4 $\pm$ 0.4	0.39 $\angle -15^{\circ}$	0.400 $\angle -14.20^{\circ}$	8.18	7.96	7.2 to 8.8
5 $\pm$ 0.5	0.32 $\angle -20^{\circ}$	0.325 $\angle -19.50^{\circ}$	9.90	9.80	9.0 to 11.0
6 $\pm$ 0.5	0.28 $\angle -23^{\circ}$	0.280 $\angle -22.40^{\circ}$	11.05	11.05	11.0 to 13.0
7 $\pm$ 0.6	0.21 $\angle -27^{\circ}$	0.220 $\angle -28.00^{\circ}$	13.55	13.20	12.8 to 15.2
8 $\pm$ 0.6	0.19 $\angle -25^{\circ}$	0.200 $\angle -26.00^{\circ}$	14.40	14.00	14.8 to 17.2
9 $\pm$ 0.6	0.17 $\angle -30^{\circ}$	0.180 $\angle -30.20^{\circ}$	15.40	15.00	16.8 to 19.2
10 $\pm$ 0.6	0.14 $\angle -31^{\circ}$	0.165 $\angle -33.70^{\circ}$	17.10	15.70	18.8 to 2.12
11 $\pm$ 0.7	0.10 $\angle -35^{\circ}$	0.144 $\angle -37.40^{\circ}$	20.00	16.80	20.6 to 23.4

Table 5.2 Return Loss Measurement Results

#### 5.4 Measurement of $\Gamma_\ell$ at 1GHz

A reflection coefficient load of controllable magnitude and phase can be generated by using the circuit arrangement shown in figure 5.1. It consists of a co-axial Tee-junction with a matched load ( $50\ \Omega$ ) connected to one arm, a variable length short-circuit stub to a second arm and a length of co-axial line to the third arm of the Tee-junction. By varying the lengths of the two co-axial lines all phase angles of the load reflection coefficient from  $0^\circ$  to  $360^\circ$  can be obtained. The magnitude of the reflection coefficient generated however depends only upon the stub length ( $d$ ) as indicated in figure 5.1

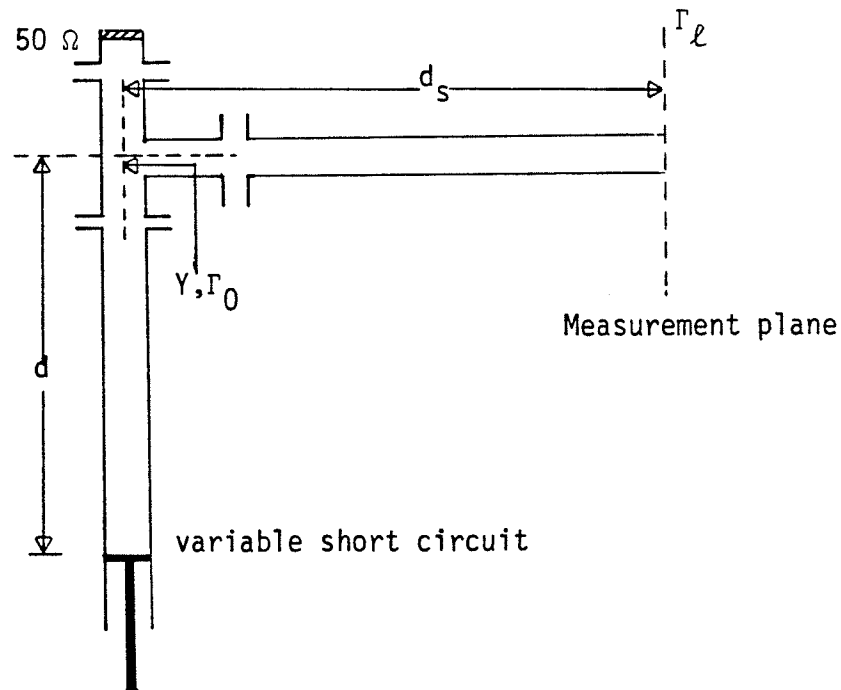


Figure 5.1 Variable Reflection Standard

A method for obtaining  $\Gamma_{\ell}$  from the lengths 'd' and 'd<sub>s</sub>' is shown below. The admittance right at the Tee-junction is given by

$$Y = Y_0 - jY_0 \cot \beta d \quad (5.1)$$

where  $Y_0 = 1/50 \text{ S}$ ,  $\beta = 2\pi/\lambda$  and

d = stub length in cm.

The corresponding reflection coefficient  $\Gamma_0$  is

$$\Gamma_0 = \frac{Y_0 - Y}{Y_0 + Y} \quad (5.2)$$

Therefore

$$\Gamma_{\ell} = \Gamma_0 e^{-2j\beta d_s} \quad (5.3)$$

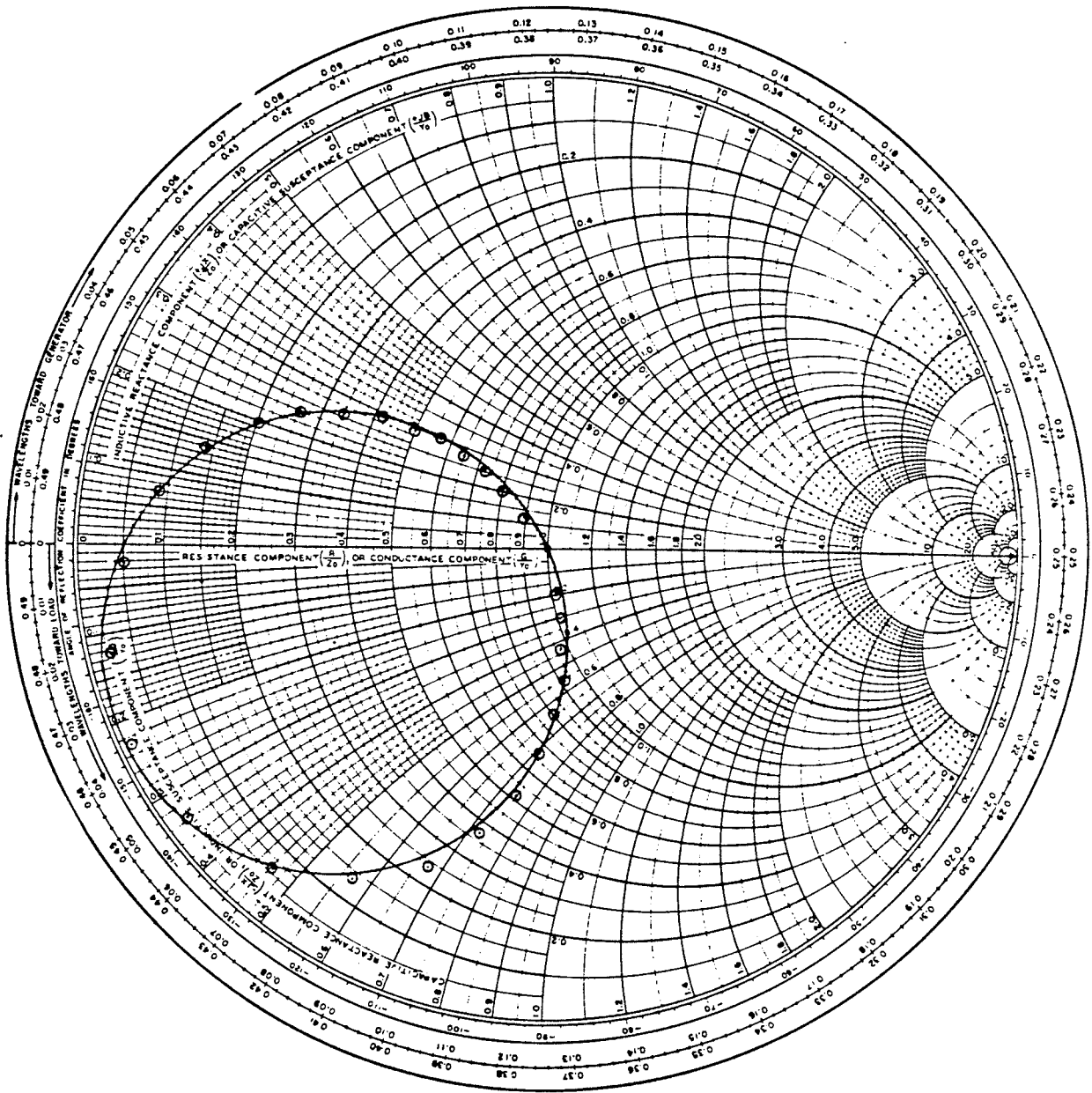
This variable reflection coefficient standard is used as a load to test the performance of the six-port system at a single frequency and over the 900-1100 MHz bandwidth. With the variable reflection coefficient standard connected to the load port of the six-port system readings of reflection coefficient for various stub length settings (of the variable reflection coefficient standard) have been taken to check the performance of the six-port system at a single frequency. To test the performance over a bandwidth of frequencies the stub length of the variable reflection coefficient standard is kept fixed and reflection coefficient readings obtained for different frequencies.

The values of reflection coefficient obtained for different stub length settings using the six-port system and the MNA are tabulated in table 5.3 along with the computed values of reflection coefficient. From

table 5.3 it is clear that the readings of reflection coefficient obtained for both magnitude and phase using the six-port system and MNA track very closely and the difference is less than 5% for all values where  $|\Gamma_{\ell}| \geq 0.2$ . In comparing these readings with the computed values of  $\Gamma_{\ell}$  it is seen that the discrepancy is less than 5% for all values of  $|\Gamma_{\ell}| > 0.4$ . For  $0.3 < |\Gamma_{\ell}| < 0.4$ , the difference is about 10% and for  $0.2 < |\Gamma_{\ell}| < 0.3$  the difference is about 15%. For  $|\Gamma_{\ell}| < 0.2$ , the accuracy is poor as one would normally expect. The computed results and the results obtained from the six-port system have been plotted on a Smith chart for comparison, see figure 5.2. The results obtained using the MNA have not been plotted separately because they track so closely with the six-port system results.

Table 5.3 Measurement of  $\Gamma_{\rho}$  at 1GHZ

Stub length setting (cm) + 0.25 cm	Reflection Coefficient ( $\Gamma_{\rho}$ )		
	Six-Port	MNA	Computed
8.5	0.099 $\angle -79.7^{\circ}$	0.00	0.13 $\angle -73.2^{\circ}$
9.0	0.150 $\angle -80.0^{\circ}$	0.15 $\angle -80^{\circ}$	0.19 $\angle -76.4^{\circ}$
9.5	0.216 $\angle -81.7^{\circ}$	0.20 $\angle -80^{\circ}$	0.24 $\angle -79.8^{\circ}$
10.0	0.285 $\angle -83.3^{\circ}$	0.28 $\angle -83^{\circ}$	0.31 $\angle -83.5^{\circ}$
10.5	0.360 $\angle -87.9^{\circ}$	0.36 $\angle -86^{\circ}$	0.37 $\angle -87.6^{\circ}$
11.0	0.440 $\angle -92.0^{\circ}$	0.44 $\angle -90^{\circ}$	0.44 $\angle -92.1^{\circ}$
11.5	0.536 $\angle -97.0^{\circ}$	0.54 $\angle -95^{\circ}$	0.53 $\angle -97.2^{\circ}$
12.0	0.630 $\angle -103.0^{\circ}$	0.62 $\angle -102^{\circ}$	0.61 $\angle -103.1^{\circ}$
12.5	0.726 $\angle -110.9^{\circ}$	0.73 $\angle -110^{\circ}$	0.70 $\angle -110.0^{\circ}$
13.0	0.820 $\angle -119.8^{\circ}$	0.82 $\angle -120^{\circ}$	0.79 $\angle -118.0^{\circ}$
13.5	0.900 $\angle -130.2^{\circ}$	0.90 $\angle -130^{\circ}$	0.88 $\angle -127.4^{\circ}$
14.0	0.960 $\angle -142.2^{\circ}$	0.97 $\angle -142^{\circ}$	0.95 $\angle -138.0^{\circ}$
14.5	0.980 $\angle -154.0^{\circ}$	1.00 $\angle -155^{\circ}$	0.99 $\angle -150.0^{\circ}$
15.0	0.960 $\angle -166^{\circ}$	0.97 $\angle -168^{\circ}$	0.99 $\angle -162.0^{\circ}$
15.5	0.914 $\angle -177.6^{\circ}$	0.91 $\angle -180^{\circ}$	0.95 $\angle -173.1^{\circ}$
16.0	0.840 $\angle -172.4^{\circ}$	0.81 $\angle 171^{\circ}$	0.88 $\angle +176.0^{\circ}$
16.5	0.760 $\angle 163.9^{\circ}$	0.74 $\angle 163^{\circ}$	0.79 $\angle 167.0^{\circ}$
17.0	0.674 $\angle 157.0^{\circ}$	0.65 $\angle 158^{\circ}$	0.70 $\angle 158.9^{\circ}$
18.0	0.524 $\angle 146.6^{\circ}$	0.52 $\angle 146^{\circ}$	0.53 $\angle 146.1^{\circ}$
18.5	0.450 $\angle 142.0^{\circ}$	0.44 $\angle 141^{\circ}$	0.45 $\angle 141.0^{\circ}$
19.0	0.380 $\angle 138.7^{\circ}$	0.38 $\angle 138^{\circ}$	0.38 $\angle 136.5^{\circ}$
19.5	0.330 $\angle 135.6^{\circ}$	0.33 $\angle 135^{\circ}$	0.31 $\angle 132.5^{\circ}$
20.0	0.260 $\angle 133.0^{\circ}$	0.26 $\angle 132^{\circ}$	0.25 $\angle 129.0^{\circ}$
20.5	0.212 $\angle 130.8^{\circ}$	0.20 $\angle 128^{\circ}$	0.19 $\angle 125.4^{\circ}$
21.0	0.156 $\angle 129.5^{\circ}$	0.16 $\angle 125^{\circ}$	0.13 $\angle 122.1^{\circ}$
21.5	0.080 $\angle 128.6^{\circ}$	0.10 $\angle 110^{\circ}$	0.08 $\angle 119.0^{\circ}$



— Computed  
 ○○○○ Six-port system and MNA

Figure 5.2 Plot of reflection coefficient with varying stub length

### 5.5 Calibration of the Six-Port System over a 220MHz bandwidth

The six-port system has been calibrated over a frequency bandwidth of 220 MHz (890-1110 MHz) at 20 MHz intervals. The calibration procedure has been explained in Chapter IV. The calibration constants determined at each calibration frequency point are presented in table 5.4. On examining  $Z \angle \phi_z$  from table 5.4 it is seen that the magnitude of  $Z$  decreases slowly from a value of 0.276 at 900 MHz to 0.049 at 1000 MHz (center frequency) and beyond 1000 MHz the value of  $Z$  increases to 0.257 at 1100 MHz. The argument of  $Z$  however remains constant at about  $170^\circ$  for frequencies below 1000 MHz and at  $-70^\circ$  for other frequencies. Ideally, the value of  $Z$  should have been zero at the design center frequency at which the five-port junction is well matched. The variation of  $Z \angle \phi_z$  with frequency has been plotted on the polar chart of figure 5.3. The calibration constant  $X_1 \angle \phi_{x1}$  varies slowly from a value of  $0.7 \angle 139.5^\circ$  at 900 MHz to a minimum value of  $0.392 \angle 51.0^\circ$  at 1020 MHz. Beyond 1020 MHz the magnitude starts increasing but, the argument still keeps decreasing gradually. The variation of  $X_1 \angle \phi_{x1}$  with frequency has been plotted on the polar chart of figure 5.4. The magnitude of the calibration constant  $X_2 \angle \phi_{x2}$  slowly decreases from a value of 0.673 at 900 MHz to a value of 0.472 at 1100 MHz.  $\phi_{x2}$  however remains steady around the value of  $200^\circ$ . The variation of the calibration constant  $X_2$  with frequency has been plotted on the graph of figure 5.5. The magnitude of the constant  $X_3 \angle \phi_{x3}$  increases slowly from a value of 0.309 at 900 MHz to 0.513 at 1100 MHz and  $\phi_{x3}$  decreases steadily from a value of  $34.5^\circ$  at 900 MHz to  $-93^\circ$  at 1100 MHz. The variation of  $x_3 \angle \phi_{x3}$  with frequency has been plotted on the graph of figure 5.6. Finally, the constants  $|B_1|$  and  $|B_3|$  stay within 0.23 to 0.26 over the 900-1100 MHz bandwidth whereas  $|B_2|$  varies from

0.3 at 900 MHz to 0.147 at 1100 MHz. Generally if the five-port junction were to be an ideal four-way power divider then the values of  $|B_i|$ ,  $i = 1, 2, 3$  would have been very close to 0.25 over the entire frequency range. From the above examination of the calibration constants we can conclude that the calibration constants are continuous and slowly varying or constant; hence, amenable to interpolation.

Table 5.4 Calibration Constants over a 220 MHz Bandwidth

Frequency (MHZ)	$z / \angle \theta_z$	$x_1 / \angle \theta_{x1}$	$x_2 / \angle \theta_{x2}$	$x_3 / \angle \theta_{x3}$	$ B_1 $	$ B_2 $	$ B_3 $
900	0.276 $\angle 176^\circ$	0.700 $\angle 139.5^\circ$	0.673 $\angle 203.0^\circ$	0.309 $\angle 34.5^\circ$	0.248	0.305	0.230
920	0.229 $\angle 173^\circ$	0.630 $\angle 130.0^\circ$	0.649 $\angle 173.4^\circ$	0.309 $\angle 13.1^\circ$	0.255	0.293	0.234
940	0.170 $\angle 166^\circ$	0.589 $\angle 116.3^\circ$	0.605 $\angle 198.6^\circ$	0.340 $\angle -11.3^\circ$	0.259	0.279	0.235
960	0.121 $\angle 167^\circ$	0.533 $\angle 104.4^\circ$	0.589 $\angle 198.6^\circ$	0.369 $\angle -30.2^\circ$	0.261	0.264	0.238
980	0.070 $\angle 176^\circ$	0.477 $\angle 90.5^\circ$	0.567 $\angle 197.0^\circ$	0.408 $\angle -47.0^\circ$	0.269	0.248	0.243
1000	0.049 $\angle 269^\circ$	0.410 $\angle 69.0^\circ$	0.510 $\angle 197.7^\circ$	0.483 $\angle -58.1^\circ$	0.272	0.231	0.250
1020	0.098 $\angle -69^\circ$	0.392 $\angle 51.0^\circ$	0.500 $\angle 198.0^\circ$	0.506 $\angle -66.7^\circ$	0.270	0.213	0.254
1040	0.150 $\angle -65^\circ$	0.395 $\angle 32.7^\circ$	0.483 $\angle 197.8^\circ$	0.522 $\angle -74.0^\circ$	0.266	0.194	0.254
1060	0.195 $\angle -66^\circ$	0.406 $\angle 16.5^\circ$	0.472 $\angle 197.5^\circ$	0.523 $\angle -80.1^\circ$	0.268	0.178	0.259
1080	0.232 $\angle -70^\circ$	0.421 $\angle 13.6^\circ$	0.475 $\angle 197.6^\circ$	0.523 $\angle -86.7^\circ$	0.265	0.162	0.260
1100	0.257 $\angle -75^\circ$	0.436 $\angle -9.0^\circ$	0.472 $\angle 183.0^\circ$	0.513 $\angle -93.0^\circ$	0.260	0.147	0.259

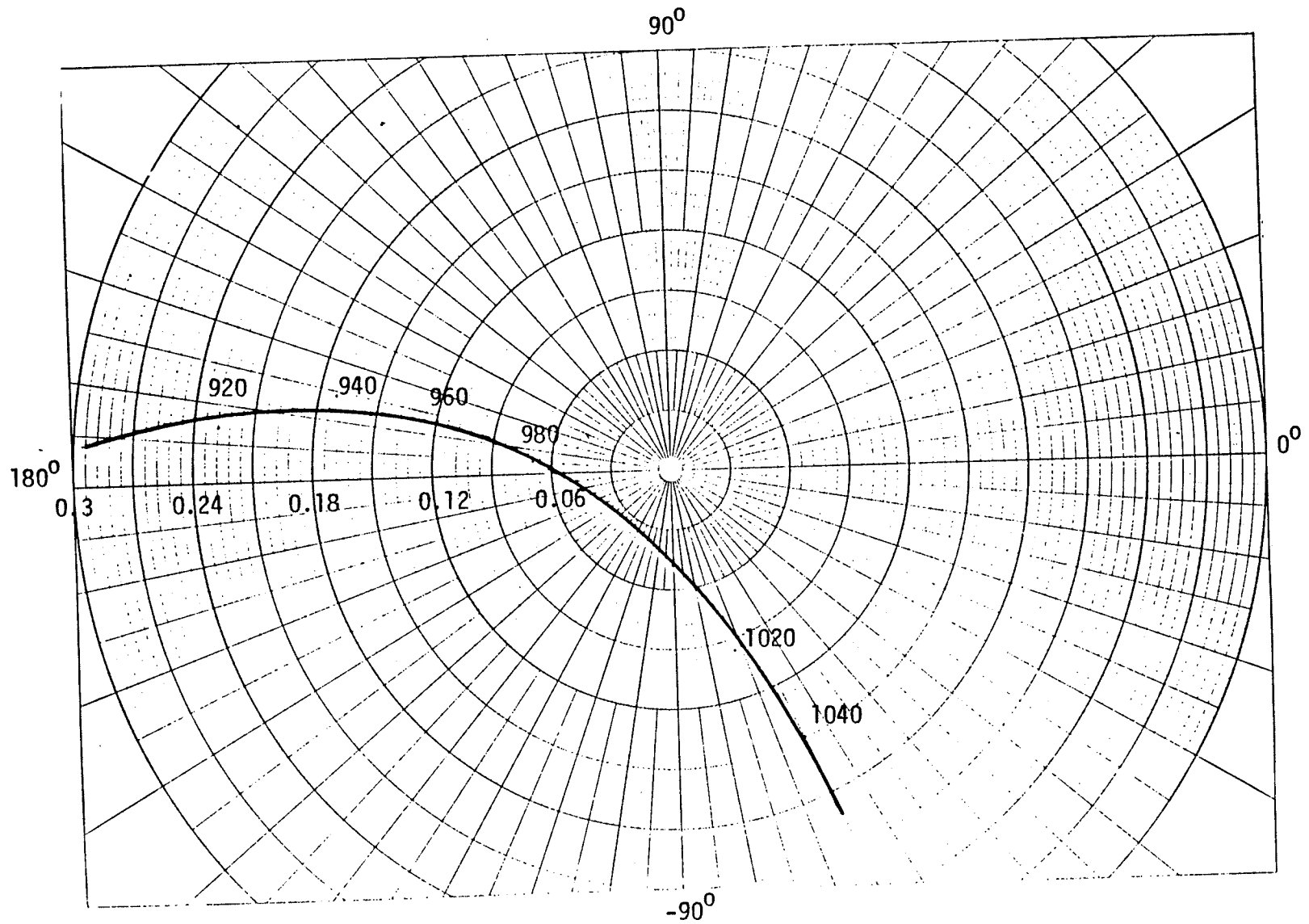


Figure 5.3 Variation of  $z/\theta_z$  with frequency (MHZ)

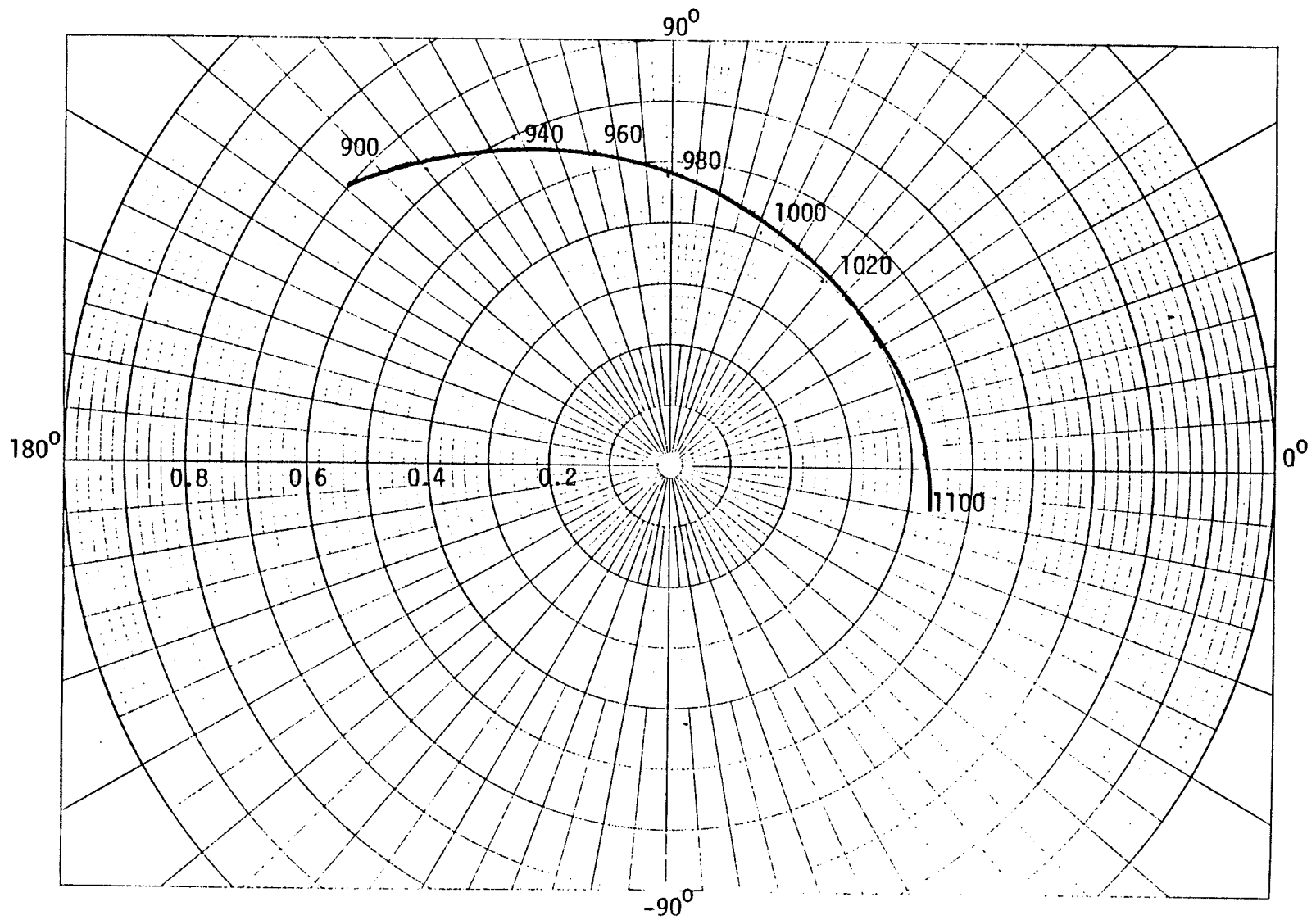


Figure 5.4 Variation of  $X_1/\theta_{x1}$  with frequency(MHZ)

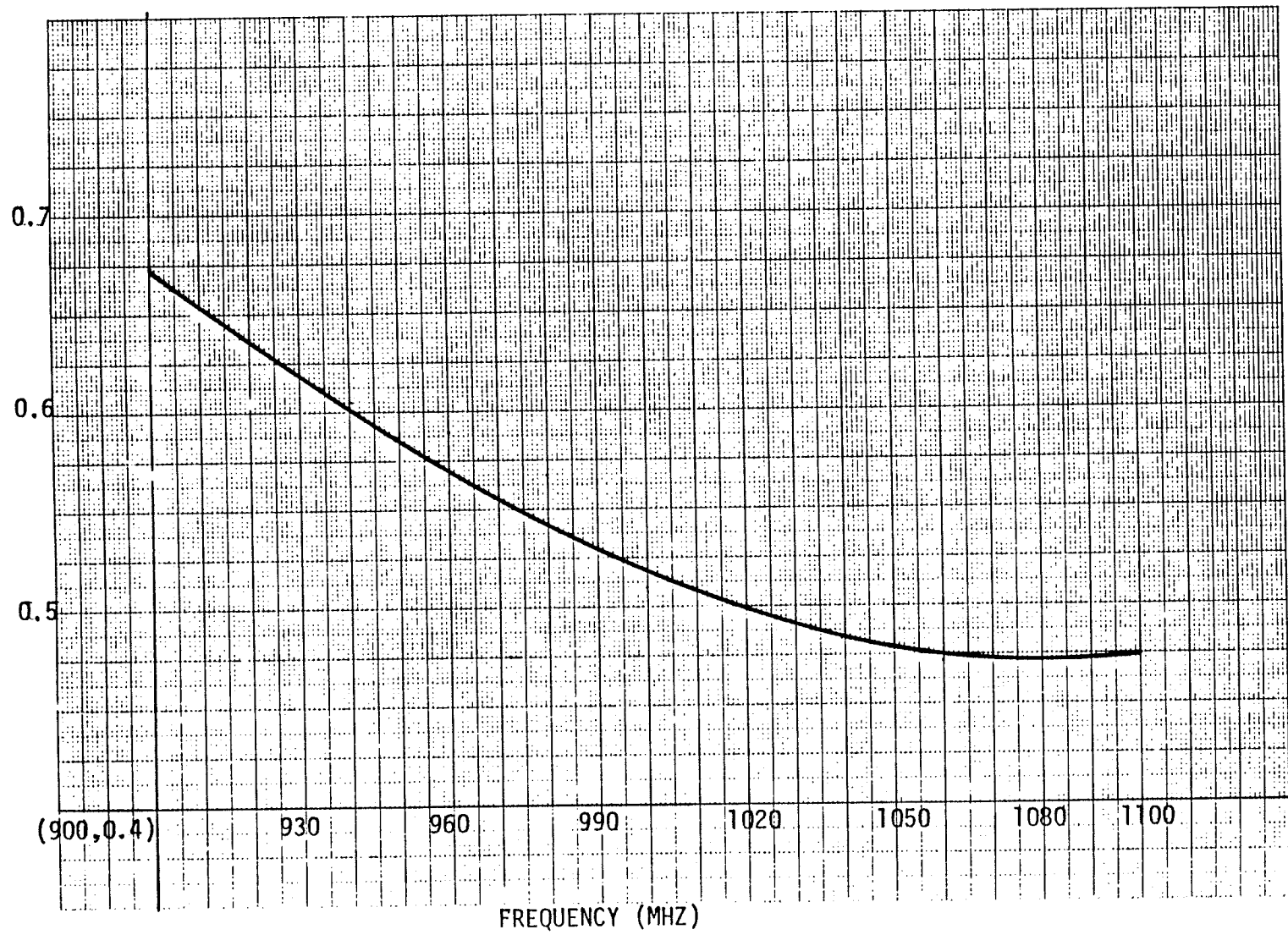


Figure 5.5 Variation of  $X_2 / \phi_{x2}$  with frequency

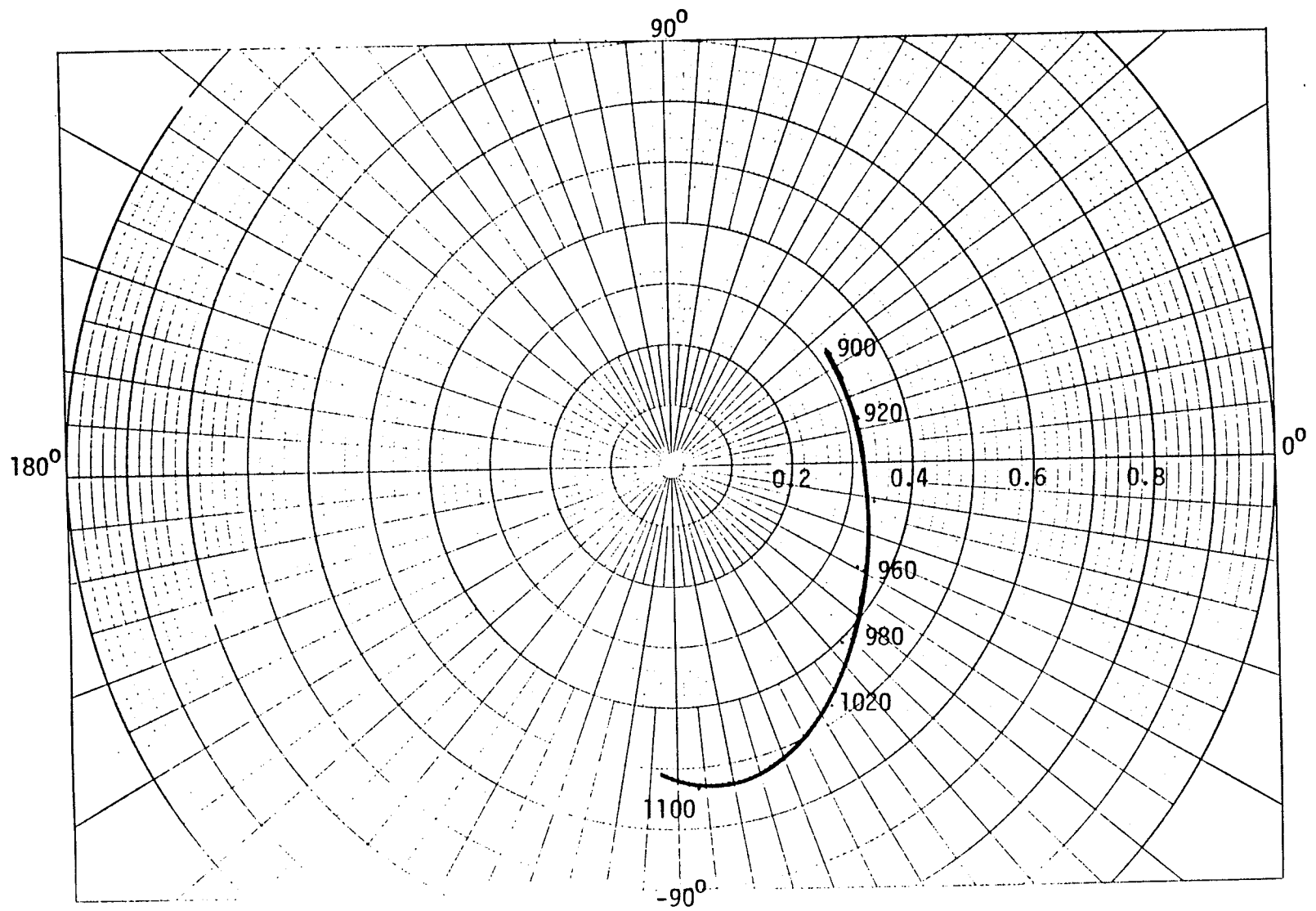


Figure 5.6 Variation of  $X_3/|\Gamma_{x3}|$  with frequency(MHZ)

### 5.6 Measurement of $\Gamma_{\ell}$ over the 220 MHz Bandwidth

With the variable reflection coefficient standard shown in figure 5.1 connected to the load port of the six-port system measurements of  $\Gamma_{\ell}$  over the 900-1100 MHz bandwidth have been performed. The measurement procedure has been explained in Chapter IV. Measurement of  $\Gamma_{\ell}$  has been repeated for two particular stub positions of the variable reflection coefficient standard. This was necessary in order to check the performance of the six-port system for a full range of values of  $|\Gamma_{\ell}|$ . The results obtained using the six-port system and the MNA for the first stub setting are tabulated in table 5.5 along with the computed values of  $\Gamma_{\ell}$ .

Table 5.5 Results of  $\Gamma_{\ell}$  over (900-1100) MHz

Frequency (MHz)	Reflection Coefficient ( $\Gamma_{\ell}$ )		
	Six-Port	MNA	Computed
900	0.570 $\angle -71.31^{\circ}$	0.57 $\angle -68^{\circ}$	0.578 $\angle -67.6^{\circ}$
910	0.594 $\angle -71.82^{\circ}$	0.60 $\angle -72^{\circ}$	0.600 $\angle -72.3^{\circ}$
920	0.626 $\angle -83.75^{\circ}$	0.61 $\angle -78^{\circ}$	0.624 $\angle -77.3^{\circ}$
930	0.644 $\angle -80.33^{\circ}$	0.63 $\angle -80^{\circ}$	0.640 $\angle -82.0^{\circ}$
940	0.681 $\angle -90.37^{\circ}$	0.68 $\angle -89^{\circ}$	0.670 $\angle -87.8^{\circ}$
950	0.707 $\angle -92.74^{\circ}$	0.70 $\angle -92^{\circ}$	0.700 $\angle -92.9^{\circ}$
960	0.738 $\angle -100.77^{\circ}$	0.73 $\angle -99^{\circ}$	0.720 $\angle -98.3^{\circ}$
970	0.749 $\angle -103.54^{\circ}$	0.74 $\angle -103^{\circ}$	0.750 $\angle -103.7^{\circ}$
980	0.781 $\angle -109.81^{\circ}$	0.78 $\angle -109^{\circ}$	0.770 $\angle -109.5^{\circ}$
990	0.811 $\angle -113.33^{\circ}$	0.80 $\angle -112^{\circ}$	0.796 $\angle -114.9^{\circ}$
1000	0.817 $\angle -120.08^{\circ}$	0.82 $\angle -121^{\circ}$	0.820 $\angle -120.7^{\circ}$
1010	0.862 $\angle -123.75^{\circ}$	0.85 $\angle -125^{\circ}$	0.845 $\angle -126.5^{\circ}$
1020	0.857 $\angle -132.22^{\circ}$	0.85 $\angle -132^{\circ}$	0.860 $\angle -132.6^{\circ}$
1030	0.909 $\angle -135.08^{\circ}$	0.90 $\angle -136^{\circ}$	0.890 $\angle -138.4^{\circ}$
1040	0.893 $\angle -145.64^{\circ}$	0.90 $\angle -144^{\circ}$	0.91 $\angle -144.5^{\circ}$
1050	0.925 $\angle -148.02^{\circ}$	0.92 $\angle -149^{\circ}$	0.93 $\angle -150.8^{\circ}$
1060	0.921 $\angle -160.14^{\circ}$	0.94 $\angle -158^{\circ}$	0.947 $\angle -157.0^{\circ}$
1070	0.967 $\angle -160.62^{\circ}$	0.96 $\angle -161^{\circ}$	0.963 $\angle -163.9^{\circ}$
1080	0.954 $\angle -174.37^{\circ}$	0.97 $\angle -171^{\circ}$	0.975 $\angle -170.0^{\circ}$
1090	0.986 $\angle -170.49^{\circ}$	0.98 $\angle -174^{\circ}$	0.987 $\angle -177.0^{\circ}$
1100	0.965 $\angle 172.14^{\circ}$	0.98 $\angle +174^{\circ}$	0.99 $\angle 177.0^{\circ}$

— Computed

••••• Six-port system and MNA

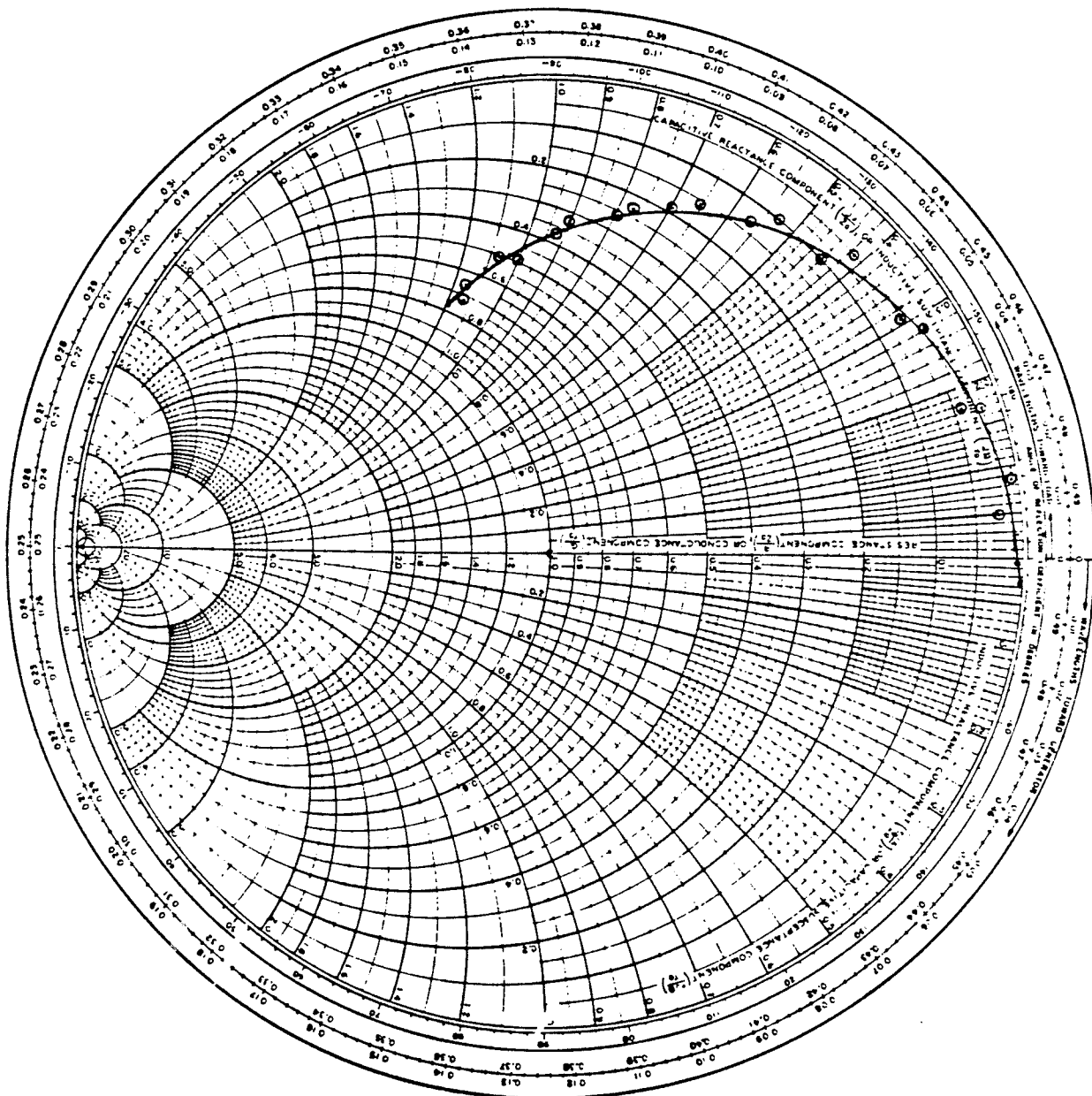


Figure 5.7 Plot of  $\Gamma_{\ell}$  with change in frequency

The computed results and the results obtained from the six-port system have been plotted on the Smith Chart of figure 5.7 for comparison. From table 5.5 it is seen that the values of  $\Gamma_{\ell}$  (magnitude and phase) obtained using the six-port system and the MNA track closely with the computed  $\Gamma_{\ell}$  with an error of less than 5%. Having evaluated the performance of the six-port system over the 900-1100 MHz bandwidth for  $0.6 \leq |\Gamma_{\ell}| < 1.0$ , the stub length on the variable reflection coefficient standard was changed and measurement for  $0.0 < |\Gamma_{\ell}| < 0.6$  performed. The results obtained using the six-port system and MNA are tabulated in table 5.6 along with the computed values of  $\Gamma_{\ell}$ . From table 5.6 it is seen that the magnitude and phase of the reflection coefficient obtained from the six-port system and the MNA track within 5% of the computed figures for all values of  $|\Gamma_{\ell}| > 0.2$ . For values of  $|\Gamma_{\ell}| < 0.2$  the agreement is poor as one would expect. The results obtained using the six-port system have been plotted on the Smith chart of figure 5.8 along with the computed values of  $\Gamma_{\ell}$  for comparison. The values obtained using the MNA have not been plotted because they track very closely with the six-port system results.

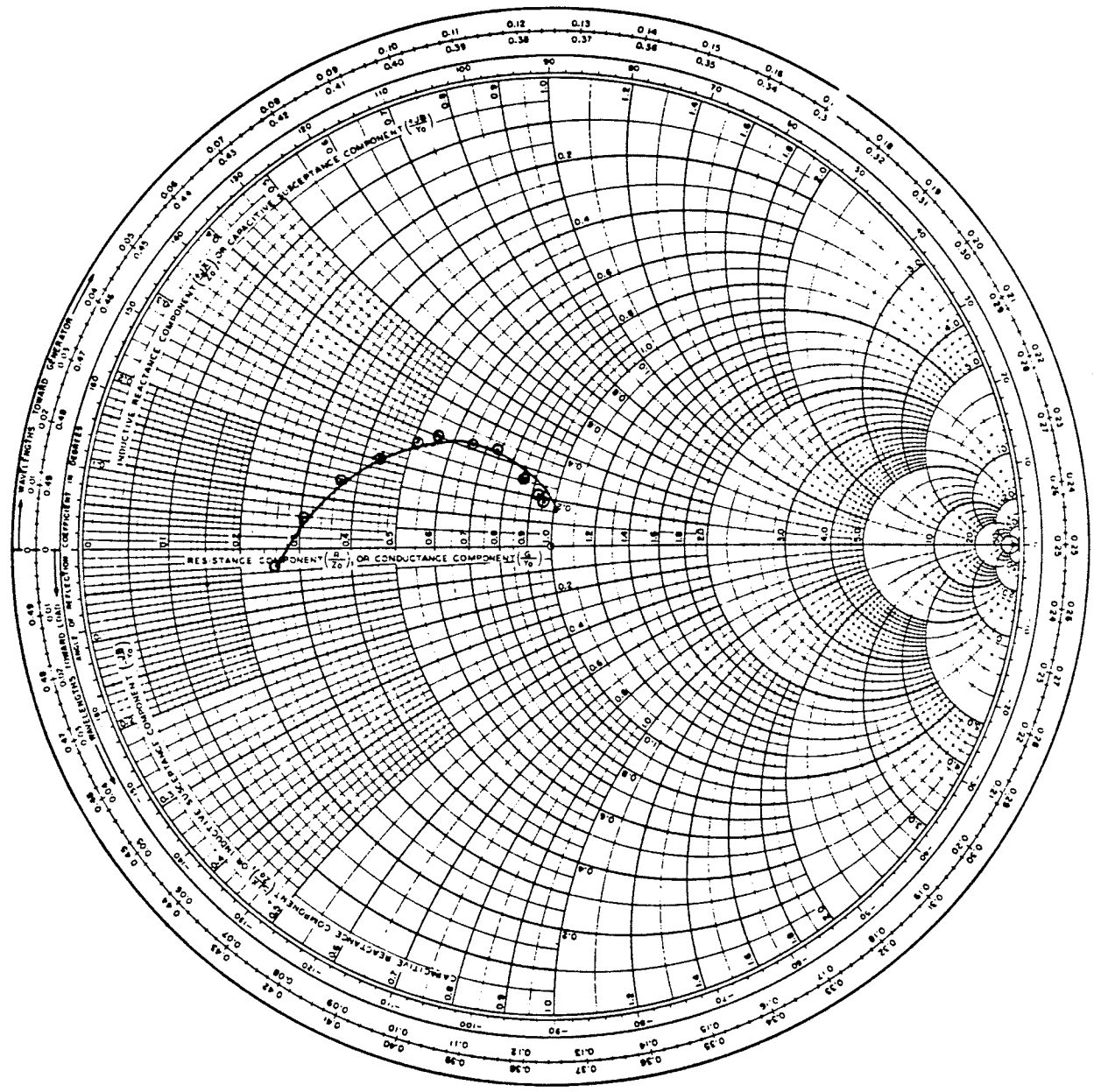


Figure 5.8 Plot of  $\Gamma_L$  with change in frequency

Table 5.6 Results of  $\Gamma_p$  over (900-1100) MHz

Frequency (MHz)	Reflection Coefficient ( $\Gamma_p$ )		
	Six-Port	MNA	Computed
900	0.590 $\angle -176.26^\circ$	0.58 $\angle -176^\circ$	0.579 $\angle -176.8^\circ$
920	0.527 $\angle 173.74^\circ$	0.53 $\angle 172^\circ$	0.520 $\angle 172.4^\circ$
940	0.466 $\angle 162.45^\circ$	0.45 $\angle 161^\circ$	0.455 $\angle 161.6^\circ$
960	0.415 $\angle 152.33^\circ$	0.42 $\angle 152^\circ$	0.400 $\angle 151.2^\circ$
980	0.360 $\angle 141.74^\circ$	0.36 $\angle 141^\circ$	0.340 $\angle 141.1^\circ$
1000	0.328 $\angle 135.04^\circ$	0.31 $\angle 133^\circ$	0.300 $\angle 132.0^\circ$
1020	0.269 $\angle 127.12^\circ$	0.25 $\angle 124^\circ$	0.240 $\angle 122.0^\circ$
1040	0.226 $\angle 119.82^\circ$	0.21 $\angle 115^\circ$	0.200 $\angle 112.4^\circ$
1060	0.144 $\angle 111.55^\circ$	0.14 $\angle 105^\circ$	0.149 $\angle 103.0^\circ$
1080	0.115 $\angle 104.06^\circ$	0.10 $\angle 100^\circ$	0.110 $\angle 94.1^\circ$
1100	0.099 $\angle 99.68^\circ$	0.00	0.065 $\angle 84.6^\circ$

## Chapter VI

### Conclusions

A six-port system based on a matched symmetric five-port junction and a directional coupler has been developed. The five-port junction has been realized on stripline in the form of a ring type circuit with simple internal structure matching. All ports of the junction are well matched at the center frequency of 1 GHz and assuming a return loss of -10 dB as sufficiently well matched, a useful bandwidth of 25% has been easily realized.

Using the symmetric five-port junction, a six-port microwave system has been synthesized in such a way that both the magnitude and the phase of a load reflection coefficient can be determined.

First, to establish the accuracy of the six-port microwave measurement system calibration constants at the center frequency of 1 GHz were determined and return loss measurements made on a short-circuit terminated attenuator. It was found from these results that the six-port accurately measured return loss down to a level of -15 dB, which corresponds to  $|\Gamma_L|$  of about 0.2. Hence, from the return loss measurements it was established that the six-port system could not accurately measure values of  $|\Gamma_L| < 0.2$ .

Next, to determine the system measurement accuracy for both magnitude and phase of the reflection coefficient at the center frequency, measurements were made using the variable reflection - coefficient load standard. It is clear from the results obtained that for all values of  $|\Gamma_L| \geq 0.2$ , the load reflection coefficient has been determined both in magnitude and phase within an error of less than 5%. Having thus established the accuracy of the six-port microwave measurement system at the center fre-

quency measurements of  $\Gamma_L$  of two load standards were made over a 20% Bandwidth (900-1100 MHz). In order to make measurements over a bandwidth of frequencies it is necessary to know the calibration constants over the entire frequency bandwidth. Upon determining the calibration constants at equal spaced frequency points in the bandwidth it was seen that all constants were either continuous and slowly varying or nearly constant and hence they are amenable to interpolation. Since the calibration constants did not vary significantly over a 20 MHz intervals it was decided that it would suffice if the calibration constants were determined at frequency intervals of 20 MHz over the 900-1100 MHz bandwidth.

For all frequencies within a particular 20 MHz interval the calibration constants are assumed to be constant. Using the calibration constants determined at eleven frequency points over the 900-1100 MHz bandwidth measurements of  $\Gamma_L$  have been made and the results indicate an error of less than 5% both in magnitude and phase for all values of  $|\Gamma_L| \geq 0.2$ . Hence, it can be concluded that the six-port system which has been developed can be successfully used to measure load reflection coefficients at any frequency over a 200 MHz frequency bandwidth centered at 1 GHz with an error of less than 5%.

Generally speaking, our calibration procedure has served its purpose. However, it should be recalled that in order to calibrate the six-port system at a frequency point a matched load, a short, an open and two offset opens ( $\pm 90^\circ$ ) were required. The offset open standards are different for each frequency point and have to be generated using a MNA. Hence, a total of 25 load standards were needed to calibrate the six-port at the eleven frequency points in the frequency band 900-1100 MHz. This is a

very laborious procedure and a more efficient procedure needs to be developed, whereby the number of load standards used to calibrate the six-port system is reduced. Additionally, the versatility of the six-port measurement system would be considerably enhanced if the five-port junction could be made broad-band over at least an octave of band-width. Finally, as an observation, the A/D converter has a dynamic input range of -5 to +5 volts and because of the linear type of amplifiers used the entire dynamic range could not be effectively used. It is hence suggested that logarithmic amplifiers be utilized to more efficiently use the full dynamic range of the A/D converter.

In summary, the major advantage of the six-port system lies in the simplicity of its amplitude detection system and its potential for use at millimeter wave frequencies where heterodyne detection is difficult. The results from the measurement of complex reflection coefficient are very encouraging. Once an efficient calibration routine is developed the six-port shall emerge as a viable and practical alternative to the existing expensive automatic network analyzer.

## REFERENCES

- 1 C.A. Hoer, "The Six-Port Coupler: A new approach to measuring voltage, current, power, impedance, and phase," IEEE Trans. Instrum. Meas., vol. IM-21, pp. 446-470, Nov. 1982.
- 2 G.F. Engen and C.A. Hoer, "Application of an arbitrary six-port junction to power-measurement problems," IEEE Trans. Instrum. Meas., Vol. IM-21, pp. 470-474. Nov. 1972.
- 3 Harry M. Cronson and Leon Susman, "A Dual Six-port automatic network analyzer," IEEE Trans. on Microwave Theory and Techniques, vol. MTT-29, No. 4, pp. 372-378, April 1981.
- 4 Glenn F. Engen, "Determination of Microwave phase and Amplitude from power measurements," IEEE Trans. Instrum. Meas., vol. IM-25, pp. 414-418, Dec. 1976.
- 5 Glenn F. Engen, "An improved circuit for implementing the six-port technique of microwave measurements," IEEE Trans. on Microwave Theory and Techniques, vol. MTT-25, No. 12, pp. 1080-1083, sec. 1977.
- 6 Gordon P. Riblet & E.R. Bertil Hansson, "The use of a matched Symmetrical five-port junction to make six-port measurements," 1981 IEEE MTT-S International Microwave Symposium digest; IEEE catalog No. 81, CH 1592-5, pp. 151-53.
- 7 Glenn F. Engen, "The Six-port Reflectometer: An Alternative Network Analyzer," IEEE Trans. on Microwave Theory and Techniques vol. MTT-25, No. 12, pp. 1075-1079, Dec. 1977.
- 8 Glenn F. Engen, "Advances in Microwave Measurement Science," proc. IEEE, Vol. 66, No. 4, pp. 374-383, April 1978.
- 9 A.L. Samuel, "An oscilloscope method of presenting impedance on the reflection coefficient plane," Proc. IRE, vol. 35, pp. 1279-1283, Nov. 1947.

[10] Shihe L. . and Renato G. Bosisio, "Calibration of Multiport Reflectometers by Means of four open/short circuits," IEEE Trans. on Microwave Theory & Techniques vol. MTT-30, No. 7, pp. 1085-1090, July 1982.

[11] R.E. Collin, "Foundations for Microwave Engineering," McGraw-Hill Book Company, 1966, Ch. 5-6.

[12] A.L. Cullen, S.K. Judah and F. Nikraves, "Impedence Measurement Using a Six-Port directional coupler," IEE proc. vol. 127, pp H. No. 2, pp. 92-97, April 1980.

[13] D. Woods "Analysis and Calibraton theory of the general 6-port reflectometer employing four amplitude detectors," proc. IEEE, vol. 126, No. 2, pp. 221-228, February 1979.

[14] E.P. Riblet and E.R. Bertil Hansson, "Aspects of the calibration of a single six-port using a load and offset reflection standards," IEEE Trans. on Microwave Theory and Techniques, vol. MTT-30, No. 12, pp. 2120-2125, Dec. 1982.

## APPENDIX A

## Determination of strip widths

The "Standard Polyguide" on which the five-port has been etched is a copper-clad, irradiated, high-density polyolefin laminate. The following specifications have been obtained from the "POLYGUIDE SPECIFICATIONS AND DESIGN INFORMATION" data book.

Designation	Dielectric thickness	Clad Copper Thickness
1/16" polyguide	$0.062 \pm 0.002$ "	10Z:0.0014" +10%

## Electrical Properties:

Dielectric Constant: The dielectric constant at 1300 McS is  $2.320 \pm 0.005$ .

Dissipation factor:  $0.0002 \pm 0.00005$  at 1McS

Attenuation: for copper clad material 0.14 dB/ft for 50 ohm line at 1300 McS.

## Design specifications

Center Frequency = 1GHZ

$$Z_0 = 43.3$$

$$Z_0' = 86.6$$

$$\epsilon = 2.328$$

We know that the velocity of propagation is given by

$$\begin{aligned} v &= \frac{c}{\lambda} \\ &= \frac{3 \times 10^{10}}{2.328} = 1.96621 \times 10^{10} \text{ cm/sec} \end{aligned}$$

Thus,

$$\lambda = \frac{1.96621 \times 10^{10}}{10^9}$$

$$\lambda = 19.662 \text{ cm}$$

The line widths corresponding to 43.3 , 50 and 86.6 ohms are, as obtained from the graph of figure A.1  $0.1125''$ ,  $0.09''$  and  $0.0316''$  respectively.

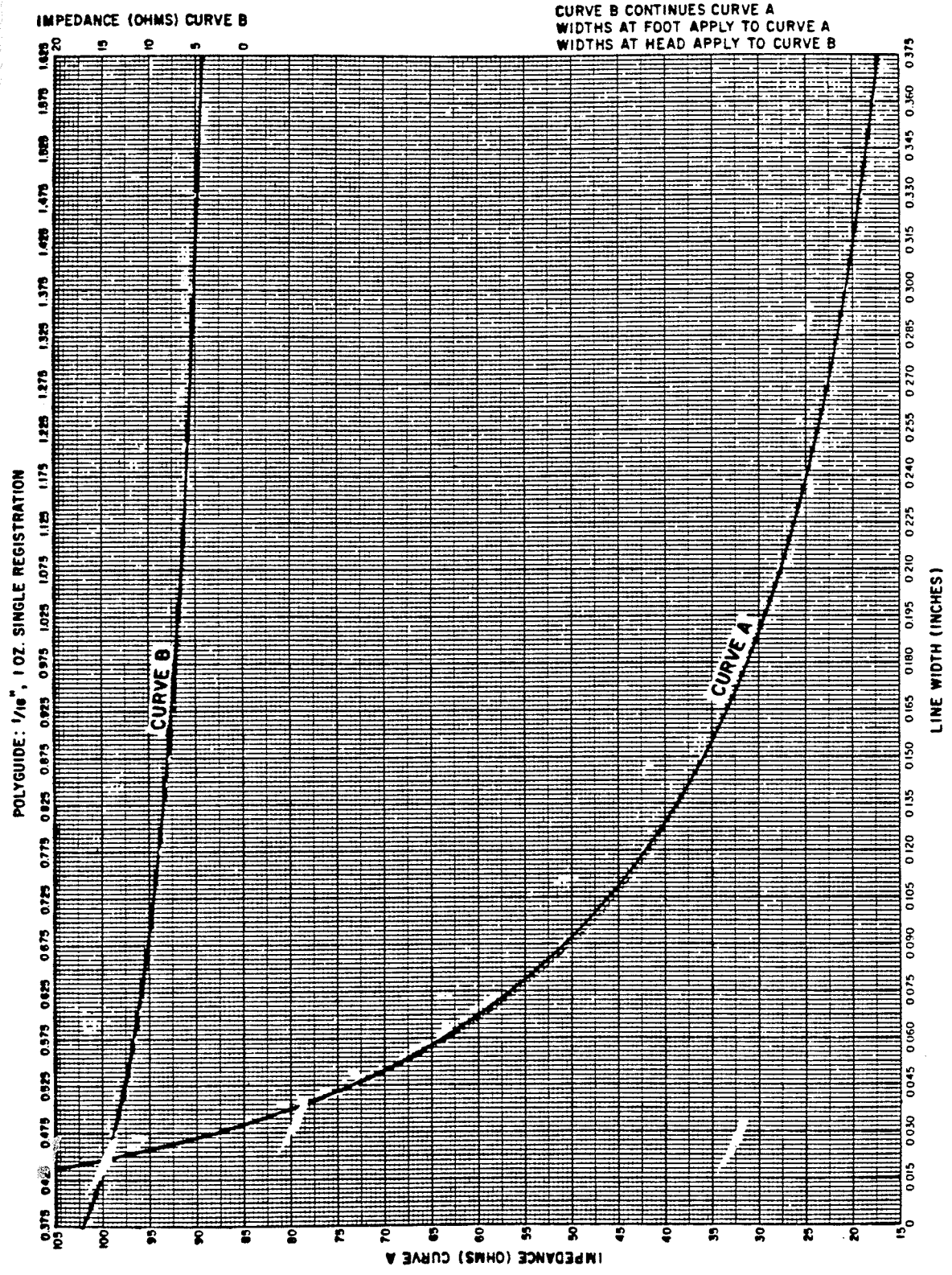
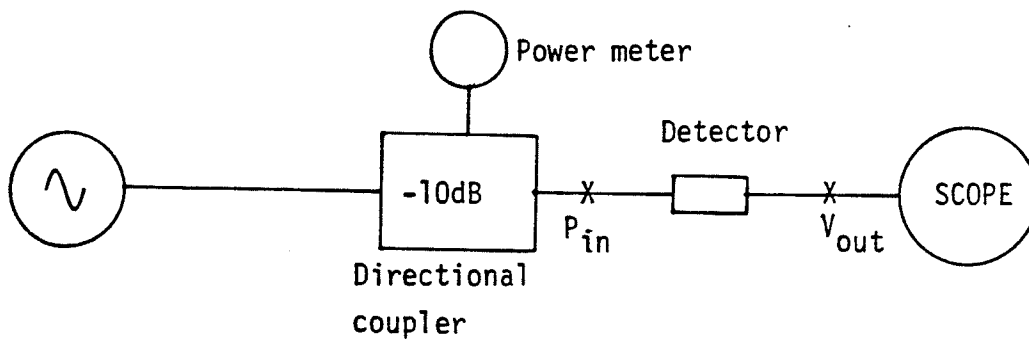


Fig. A.1 Impedance Vs Line widths for 1/16", 10 Z Polyguide

## APPENDIX B

## Detector characterisation

Each of the four detectors used (model-Wiltron #73N50) have been characterized by taking a set of readings of the input power and the output volts making use of an arrangement similar to the one shown below. The readings have been tabulated in table B.1.



Using the results of table B.1 each detector is characterized by a second order polynomial of the form

$$P = a + bv + cv^2 \quad (B.1)$$

where  $P$  is the input power (dBm) and  $v$  is the output voltage.

For detector #1

$$a = 6.163; b = 207.09 \text{ and } c = 19.161$$

For detector #2

$$a = 0.959; b = 75.33 \text{ and } c = 17.88$$

For detector #3

$$a = -0.027; b = 179.45 \text{ and } c = 11.186$$

For detector #4

$$a = -1.38; b = 123.9 \text{ and } c = 13.88.$$

Detector#1		Detector#2		Detector#3		Detector#4	
Input Power (dBm)	Output Volts						
-28.30	0.0	-28.15	0.0	-28.71	$2.45 \times 10^{-2}$	-26.34	$2.94 \times 10^{-2}$
-26.63	0.0	-26.30	$9.79 \times 10^{-3}$	-26.68	$2.84 \times 10^{-2}$	-25.01	$3.42 \times 10^{-2}$
-24.54	$4.89 \times 10^{-3}$	-26.05	$1.08 \times 10^{-2}$	-25.40	$2.94 \times 10^{-2}$	-24.38	$3.91 \times 10^{-2}$
-23.44	$9.78 \times 10^{-3}$	-24.83	$1.96 \times 10^{-2}$	-23.32	$3.91 \times 10^{-2}$	-23.15	$4.89 \times 10^{-2}$
-22.80	$1.47 \times 10^{-2}$	-23.40	$3.91 \times 10^{-2}$	-22.18	$4.40 \times 10^{-2}$	-22.06	$5.87 \times 10^{-2}$
-21.55	$1.96 \times 10^{-2}$	-22.47	$5.38 \times 10^{-2}$	-21.36	$5.4 \times 10^{-2}$	-21.31	0.068
-20.61	$2.45 \times 10^{-2}$	-21.53	$7.34 \times 10^{-2}$	-20.47	$5.87 \times 10^{-2}$	-20.88	$7.34 \times 10^{-2}$
-19.73	$3.43 \times 10^{-2}$	-20.92	$8.81 \times 10^{-2}$	-19.69	0.068	-19.19	0.107
-18.52	$4.89 \times 10^{-2}$	-19.47	0.1316	-18.72	$8.27 \times 10^{-2}$	-18.36	0.13
-17.74	$5.87 \times 10^{-2}$	-18.23	0.1761	-17.94	$9.3 \times 10^{-2}$	-17.48	0.15
-16.47	$7.83 \times 10^{-2}$	-17.15	0.23	-16.50	0.122	-16.06	0.21
-15.20	0.113	-16.03	0.298	-15.31	0.157	-15.54	0.23
-14.30	0.14	-15.24	0.36	-14.47	0.19	-14.93	0.26
-12.56	0.215	-13.82	0.49	-13.48	0.235	-13.07	0.39
-11.58	0.274	12.35	0.67	-12.48	0.298	-12.78	0.416
-10.56	0.35	-11.80	0.75	-11.12	0.4	-11.41	0.56
-9.15	0.49	-10.80	0.91	-10.27	0.49	-10.32	.704

-8.57	0.57	-9.76	1.12	-9.07	0.641	-9.05	0.924
-7.41	0.75	-8.38	1.45	-8.01	0.82	-8.28	1.08
-5.99	1.05	-7.31	1.76	-7.23	0.98	-7.58	1.25
-4.60	1.43	-6.84	1.88	-6.54	1.14	-7.00	1.40
-3.38	1.86	-5.13	2.52	-5.58	1.41	-6.46	1.57
-3.24	1.90	-4.17	2.96	-4.84	1.66	-5.83	1.77
-2.87	2.05	-3.30	3.41	-4.03	1.97	-4.67	2.2
-1.63	2.63	-2.53	3.86	-3.26	2.30	-3.91	2.56
-0.20	3.46	-2.15	4.1	-2.55	2.67	-2.94	3.06
0.96	4.29	-1.67	4.41	-1.69	3.17	-2.00	3.63
1.33	4.58	-1.29	4.70	-0.24	4.19	-1.08	4.26
1.73	4.90	-0.94	4.93	0.43	4.74	-0.43	4.76

Table B.1 Detector characteristics

## APPENDIX C

## PROGRAM LISTING

```

REF - 6P      10 DISP "MEASUREMENT OF REF. COE
              FF USING 6-PORT NW!"
              20 WAIT 4000
              30 CLEAR
              40 OPTION BASE 1
              50 DEG
              60 ASSIGN# 1 TO "CONST1"
              70 DIM N(101),F0(101),X(3),C(3)
                ,S(3),B(3),P(3),J4(101),J1(1
                01)
              80 OUTPUT 705 ; "MIR0F0"
              90 OUTPUT 716 USING "K,K" ; "B"
                ;3;"R1YPMPOM"
            100 CLEAR
            110 DISP "ENTER LO AND HI FREQUE
                NCIES"
            120 INPUT F1,F2
            130 R1=F2-F1
            140 CLEAR
            150 DISP "NUMBER OF FREQUENCY IN
                TERVALS TO BE SWEPT?"
            160 INPUT N1
            170 CLEAR
            180 N3=N1+1
            190 N2=N1/5
            200 N0=1.5*N2
            210 FOR I=1 TO N3
            220 F0(I)=(I-1)*R1/N1+F1
            230 F0(I)=INT(F0(I)*10)/10
            240 N(I)=INT((F0(I)-10)*.5289399
                6755+109 4)
            250 NEXT I
            260 FOR T=1 TO N3
            270 K1=N(T)-25
            280 K1=K1-3
            290 C2=1
            300 K1=K1+3
            310 OUTPUT 705 ; "V";K1;"E"
            320 WAIT 30
            330 ENTER 716 ; F3
            340 C1=F3/1000000-F0(T)
            350 IF ABS(C1)<10 THEN GOTO 400
            360 IF C1>0 THEN K1=K1-10
            370 IF C1<0 THEN K1=K1+10
            380 IF C2<4 THEN C2=C2+1 ELSE 29
                0
            390 GOTO 310
            400 OUTPUT 716 "YPMPD";F0(T);"MR
                C"
            410 WAIT 30
            420 ENTER 716 ; F4
            430 F4=F4/1000
            440 WAIT 30
            450 ENTER 716 ; F5
            460 F5=F5/1000
            470 F6=ABS(F5-F4)
            471 IF F6>10 THEN GOTO 420
            480 K2=5/1022
            490 C=1
            500 WAIT 30

```

```

510 OUTPUT 706 USING "#,K,K" ; "
H",C,"AJ","F"
520 S=0
530 FOR J=1 TO 10
540 WAIT 30
550 ENTER 706 USING "#,W" ; V(1)
560 S=S+V(1)
570 NEXT J
580 V(1)=K2*S/10
590 X=V(1)
600 P(1)=6.162983+207.0921*X+19.
16073*X^2
610 C=2
620 WAIT 300
630 OUTPUT 706 USING "#,K,K" ; "
H",C,"AJ","F"
640 S=0
650 FOR J=1 TO 10
660 WAIT 300
670 ENTER 706 USING "#,W" ; V(2)
680 S=S+V(2)
690 NEXT J
700 V(2)=K2*S/10
710 X=V(2)
720 R=10*(.9590646+75.32981*X+17
.8778*X^2)
730 C=4
740 WAIT 300
750 OUTPUT 706 USING "#,K,K" ; "
H",C,"AJ","F"
760 S=0
770 FOR J=1 TO 10
780 WAIT 300
790 ENTER 706 USING "#,W" ; V(3)
800 S=S+V(3)
810 NEXT J
820 V(3)=K2*S/10
830 X=V(3)
840 P(3)=-.02710391+179.4503*X+1
1.18641*X^2
850 C=8
860 WAIT 300
870 OUTPUT 706 USING "#,K,K" ; "
H",C,"AJ","F"
880 S=0
890 FOR J=1 TO 10
900 WAIT 300
910 ENTER 706 USING "#,W" ; V(4)
920 S=S+V(4)
930 NEXT J
940 V(4)=K2*S/10
950 X=V(4)
960 P(2)=-1.375671+123.8964*X+13
.8794*X^2
970 OUTPUT 706 USING "H"
980 Q=IP((F0(T)-890)/20)+1
990 READ# 1,Q ; Z,A9,X(1),X(2),X
(3),C(1),C(2),C(3),S(1),S(2)
,S(3),B(1),B(2),B(3)
1000 N=3

```

```

1010 M=1
1020 DIM F(3,3),W(3,1),I1(3)
1030 FOR I=1 TO 3
1040 F(I,1)=P(I)/R/B(I)*Z^2-X(I)
      ^2
1050 F(I,2)=P(I)/R/B(I)*Z*COS(A9
      )-C(I)
1060 F(I,3)=S(I)-P(I)/R/B(I)*Z*S
      IN(A9)
1070 W(I,1)=1-P(I)/R/B(I)
1080 NEXT I
1090 GOSUB 1110
1100 GOTO 1070
1110 W1=N<=0 OR M<=0
1120 IF W1=0 THEN 1160
1130 PRINT "ERROR IN SUBROUTINE"
1140 PRINT "N=";N;"M=";M @ PAUSE
      @ GOTO 1110
1150 DIM W2(3),X2(3)
1160 GOSUB 1540
1170 FOR J=1 TO M
1180 FOR I=1 TO N
1190 W2(I)=W(I,J)
1200 NEXT I
1210 GOSUB 1270
1220 FOR I=1 TO N
1230 W(I,J)=X2(I)
1240 NEXT I
1250 NEXT J
1260 RETURN
1270 W1=N<=0
1280 IF W1=0 THEN 1310
1290 PRINT "ERROR IN SUBROUTINE
      " @ PRINT "N=";N @ PAUSE
1300 GOTO 1270
1310 I2=I1(1) @ X2(1)=W2(I2)
1320 FOR C=2 TO N
1330 I2=I1(C) @ S=0
1340 FOR D=1 TO C-1
1350 S=S+F(I2,D)*X2(D)
1360 NEXT D
1370 X2(C)=W2(I2)-S
1380 NEXT C
1390 I2=I1(N)
1400 IF F(I2,N)<>0 THEN 1420
1410 PRINT "ERROR IN SUBROUTINE"
      @ PRINT "DIVISION BY ZERO"
      @ PAUSE
1420 X2(N)=X2(N)/F(I2,N)
1430 FOR C=N-1 TO 1 STEP -1
1440 I2=I1(C)
1450 S=0
1460 FOR D=C+1 TO N
1470 S=S+F(I2,D)*X2(D)
1480 NEXT D
1490 IF F(I2,C)<>0 THEN 1510
1500 GOTO 1410
1510 X2(C)=(X2(C)-S)/F(I2,C)
1520 NEXT C
1530 RETURN

```

```

1540 DIM S1(3)
1550 FOR I=1 TO N
1560 I1(I)=I @ R=0
1570 FOR J=1 TO N
1580 IF R-ABS(F(I,J))>=0 THEN 16
00
1590 R=ABS(F(I,J))
1600 NEXT J
1610 IF R<>0 THEN 1630
1620 PRINT "ERROR IN SUBROUTINE"
@ PRINT "MATRIX WITH ZERO
ROW" @ PAUSE
1630 S1(I)=1/R
1640 NEXT I
1650 FOR K=1 TO N-1
1660 W3=0
1670 FOR I=K TO N
1680 I2=I1(I) @ S2=ABS(F(I2,K))*
S1(I2)
1690 IF S2-W3<=0 THEN 1710
1700 W3=S2 @ I3=I
1710 NEXT I
1720 IF W3<>0 THEN 1740
1730 GOTO 1860
1740 IF I3-K=0 THEN 1760
1750 J=I1(K) @ I1(K)=I1(I3) @ I1
(I3)=J
1760 K1=I1(K) @ P=F(K1,K)
1770 FOR I=K+1 TO N
1780 I2=I1(I) @ E=-F(I2,K)/P @ F
(I2,K)=-E
1790 FOR J=K+1 TO N
1800 F(I2,J)=F(I2,J)+E*F(K1,J)
1810 NEXT J
1820 NEXT I
1830 NEXT K
1840 K1=I1(N)
1850 IF F(K1,N)<>0 THEN RETURN
1860 PRINT "ERROR IN SUBROUTINE"
@ PRINT "MATRIX IS MACHINE
SINGULAR" @ PAUSE @ RETURN
1870 J1(T)=ATN2(W(3,1),W(2,1))
1880 J2=W(2,1)/(2*COS(J1(T)))
1890 J3=W(3,1)/(2*SIN(J1(T)))
1900 J5=SQR(ABS(W(1,1)))
1910 J4(T)=(J5+J2+J3)/3
1920 NEXT T
1930 ASSIGN# 1 TO *
1940 PRINT "FREQ ; REF. COEFF.
"
1950 PRINT "-----
-"
1960 PRINT "[MHZ] ; MAG ; PHASE"
1970 PRINT "-----
-"
1980 FOR I=1 TO N3
1990 PRINT USING 2010 ; F0(I),J4
(I),J1(I)
2000 NEXT I
2010 IMAGE 5D,2X,0.3D,2X,4D.2D, /
/

```

```
2020 PEN 1 @ GCLEAR
2030 SCALE F0(1)-2*R1/N1,F0(N3)+
2*R1/N1,-.2,1.2
2040 XAXIS 0,R1/N1,F0(1)-R1/N1,F
0(N3)+R1/N1
2050 YAXIS F0(1)-R1/N1,.1,0,1
2060 GOSUB 2150
2070 FOR I=F0(1) TO F0(N3) STEP
R1/N1
2080 GOSUB 2110
2090 NEXT I
2100 GOTO 2260
2110 MOVE I,J4(K)
2120 IMOVE 0,.01 @ IDRAW 0,-.02
2130 IMOVE .3,.01 @ IDRAW -.6,0
2140 RETURN
2150 LDIR 90
2160 FOR X=F0(1) TO F0(N3) STEP
R1/N1
2170 MOVE X,-.19
2180 LABEL VAL$(X)
2190 NEXT X
2200 LDIR 0
2210 FOR Y=0 TO 1 STEP .1
2220 MOVE F0(1)-1.8*R1/N1,Y
2230 LABEL VAL$(Y)
2240 NEXT Y
2250 RETURN
2260 COPY
2270 END
```

6PCAL

```

10 DISP " THIS IS A CALIBRATION
   ROUTINE FOR THE SIX-PORT"
11 WAIT 4000
12 CLEAR
20 DISP " THE SIX-PORT CAN BE C
   ALIBRATED AT ANY FREQ BETWEE
   N 900-1100MHZ"
21 WAIT 4000
30 CLEAR
40 OPTION BASE 1
50 DIM N(101),F0(101),V(4),V1(3
   ),V2(3),V3(3),V4(3)
60 DIM P(3,6),R(6),A(3,3),C(3),
   S(3),B(3),T(3),X(3)
70 DIM R0(3),R1(3),R2(3),R3(3)
80 DEG
90 O1=180
100 O2=90
110 O3=-90
120 CLEAR
130 DISP "ENTER LO AND HI FREQUE
   NCIES IN MHZ"
140 INPUT F1,F2
150 R1=F2-F1
160 CLEAR
170 IF F2#F1 THEN 220
180 N1=1
190 N3=1
200 N2=.2
210 GOTO 270
220 DISP "NUMBER OF FREQUENCY IN
   TERVALS TO BE SWEPT?"
230 INPUT N1
240 CLEAR
250 N3=N1+1
260 N2=N1/5
270 N0=1.5*N2
280 OUTPUT 705 ; "M1R0F0"
290 WAIT 300
300 OUTPUT 716 USING "K,K" ; "B"
   ;3;"R1YPMPOM"
310 WAIT 300
320 CLEAR
330 FOR I=1 TO N3
340 F0(I)=(I-1)*R1/N1+F1
350 F0(I)=INT(F0(I)*10)/10
360 N(I)=1INT((F0(I)-10)*.5289399
   6755+109.4)
370 NEXT I
380 FOR T=1 TO N3
390 K1=N(T)-25
400 K1=K1-3
410 C2=1
420 K1=K1+3
430 OUTPUT 705 ; "V";K1;"E"
440 WAIT 300
450 ENTER 716 ; F3
460 C1=F3/1000000-F0(T)
470 IF ABS(C1)<10 THEN GOTO 530
480 IF C1>0 THEN K1=K1-10

```

```

490 IF C1<0 THEN K1=K1+10
500 IF C2<4 THEN C2=C2+1 ELSE 41
    0
510 GOTO 430
520 WAIT 300
530 OUTPUT 716 "YPMPD";F0(T);"MR
    C"
540 WAIT 300
550 ENTER 716 ; F4
560 F4=F4/1000
570 WAIT 300
580 ENTER 716 ; F5
590 F5=F5/1000
600 F6=ABS(F5-F4)
610 FOR L=1 TO 5
620 IF L#1 THEN 650
630 A$="USE MATCHED LOAD"
640 GOTO 750
650 IF L#2 THEN 680
660 A$="USE OPEN"
670 GOTO 750
680 IF L#3 THEN 710
690 A$="USE SHORT "
700 GOTO 750
710 IF L#4 THEN 730
720 A$="USE 90 DEG OFFSET"
730 IF L#5 THEN 750
740 A$="USE 270 DEG OFFSET"
750 DISP A$
760 INPUT D$
770 CLEAR
780 K2=5/1022
790 C=1
800 WAIT 300
810 OUTPUT 706 USING "#,K,K" ; "
    H",C,"AJ","F"
820 S=0
830 FOR J=1 TO 10
840 WAIT 300
850 ENTER 706 USING "#,W" ; V(1)
860 S=S+V(1)
870 NEXT J
880 V(1)=K2*S/10
890 X=V(1)
900 P(1,L)=6.162983+207.0921*X+1
    9.16073*X^2
910 C=2
920 WAIT 300
930 OUTPUT 706 USING "#,K,K" ; "
    H",C,"AJ","F"
940 S=0
950 FOR J=1 TO 10
960 WAIT 300
970 ENTER 706 USING "#,W" ; V(2)
980 S=S+V(2)
990 NEXT J
1000 V(2)=K2*S/10
1010 X=V(2)
1020 R(L)=10*(.9590646+75.32981*
    X+17.8778*X^2)

```

```

1030 C=4
1040 WAIT 300
1050 OUTPUT 706 USING "#,K,K" ;
      "H",C,"AJ","F"
1060 S=0
1070 FOR J=1 TO 10
1080 WAIT 300
1090 ENTER 706 USING "#,W" ; V(3
      )
1100 S=S+V(3)
1110 NEXT J
1120 V(3)=K2*S/10
1130 X=V(3)
1140 P(3,L)=-.02710391+179.4503*
      X+11.18641*X^2
1150 C=8
1160 WAIT 300
1170 OUTPUT 706 USING "#,K,K" ;
      "H",C,"AJ","F"
1180 S=0
1190 FOR J=1 TO 10
1200 WAIT 300
1210 ENTER 706 USING "#,W" ; V(4
      )
1220 S=S+V(4)
1230 NEXT J
1240 V(4)=K2*S/10
1250 X=V(4)
1260 P(2,L)=-1.375671+123.8964*X
      +13.8794*X^2
1270 OUTPUT 706 USING "H"
1280 NEXT L
1290 FOR I=1 TO 3
1300 B(I)=P(I,1)/R(I)
1310 R0(I)=P(I,2)/(R(2)*B(I))
1320 R1(I)=P(I,3)/(R(3)*B(I))
1330 R2(I)=P(I,4)/(R(4)*B(I))
1340 R3(I)=P(I,5)/(R(5)*B(I))
1350 NEXT I
1360 FOR I=1 TO 3
1370 D1=SIN(02)-SIN(03)-SIN(02-0
      3)
1380 D2=SIN(03)-SIN(01)-SIN(03-0
      1)
1390 D3=SIN(01)-SIN(02)-SIN(01-0
      2)
1400 A(I,1)=(R1(I)-R0(I))*D1+(R2
      (I)-R0(I))*D2+(R3(I)-R0(I))
      *D3
1410 A(I,2)=(R1(I)*COS(01)-R0(I)
      )*D1+(R2(I)*COS(02)-R0(I))*
      D2+(R3(I)*COS(03)-R0(I))*D3
1420 A(I,3)=-R1(I)*SIN(01)*D1-R2
      (I)*SIN(02)*D2-R3(I)*SIN(03
      )*D3
1430 NEXT I
1440 Z5=ATN((A(2,1)*A(1,2)-A(1,1
      )*A(2,2))/(A(1,1)*A(2,3)-A(
      2,1)*A(1,3)))
1450 Z6=ATN((A(2,1)*A(3,2)-A(3,1
      )*A(2,2))/(A(3,1)*A(2,3)-A(
      2,1)*A(3,3)))

```

```

1460 Z7=ATN((A(3,1)*A(1,2)-A(1,1)
) *A(3,2))/(A(1,1)*A(3,3)-A(
3,1)*A(1,3))
1470 B5=SQR((A(2,1)*A(1,2)-A(1,1)
)*A(2,2))^2+(A(1,1)*A(2,3)-
A(2,1)*A(1,3))^2)
1480 B6=SQR((A(2,1)*A(3,2)-A(3,1)
)*A(2,2))^2+(A(3,1)*A(2,3)-
A(2,1)*A(3,3))^2)
1490 B7=SQR((A(3,1)*A(1,2)-A(1,1)
)*A(3,2))^2+(A(1,1)*A(3,3)-
A(3,1)*A(1,3))^2)
1500 A8=Z5
1510 IF B5>B6 THEN 1530
1520 A8=Z6
1530 IF B6>B7 THEN 1550
1540 A8=Z7
1550 Z2=A8+180
1560 U1=(-A(1,3)*SIN(A8)-A(1,2)*
COS(A8))/A(1,1)
1570 U2=(-A(1,3)*SIN(Z2)-A(1,2)*
COS(Z2))/A(1,1)
1580 A9=A8
1590 IF U1>U2 THEN 1610
1600 A9=Z2
1610 GOTO 1620
1620 X5=-(A(1,2)*COS(A9)+A(1,3)*
SIN(A9))/A(1,1)
1630 X6=-(A(2,2)*COS(A9)+A(2,3)*
SIN(A9))/A(2,1)
1640 X7=-(A(3,2)*COS(A9)+A(3,3)*
SIN(A9))/A(3,1)
1650 X1=X5
1660 IF A(1,1)>A(2,1) THEN 1680
1670 X1=X6
1680 IF A(2,1)>A(3,1) THEN 1700
1690 X1=X7
1700 Z=ABS(X1)-SQR(X1^2-1)
1710 OUTPUT 706 USING "H"
1720 FOR I=1 TO 3
1730 V1(I)=P(1,2)/R(2)/B(I)*(1+2
)*Z*COS(A9)+Z^2)
1740 V2(I)=P(1,3)/R(3)/B(I)*(1-2
)*Z*COS(A9)+Z^2)
1750 V3(I)=P(1,4)/R(4)/B(I)*(1-2
)*Z*SIN(A9)+Z^2)
1760 V4(I)=P(1,5)/R(5)/B(I)*(1+2
)*Z*SIN(A9)+Z^2)
1770 NEXT I
1780 FOR I=1 TO 3
1790 C(I)=.25*(V1(I)-V2(I))
1800 S(I)=.25*(V4(I)-V3(I))
1810 X(I)=SQR(C(I)^2+S(I)^2)
1820 NEXT I
1830 PRINT F0(T),Z,A9,X(1),X(2),
X(3),C(1),C(2),C(3),S(1),S(
2),S(3),B(1),B(2),B(3)
1840 NEXT T
1850 END

```